

1992

Electroabsorbtion in Multiple Quantum Well Structures

Hatem Abdelkader
University of Rhode Island

Follow this and additional works at: https://digitalcommons.uri.edu/oa_diss

Terms of Use

All rights reserved under copyright.

Recommended Citation

Abdelkader, Hatem, "Electroabsorbtion in Multiple Quantum Well Structures" (1992). *Open Access Dissertations*. Paper 387.

https://digitalcommons.uri.edu/oa_diss/387

This Dissertation is brought to you by the University of Rhode Island. It has been accepted for inclusion in Open Access Dissertations by an authorized administrator of DigitalCommons@URI. For more information, please contact digitalcommons-group@uri.edu. For permission to reuse copyrighted content, contact the author directly.

1992

Electroabsorption in Multiple Quantum Well Structures

Hatem Abdelkader

Follow this and additional works at: <http://digitalcommons.uri.edu/theses>

Terms of Use

All rights reserved under copyright.

ELECTROABSORPTION IN MULTIPLE QUANTUM WELL STRUCTURES

BY

HATEM ABDELKADER

A DISSERTATION SUBMITTED IN PARTIAL FULFILLMENT OF THE

REQUIREMENTS FOR THE DEGREE OF

DOCTOR OF PHILOSOPHY

IN

ELECTRICAL ENGINEERING

UNIVERSITY OF RHODE ISLAND

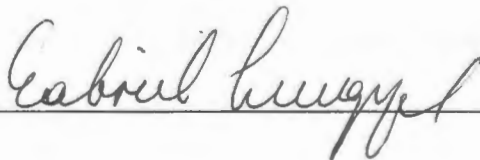
1992

DOCTOR OF PHILOSOPHY DISSERTATION
OF
HATEM ABDELKADER

APPROVED:

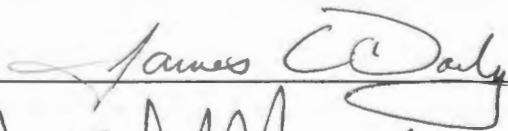
Dissertation Committee

Major Professor











DEAN OF THE GRADUATE SCHOOL

UNIVERSITY OF RHODE ISLAND

1992

Abstract

We studied electroabsorption in GaAs/AlGaAs Multiple Quantum Well (MQW) structures. The waveguide used for this study was designed as a phase modulator with an active layer containing six 75 Å GaAs quantum wells and 80 Å Al_{0.35}Ga_{0.65}As barriers.

Electroabsorption in MQW structures is dependent on, among other things, the light polarization, the orientation of the crystal optical axes, and the direction of the applied electric field.

In the first study we measured the spectral dependence of the quadratic electro-optic coefficient for TM polarized light (s_{33} near the absorption band edge. The light hole exciton resonance occurs at 820 nm for the particular device we used. The spectral range studied was from 840 nm to 880 nm. In this region, the quadratic coefficient demonstrated large values ($1.2 \times 10^{-8} \text{ cm}^2/\text{kV}^2$ at 840 nm) near the band edge. This is about two orders of magnitude larger than that observed in bulk material. It also falls rapidly as the wavelength increases further away from the band edge.

A knowledge of this material parameter permits the calculation of the change in refractive index with an applied field, which is very useful in phase modulator design. This along with the change in the absorption coefficient as a function of the applied field (also measured) determines the operational characteristics of

the phase modulator at a given wavelength.

In the second study, we investigated the effect of the crystal optical axes orientation on electroabsorption in MQW's. We reported, for the first time, a difference in the change in electroabsorption by almost a factor of 2 between $[-1,1,0]$ and $[1,1,0]$ oriented structures. This makes the former orientation better suited for intensity modulator/switching devices as one gets larger change in the absorption coefficient with lesser applied voltage.

We attributed that orientation dependence in the absorption coefficient between the two orientations to the anisotropy of the valence subband structure brought about by band mixing due to the quantum wells periodic potential.

In the third study, we devised a novel technique to extract the spectral dependence of the absorption coefficient in these structures from measurements of the transmitted light intensity as a function of the applied voltage at a single fixed wavelength.

Results are in very good agreement with the measurement of the spectral dependence of the absorption coefficient by varying the wavelength. This technique is a rather simple one and does not require a coherent tunable light source which is very expensive and not readily available in every lab.

Acknowledgments

I gratefully acknowledge the assistance of the laboratories in Munich, Germany, and its department, as well as the support of the...

I would like to thank Dr. [Name] for his help in Lengyel, front view, and other aspects of a friend and mentor. **DEDICATED TO MOM AND DAD**

I would then like to thank Dr. [Name] Hartl for serving as my advisor.

I am grateful to Dr. [Name] W. Ohley and Dr. [Name] RA during the course of my...

I would like to thank Dr. [Name] Schaumburg for his help and support.

I take this opportunity to thank my valuable director, Dr. [Name]

I would also like to thank my family and friends for their support.

Acknowledgments

I gratefully acknowledge the financial assistance of the Siemens Research Laboratories in Munich, FRG, without which this work would not have been possible, and its department FKE1 for the preparation of the samples used in the studies, as well as the Siemens Research and Technology Laboratories at Princeton, N.J.

I would like to extend my heartfelt thanks to my major professor, Dr. Gabriel Lengyel, from whom I learned a lot not only in the area of my research, but also in other aspects of life. I am deeply indebted to him for standing by me both as a friend and mentor during my doctoral work.

I would then like to thank Professors G. Fischer, J. Bonner, J. Daly, and K. Hartt for serving on my dissertation committee.

I am grateful to the department of Electrical Engineering, in particular to Dr. W. Ohley and Dr. H. Sunak for giving me the opportunity to work as a TA or RA during the course of my doctoral program.

I would like to thank Dr. George Valliath, who is presently with Motorola Inc in Schaumburg, IL. I have learned invaluable skills as an experimentalist from him.

I take this opportunity to thank my very good friend Steve Bastien for the valuable discussions we had, and for his support during the past five years.

I would also like to extend my thanks to my colleagues: Tony Deus, Jeff Adams,

Clark Engert, Dane Kottke, Marry-Kay Kottke, Seth Suppapola, Antonia Papandreou, Robin Murray, Gustavo Ruiz-Riquer , Mike Plattak, Anjali Singh, Sridahr Balakrishnan, Ram Palissery and Tom Quattromani.

Throughout my work I was sustained by the strength I received from my Lord and my God. I dedicate this work to the memory of my father. I am especially grateful to my family, my mother Layla, my sister Manal, and my brother Khalid. They stood by me and encouraged me to do my best and gave me the impetus to pursue my study, though far away.

Thank you!

Hatem Abdelkader

October, 1992.

Preface

Recent advances in semiconductor technology have led to the fabrication of microstructures which are small enough to manifest the quantum nature of charge carriers in these structures on a macroscopic scale. The majority of these microstructures are in the form of alternating layers of wide and narrow energy gap materials which produce a series of 'potential wells' due to the alternating energy gaps. The thickness of these wells is of the order of 100 \AA , which causes the carriers, that are confined in the potential wells, to behave like the well-known quantum mechanical particle-in-a-box and exhibit the corresponding discrete energy levels. The term 'quantum well' arises from these characteristics. These quantum wells, when incorporated in semiconductor devices like lasers and modulators as part of their active regions, exhibit novel physical properties which holds the potential for revolutionizing opto-electronics.

Large strides have been made in characterizing these new semiconductor structures and still larger terrains remain to be explored. This thesis documents the study of two important properties of the quantum well structures, viz., the quadratic electro-optic coefficient for TM polarized light and the orientation dependence of the change in the absorption coefficient.

The electro-optic coefficients describe the change in the refractive index due to an applied electric field, a phenomenon which is exploited in optical phase modulation and diode laser tuning. These coefficients are well researched in bulk materials, but scant literature is found regarding them for quantum well

structures. Knowledge of these coefficients is very important in semiconductor tunable laser and modulator design. Also important is the absorption coefficient and its dependence on the applied electric field. This quantity is intimately related to the refractive index, and so, a study of the refractive index and its field dependence is not complete, if the absorption coefficient and its field dependence are not studied.

The other property studied is the orientation dependence of the change in the absorption coefficient between $[-1,1,0]$ and $[1,1,0]$ oriented devices. In this study we reported a factor of 2 difference between the two orientation. This favors the $[-1,1,0]$ for applications that involve intensity modulator/switching devices.

This dissertation has been prepared according to the MANUSCRIPT PLAN. The main part of this dissertation consists of manuscripts I - III, which have been written in the contemporary format required for publication in journals. Appendices have been added to include detailed information normally excluded from manuscripts; however, necessary for completeness of this work. References pertaining to each manuscript are cited at the end of the respective manuscript. The bibliography at the end of the dissertation lists all possible sources used in the writing of this dissertation.

This work is an outgrowth of a study funded by the Research Laboratories of the Siemens Corp., Munich, and its US research branch, the Research and Technology Laboratories, Princeton, N. J. The study was aimed at characterizing and developing efficient phase modulators with a view to integration of modulator and laser. This work is still in progress at the University of Rhode Island.

Contents

Abstract	ii
Acknowledgments	v
Preface	vii
Table of Contents	ix
List of Figures	xii
1 Spectral dependence of the quadratic electro-optic coefficient, for TM polarization, in 75Å GaAs/AlGaAs Multiple Quantum Well devices.	1
1.1 Introduction	3
1.2 Test samples	5
1.3 Experimental setup	6
1.3.1 The source	6
1.3.2 The interferometer	7
1.3.3 The detection system	8

1.4	Phase change versus voltage measurements	9
1.5	Evaluation of s_{33}	11
1.6	Results	14
1.7	Conclusion	16
1.8	Appendix A	17
1.8.1	The electro-optic effect in zincblend type crystals	17
1.8.2	Zincblend Crystal Structure	18
1.8.3	Perturbed Index Ellipsoid	18
1.8.4	Symmetry Properties in Zincblend	21
1.8.5	The Linear Electro-optic Coefficient $[r_{ijk}]$	22
1.8.6	The Quadratic Electro-optic Coefficient $[s_{ijkl}]$	26
1.9	Figure captions	34
2	Orientation dependence in the change of electroabsorption for [-1,1,0] and [1,1,0] oriented GaAs/AlGaAs multiple quantum well structures	42
2.1	Introduction	44
2.2	Test samples	45
2.3	Measurements and results	46
2.4	Results and explanation	49
2.5	Transverse sample measurements	51

2.6	Effect of stress/strain on the QW electronic states and optical properties	53
2.7	Effect of refractive index change due to the linear electrooptic effect on the confinement factor Γ	55
2.8	Summary and conclusion	56
2.9	Appendix A	57
2.9.1	Absorption coefficient calculation	57
2.9.2	Envelope function description of electronic states in the multiband effective mass scheme	62
2.10	Figure captions	74
3	Extraction of the spectral dependence of the absorption coefficient in III-V multiple quantum well structures from transmitted light intensity measurements as a function of applied field at a single wavelength	85
3.1	Introduction	87
3.2	Sample, experimental setup and measurements	88
3.3	Technique	90
3.4	Results	94
3.5	Conclusion	95
3.6	Acknowledgement	96
3.7	Appendix A	97
3.8	Figure captions	104

List of Figures

1.1	Cross section of the waveguide multiple quantum well sample. . .	35
1.2	Block diagram of the experimental setup for measuring s_{33}	36
1.3	Normalized measured interference pattern "F(V)", and transmitted light intensity "f(V)" at 850 nm.	37
1.4	Normalized measured interference pattern "F(V)", and transmitted light intensity "f(V)" at 875 nm.	38
1.5	Calculated quadratic electro-optic coefficient s_{33} versus wavelength. . .	39
1.6	Comparison between the quadratic electro-optic coefficients s_{31} (TE) solid line and s_{33} (TM) dotted line as a function of the detuning from the exciton absorption edge for the [-1,1,0] orientation.	40
1.7	Calculated change in refractive index Δn as a function of applied field for the [-1,1,0] orientation.	41
2.1	Cross section of the Multiple Quantum Well waveguide sample. . .	76
2.2	Schematic illustration of how both [-1,1,0] and [1,1,0] samples were cut from the same wafer which was grown on a (001) plane.	77
2.3	Experimental setup for measuring the change in electroabsorption.	78
2.4	Normalized P_i and I_{ph} vs. applied voltage for TE polarization at 850 nm, a) [-1,1,0] orientation, b) [1,1,0] orientation.	79

2.5	Normalized P_t and I_{ph} vs. applied voltage for TM polarization at 850 nm, a) [-1,1,0] orientation, b) [1,1,0] orientation.	80
2.6	Change in the absorption coefficient in A.U. vs. applied voltage at 850 nm (hh exciton is at 830 nm, lh exciton is at 820 nm). a) TE polarization, b)TM polarization.	81
2.7	Cross section of the Double heterostructure sample used.	82
2.8	Change in the absorption coefficient in A.U. vs. applied voltage in DH structures at 800 nm for TE polarization.	83
2.9	Cross section of the Multiple Quantum Well transverse sample.	84
3.1	Cross section of the transverse MQW structure.	106
3.2	Experimental setup used to measure P_t and I_{ph}	107
3.3	Measured P_t , and I_{ph} at $\lambda=860$ nm as a function of voltage.	108
3.4	Absorption coefficient at 860 nm as a function of applied electric field.	109
3.5	Heavy hole exciton energy $E_{hh}(F)$ as a function of applied electric field.	110
3.6	Normalized oscillator strength for the heavy hole exciton as function of applied electric field.	111
3.7	HWHM of the heavy hole Lorentzian line shape as a function of applied electric field.	112
3.8	Schematic illustration of the technique used to deduce the spectral dependence of electroabsorption.	113

3.9	Calculated spectral dependence of the absorption coefficient for different values of applied field.	114
3.10	Measured spectral dependence of absorption coefficient for different values of applied voltage/field.	115
3.11	Perturbed electron and hole wavefunctions for different values of applied field. a) for electrons, b) for holes.	116
3.12	Calculated exciton binding energy as a function of applied field. .	117

Manuscript 1

Spectral dependence of the quadratic electro-optic coefficient, for TM polarization, in 75Å GaAs/AlGaAs Multiple Quantum Well devices.

ABSTRACT

The authors

investigate

the

dependence

of the

quadratic

electro-optic

coefficient

for

TM

polarization

in

75Å

GaAs/AlGaAs

Multiple

Quantum

Well

devices.

TITLE:

Spectral dependence of the quadratic electro-optic coefficient, for TM polarization, in 75Å GaAs/AlGaAs Multiple Quantum Well devices.

ABSTRACT:

We have measured the wavelength dependence, for TM polarization, of the quadratic electro-optic coefficient s_{33} for 75Å GaAs/Al_{0.35}Ga_{0.65}As structures near the absorption edge. Waveguides oriented along the $[\bar{1}, 1, 0]$ and $[1, 1, 0]$ directions were used for measurement. Results show a rapid decrease in s_{33} (cm^2/kV^2) as λ increased further away from the absorption edge. We have also plotted the quadratic electrooptic coefficient versus the detuning energy from the exciton fundamental absorption edge in meV for TM polarized light s_{33} and compare it with s_{13} for TE polarization. The change in refractive index for TM polarization as a function of applied field and wavelength is also presented as an aid to device design.

1.1 Introduction

In electro-optic devices it is sometimes necessary to determine the change in refractive index due to an applied field. The change in the refractive index is a function of three factors which are:

1. The direction of the polarizing field ($E_{\text{electrical}}$),
2. the orientation of the crystal optical axes,
3. and the polarization of the optical electric field.

The behavior of the refractive index under the influence of an applied field is governed largely by the linear and quadratic electro-optic coefficients of the material. These coefficients are traditionally defined as the expansion coefficients of the change in the dielectric impermeability tensor $\eta_{ij} = \epsilon_0(\epsilon^{-1})_{ij}$ as a function of the external field or

$$\Delta\eta_{ij} = r_{ijk}E_k + s_{ijkl}E_kE_l,$$

where E_i are the components of the electric field and r_{ijk} and s_{ijkl} are the elements of the 3rd rank linear electro-optic tensor and the 4th rank quadratic electro-optic tensor respectively. The higher order expansion terms have been neglected and summation over repeated indices is assumed. The dielectric impermeability tensor η relates the *optical* electric field to the *optical* displacement vector

$$E_i = \frac{\eta_{ij}}{\epsilon_0} D_j.$$

When diagonalized, the elements of the tensor η are related to the refractive indices by

$$\eta_i = \left(\frac{1}{n_i^2} \right),$$

where η_i are the diagonal elements and the n_i are the refractive indices along the principal axes of the crystal. Again the summation over repeated indices has been assumed.

The electro-optic coefficients for bulk GaAs and other crystals have been extensively studied and cataloged [1], [2]. In quantum well structures, however, the research has been relatively limited, mainly due to the relative newness of the field.

In this paper we present the quadratic electro-optic coefficient, as a function of wavelength, for a GaAs/Al_{0.35}Ga_{0.65}As quantum well (QW) structure, near its band gap. The electric field was applied parallel to the [1,0,0] direction which, in the case of our *p-i-n* structure, corresponded to a field perpendicular to the layers. The polarization of the optical wave was perpendicular to the QW layers, i. e., in the TM mode. For such a configuration there is one coefficient, the s_{33} , that is involved (see appendix A).

Where an ambiguity could arise between the coefficients of the quantum well and those of the bulk, the former will be referred to as r_Q and s_Q , where Q signifies the quantum well, and the bulk coefficients will be referred to as r_B and s_B .

From the measurements, we also calculate the change in the refractive index. This is helpful in device design and determination of its operational characteristics.

1.2 Test samples

The samples were grown by metallo-organic vapor phase epitaxy (MOVPE) on a (001) substrate of n-doped GaAs at the Siemens Research laboratories in Munich, Germany. The active region contained six GaAs QW's each 75 Å thick, separated by five 80 Å thick $Al_{.35}Ga_{.65}As$ barrier layers. Figure (1.1) shows a cross section of the MQW sample used.

The MQW layers and the index grading layers in the QW device were not intentionally doped. The residual doping in these layers was found to lie in the middle 10^{16} cm^{-3} range. The doping of the cover layers ranged between 2 and $5 \times 10^{17} \text{ cm}^{-3}$ leading to a *p-i-n* sequence in the doping profile.

A stripe of 3 μm width was then formed by sputter etching a ridge into the top AlGaAs cover layer to form the ridge waveguide. The height of the ridge was designed to allow single lateral mode operation. The etched surface was passivated with a .3 μm sputtered Al_2O_3 and finally the metal contact was evaporated on the finished wafer.

The samples were identical except for the orientation of the waveguides, where the optical axis was oriented along the [-1,1,0] direction in some samples while along the [1,1,0] in others. The length of the QW waveguide modulator was 1 mm. Both facets were AR-coated to improve transmission and to reduce Fabry-Perot resonances.

1.3 Experimental setup

The experimental set-up is divided, for the purposes of description, into three parts. The first is the source, which covers the lasers and the polarizing elements. The second deals with the interferometer itself, and the last deals with the detector arrangements. Figure (1.2) depicts the experimental setup.

1.3.1 The source

The source of tunable radiation for this experiment was a Coherent 599-01 Dye Laser, with Styryl 9M as the lasing dye. The useful lasing range of this dye was 800–920 nm. The linewidth of the output radiation was about 27 GHz. The laser was run at a power output of 80 mW, though the maximum output power was about 500 mW.

The pump for the dye laser was a Coherent Innova 70-4 Argon Ion Laser, with a maximum power output of 6 W. The laser produced a multiline output which ranged in wavelength from 488–514 nm. About 3 W was required to produce the required 80 mW from the dye laser.

The output from the dye laser was guided to the interferometer using beam-steering elements. A polarizer and an attenuator (neutral density filter) were used to ensure the desired polarization and intensity respectively.

Not shown in the diagram is a beam-splitter, located just before the polarizer,

which sampled a portion of the beam and directed it to a SPEX 1702 spectrometer for wavelength measurement. Also not shown, is a He-Ne laser which was used for the alignment of the interferometer. It was arranged such that the output of the dye laser and the He-Ne beam would reach the interferometer collinearly.

1.3.2 The interferometer

The operation of this interferometer is simple. Light from the source is split into two parts by a beamsplitter. One beam travels along one arm and the other travels along the other arm of the interferometer. These two beams meet again and interfere. Normally, concentric or parallel fringes are seen on the screen. These fringe patterns move as the difference in optical path length between the two arms of the interferometer changes.

If the alignment between the two arms is very good, then the size of the fringes grow large enough such that the entire image on the screen increases or decreases in brightness as the optical path length changes. Achieving this is very important as the the measurements were done using a photodiode, which only measures average intensities. If the fringes were small, even though the fringes move, no change in average intensity would be observed.

The mirror located in the reference arm was equipped with a piezo-electric translation positioner to adjust the difference in path length. This positioner could move distances as small as $0.1 \mu\text{m}$. The optical path length depends on the physical length as well as the refractive index of the path. The positioner changes the optical path length by changing the physical length, while the phase modulator

changes it by changing the refractive index. On application of a voltage, the phase modulator changes the path length of this arm and a change in interference pattern is measured by the photodetector. This is the basic raw data used to evaluate the electro-optic coefficient s_{33} .

1.3.3 The detection system

The detection system consists of an infra-red TV camera and a silicon photodiode. The camera is used for alignment of the interferometer, and the photodiode is used for the phase vs. voltage measurements.

The photodiode is connected in series with a $100\text{ k}\Omega$ resistor and a voltage source. The latter is used to reverse-bias the photodiode to the the required 15 V. The photocurrent is measured by measuring the potential drop across the series resistance, using a Keithley System DMM. This DMM is controlled by an HP9000 Series 300 computer, through an IEEE-488 interface.

The voltage for the phase modulator is provided by an HP System DC Power Supply, which is also controlled by the computer. For a measurement cycle, the computer causes the DC Power Supply to ramp from 0 to 6 V in steps of 0.1 V, producing 61 voltage points. At each voltage the DMM measures the output of the photodiode. Although the DMM is capable of taking a measurement every 1 ms, the voltage source takes about 10 ms to change from one voltage to the next. This means that the measurement cycle, of 61 points, can be completed in < 1 s. Speed is very important for good measurements. The interference pattern has the tendency to drift slowly, with a time period of the order of a couple of minutes. This is probably caused by a slow drift in the laser line due to heating

effects. This means that, with a 1 s measurement cycle, the data will be very reliable as the drift will be negligible. Another advantage of high speed is that several cycles can be performed within a short period, and the results averaged to produce data curves. In a typical measurement, about 25 measurement cycles are performed in about half a minute. These measurements are averaged to produce the final data curves.

For each wavelength, the entire measurement procedure consists of three steps. The first is the measurement of the intensity of the reference arm, which is done with the device arm blocked. The device arm is the arm of the interferometer which contains the phase modulator. Next, the voltage dependence of the device arm intensity is measured, with the reference arm blocked. This is done as described in the previous paragraph, with each measurement cycle taking about 1 s. The change in intensity of light passing through the device is due to the change in absorption coefficient in the modulator with applied field. The last step is the measurement of the interference change with voltage, with both arms unblocked. The result of this measurement is labelled $F(V)$, and the change in device arm intensity is labelled $f(V)$. These two quantities, along with the reference arm intensity R , are used to calculate the electro-optic coefficients.

1.4 Phase change versus voltage measurements

The phase change produced in the light guided through the device was measured using the Mach-Zehnder interferometer described above. The device to be tested was placed in one arm of the interferometer. The light was launched into, and collected from the device using a pair of microscope objectives. The polarization

was perpendicular to the layers, i.e., TM. The output microscope objective was positioned such that it produced an image of the device near-field on the IR TV camera. A pair of similar objectives was also placed in the reference arm in order to focus the light onto the image of the device near-field in the camera and also to compensate for the change in path length introduced in the device arm due to the presence of the device-arm microscope objectives.

The interference pattern was imaged on the IR TV camera as well as on a photodiode. The camera helped in alignment, while the photodiode was used in the actual measurement.

The application of a reverse bias causes the refractive index of the guiding layers in the device to change, resulting in a phase shift of the guided wave. This shift can be observed as a change in intensity of the interference pattern. If the interferometer was not well aligned then a shift in the fringe pattern would be seen. In our case, the two arms were aligned so that the phase shift was seen only as an intensity change. This intensity change labeled $F(V)$, measured by the photodiode, is shown in Figure (1.3,1.4) for two different wavelengths. Moving from peak to trough on the plot corresponds to a phase shift of 180° . These figures also show the measured intensity modulation, labeled $f(V)$, caused by the device due to electro-absorption. This was measured with the reference arm of the interferometer blocked. The next step was to extract the phase versus voltage relations from the measured data. It can be shown that the phase change as a function of voltage $\phi(V)$, can be expressed using the measured data as [3]

$$A_0 \cos(\phi(V)) = \frac{F(V) - f(V) - R}{\sqrt{f(V) - K}} \quad (1.1)$$

where $F(V)$ is the measured interference curve while $f(V)$ is the measured intensity variation with one arm of the interferometer blocked Figure (1.3). R is the

intensity of the reference arm in the interferometer. The constant K was chosen such that the RHS of Equation (1.1) was cosine in form. This cosine data is then fitted to an equation of the form

$$A_0 \cos(aV^2 + c) \quad (1.2)$$

where the $\phi(V)$ is assumed to have the form

$$\phi(V) = aV^2 + c \quad (1.3)$$

to reflect the quadratic nature of the phase change produced by the quadratic electro-optic coefficient. There is no linear electrooptic effect for TM polarization (see appendix A). The constants A_0 , a , and c become the non-linear least-square fit parameters. The a is directly related to the quadratic electro-optic coefficient while the c represents only a constant phase shift at $V = 0$ which depends on, among other things, the length of the device and the difference in path length between the two arms of the interferometer. Consequently a alone completely determine the significant information contained in $\phi(V)$. Having obtained $\phi(V)$ as a quadratic we can proceed to evaluate the quadratic electro-optic coefficient s_{33} .

1.5 Evaluation of s_{33}

The electro-optic coefficient s_Q for the quantum well device is obtained using a technique similar to that used in [3], namely, a least-squares fit to the measured data $\phi(V)$. The main difference from [3] is that for TM polarized light, symmetry considerations do not allow a linear component for the phase change $\phi(V)$ in the applied voltage, i.e. $\phi(V)$ is a pure quadratic in the applied voltage V . This technique is repeated here with the necessary modifications only for better

understanding.

The phase $\phi(V)$ can be written in terms of the change in the propagation constant β as

$$\phi(V) = \Delta\beta(V)L \quad (1.4)$$

where L is the length of the device. The $\Delta\beta(V)$ depends, in turn, on the refractive indices of the various layers in the device. Thus, if there are M layers, the $\Delta\beta$ can be written as

$$\Delta\beta(V) \cong \left(\frac{\partial\beta}{\partial n_1}\right)\Delta n_1(E_1) + \left(\frac{\partial\beta}{\partial n_2}\right)\Delta n_2(E_2) + \dots + \left(\frac{\partial\beta}{\partial n_M}\right)\Delta n_M(E_M) \quad (1.5)$$

where the right hand side represents the linear terms of a Taylor's expansion. As the Δn s are small, this approximation is regarded as adequate. The above equation can be written more compactly as

$$\Delta\beta(V) = \sum_{i=1}^M \left(\frac{\partial\beta}{\partial n_i}\right)\Delta n_i(E_i) \quad (1.6)$$

where E_i is the field in the i th layer due to an applied voltage V . The $\Delta n_i(E_i)$ is the change in the refractive index of the i th layer due to a field E_i . In order to get Eq. (1.6) into a more desirable form, it is divided into two sums as

$$\Delta\beta(V) = \sum_{j=1}^{M_1} \left(\frac{\partial\beta}{\partial n_j}\right)\Delta n_j(E_j) + \sum_{k=1}^{M_2} \left(\frac{\partial\beta}{\partial n_k}\right)\Delta n_k(E_k) \quad (1.7)$$

where the first sum covers only the GaAs quantum wells and M_1 is the number of wells. The second sum represents the other layers which are not wells and obviously $M_1 + M_2 = M$. The first sum in the equation contains the term $\Delta n_j(E_j)$ which is the change in refractive index of the quantum well. This can be related to the electro-optic coefficients by

$$\Delta n_j = -\frac{1}{2}n_Q^3 s_Q E_j^2 + \Delta n_{fc}, \quad (1.8)$$

where the subscript Q refers to the quantum well and n_Q is the refractive index. The s does not carry the subscript j as they are assumed to be the same for all j . The Δn_{fc} is the change in the refractive index due to the presence of free carriers. This is important if any of the layers were not fully depleted, as could occur if the doping were too high in the i -layers. This was important in our case as the unintentional doping in the i -layer was about $7 \times 10^{16} \text{cm}^{-3}$. The expression used for Δn_c was [4]

$$\Delta n_c = \frac{R_o \lambda^2}{2\pi n m_e} N_d, \quad (1.9)$$

Where N_d is the concentration of free carriers removed by the field. Values for n_B were obtained using the equations developed by Afromovitz [5]. Of course, we also need to know the refractive index n_Q , of the quantum wells, as a function of wavelength. For this, we used the analytic expression used by Sonek *et. al.* [6] for the dielectric constant

$$\epsilon(\omega) = \epsilon_{MQW}(\omega) + \sum_{z=1}^2 4\pi\beta\omega_z^2 / (\omega_z^2 - \omega^2 - i\omega\Gamma_z) \quad (1.10)$$

where ϵ_{MQW} is the background dielectric constant of the quantum wells without the presence of the exciton. The ω_z are the exciton frequencies (hh, lh) and the Γ_z are the corresponding exciton linewidths. For TM polarization only the electron-light hole exciton is present. The derivatives ($\partial\beta/\partial n$) are assessed numerically using a program which calculates the properties of the propagating modes in the waveguides. Finally, the E versus V relation was calculated by solving Poisson's equation numerically for the given geometry and doping profile of the multi-layer structure.

Continuing, using Eq. (1.8) in Eq.(1.7) we get

$$\Delta\beta(V) = C_1 s_Q + C_2 = \phi(V)/L, \quad (1.11)$$

where

$$C_1 = -\frac{1}{2}n_Q^3 \sum_{j=1}^{M_1} \left(\frac{\partial \beta}{\partial n_Q} \right)_j E_j^2 \quad (1.12)$$

$$C_2 = \sum_{k=1}^{M_2} \left(\frac{\partial \beta}{\partial n_k} \right)_k \Delta n_k(E_k) + \sum_{i=1}^M \left(\frac{\partial \beta}{\partial n_i} \right)_k (\Delta n_{fc})_i \quad (1.13)$$

We are now in a position to solve for s_Q of the quantum well. Using Eq. (1.11), a linear least-square error fit to the data $\phi(V)$ yields the desired quantities.

1.6 Results

Figure (1.5) shows the calculated quadratic electro-optic coefficient s_{33} as a function of wavelength for both the $[-1,1,0]$ and the $[1,1,0]$ orientations. We see a difference between the two orientations and that the difference decreases as the wavelength increases. It is clear that s_{33} is large compared to that of bulk materials based devices by roughly more than one order of magnitude. This makes the quantum well based devices more attractive. Even though the absorption may be high in this spectral region (≈ 50 meV from edge) the high s_{33} allows for very short modulator lengths which might make the effects of absorption tolerable. This is especially important for integration of the laser and modulator on the same wafer. In the simpler schemes, the laser and modulator would have the same absorption edge and generally the lasing would be about 40 meV below the edge, which might be a wavelength where a sufficiently short phase modulator could function without too much loss or intensity modulation. This will however, be limited to digital modulation schemes due to the quadratic nature of the modulation. Also, we note the rapid decrease of s_{33} as we go away from the absorption edge.

We have also plotted the quadratic electrooptic coefficient versus detuning from the exciton fundamental absorption edge in meV for both polarizations on the same graph for the sake of comparison, figure (1.6) shows the result. For TE polarized light, the quadratic electrooptic coefficient involved is the s_{13} (see appendix A), while for TM polarized light s_{33} is the coefficient involved as previously indicated. s_{13} was measured in [3], s_{13} and s_{33} are equal in magnitude at some 90 meV away from the exciton fundamental absorption edge. Closer to the exciton absorption edge, $s_{13}(\lambda)$ is greater than $s_{33}(\lambda)$. The reason for that is the Quantum Confined Stark Effect (QCSE) is stronger in the TE polarized light case because both the e-hh and e-lh transitions are allowed, however, for TM polarization quantum mechanical selection rules forbid the e-hh transition. Since the e-hh transition occurs at a larger wavelength, the absorption edge for TE polarized light is closer than that for TM polarized light (the hh exciton position is at 830 nm, while the lh exciton resonance occurs at 820 nm), this translates to a larger quadratic electrooptic coefficient ($s_{13} > s_{33}$), and consequently a larger electrorefraction results in the TE polarization.

The fact that the rate of decrease of the quadratic electrooptic coefficient is different for different polarizations makes it possible to design modulators which depend only moderately on polarization, an important consideration in the design and operation of fiber optic communication systems.

Also, the change in refractive index as a function of the electric field for different wavelengths was calculated. Figure (1.7) shows the result. The calculation of $\Delta n(\lambda, E)$ is based on

$$\Delta n(\lambda, E) = -\frac{1}{2}n_Q^3 s_{33} E^2 \quad (1.14)$$

1.7 Conclusion

The wavelength dependence of the quadratic electro-optic coefficient s_{33} has been measured near the band edge for QW structures for a TM polarized light. This was obtained by measurement of the phase changes induced in a waveguide structure by an applied electric field using interferometric techniques. The results indicates that the s_{33} shows a dramatic increase near the edge.

We have discussed the utilization of the large quadratic coefficient for digital phase modulator integration with a laser.

We have also shown a comparison between the values of the quadratic electrooptic coefficient in both TE and TM polarizations. Results show that s_{13} is larger than s_{33} , and that it decreases faster.

We have also presented a set of data curves for the Δn as a function of applied field with wavelength as parameter as an aid to modulator design and operational characteristics evaluation.

1.8 Appendix A

In this Appendix we determine the non zero elements of the electro-optic tensor that are involved in our measurements.

1.8.1 The electro-optic effect in zincblend type crystals

In certain types of crystals, the application of an electric field results in a change in both the dimensions and orientation of the index ellipsoid. This is referred to as the electro-optic effect.

The propagation of optical radiation in a crystal can be described completely in terms of the impermeability tensor η_{ij} ($\eta = \epsilon_0 \epsilon^{-1}$). The two directions of polarization as well as their corresponding indices of refraction can be found by using the index ellipsoid which assumes its simplest form in the principal coordinate system:

$$\eta_1 x^2 + \eta_2 y^2 + \eta_3 z^2 = 1 \quad (1.15)$$

where x, y, z are the principal axes, that is the directions in the crystal along which \mathbf{D} and \mathbf{E} are parallel ($\mathbf{D} \parallel \mathbf{E}$). $\eta_1 = \frac{1}{n_x^2}$, $\eta_2 = \frac{1}{n_y^2}$ and $\eta_3 = \frac{1}{n_z^2}$ are the principal values of the impermeability tensor η_{ij} . In the unperturbed zincblend crystal, due to its cubic symmetry, the index ellipsoid is a sphere, thus $\eta_1 = \eta_2 = \eta_3 = \frac{1}{n_o^2}$

According to the quantum theory of solids, the optical dielectric impermeability tensor depends on the distribution of charges in the crystal. The application of an electric field will result in a redistribution of the bond charges and possibly a slight deformation of the ion lattice. The net result is a change in the optical

impermeability tensor. The electro-optic coefficients are defined traditionally as:

$$\eta_{ij}(E) - \eta_{ij}(0) = \Delta\eta_{ij} = r_{ijk}\mathbf{E}_k + s_{ijkl}\mathbf{E}_k\mathbf{E}_l \quad (1.16)$$

where \mathbf{E} is the applied electric field, r_{ijk} is the linear (or Pockels) electro-optic coefficient and s_{ijkl} is the quadratic (or Kerr) electro-optic coefficient.

1.8.2 Zincblend Crystal Structure

It can be viewed as two fcc structures displaced from each other by $1/4$ of a body diagonal. About each atom, there are 4 equally distant atoms of the opposite kind arranged at the corners of a regular tetrahedron. In crystallography, different structures are grouped into families. The zincblend type crystals belong to the family $\bar{4}3m$. Very shortly we explain what it means and how this grouping helps identify the non zero elements in the linear and quadratic electro-optic coefficient-tensors.

1.8.3 Perturbed Index Ellipsoid

Applying an electric field \mathbf{E} to a crystal changes the dimensions and the orientation of the index ellipsoid and makes it to deviate from equation (1.15) due to the appearance of mixed terms. The most general form of an index ellipsoid in the presence of an applied electric field is given by the quadratic form:

$$\eta_{ij}(E)x_i x_j = 1 \quad (1.17)$$

which can be written as:

$$\eta_{11}x_1^2 + \eta_{12}x_1x_2 + \eta_{13}x_1x_3 + \eta_{21}x_2x_1 + \eta_{22}x_2^2 + \eta_{23}x_2x_3 + \eta_{31}x_3x_1 + \eta_{32}x_3x_2 + \eta_{33}x_3^2 = 1 \quad (1.18)$$

in the above equations $i, j = 1, 2$ and 3 refer to the $x, y,$ and z axes respectively. In this case, x, y and z are not the principal axes any more. It can be easily shown [7] that the dielectric tensor ϵ_{ij} is a symmetric tensor provided that the medium is lossless and optically inactive, i.e. $\epsilon_{ij} = \epsilon_{ji}$. According to the definition of η_{ij} we conclude that η_{ij} must also be a symmetric tensor, hence $\eta_{ij} = \eta_{ji}$. Consequently, the indices i and j can be permuted and (1.18) can be written as:

$$\eta_{11}x^2 + \eta_{22}y^2 + \eta_{33}z^2 + 2\eta_{23}yz + 2\eta_{31}zx + 2\eta_{12}xy = 1 \quad (1.19)$$

Note that when the electric field vanishes, the index ellipsoid (1.19) reduces to (1.15). We are now going to use the standard contracted index notation which is the replacement of the double subscript by a single one. It is important to remember that the contraction of indices is just a matter of convenience. In this customary notation:

$$\begin{aligned} 11 &\longrightarrow 1 \\ 22 &\longrightarrow 2 \\ 33 &\longrightarrow 3 \\ 23, 32 &\longrightarrow 4 \\ 13, 31 &\longrightarrow 5 \\ 12, 21 &\longrightarrow 6 \end{aligned} \quad (1.20)$$

In this sense, in (1.19):

$$\begin{aligned}
 \eta_{11} &= \eta_1 + \Delta\eta_1 \\
 \eta_{22} &= \eta_2 + \Delta\eta_2 \\
 \eta_{33} &= \eta_3 + \Delta\eta_3 \\
 \eta_{23} &= \Delta\eta_4 \\
 \eta_{31} &= \Delta\eta_5 \\
 \eta_{12} &= \Delta\eta_6
 \end{aligned}
 \tag{1.21}$$

If we look at equation(1.16) we can figure out the dimension of the electro-optic tensor. For instance, the dimension of r_{ijk} will be 6×3 (6 is the number of repeated or contracted indices and 3 is the possible combinations for the direction of the electric field E_k which are E_x, E_y and E_z). Similarly the dimension of s_{ijkl} is 6×6 (again 6 is the number of contracted indices and the other 6 is the number of possible combinations for the direction of the electric field $E_k E_l$ which are: $E_x^2, E_y^2, E_z^2, E_y E_z, E_x E_x,$ and $E_x E_y$). So,

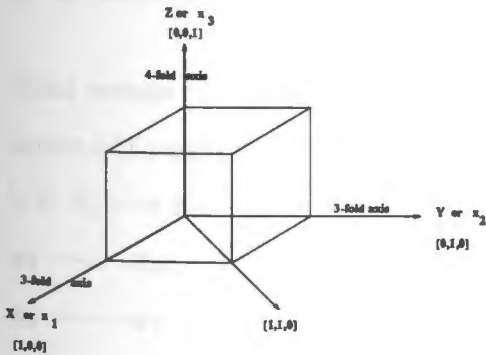
$$\begin{aligned}
 \Delta\eta_{ij} &= \eta_{ij}(E) - \eta_{ij}(0) \\
 &= r_{ijk}E_k + s_{ijkl}E_k E_l
 \end{aligned}$$

can be written in the form:

$$\begin{aligned}
 \Delta\eta_{ij} = & \begin{bmatrix} r_{11} & r_{12} & r_{13} \\ r_{21} & r_{22} & r_{23} \\ r_{31} & r_{32} & r_{33} \\ r_{41} & r_{42} & r_{43} \\ r_{51} & r_{52} & r_{53} \\ r_{61} & r_{62} & r_{63} \end{bmatrix} \times \begin{bmatrix} E_x \\ E_y \\ E_z \end{bmatrix} \\
 & + \begin{bmatrix} s_{11} & s_{12} & s_{13} & s_{14} & s_{15} & s_{16} \\ s_{21} & s_{22} & s_{23} & s_{24} & s_{25} & s_{26} \\ s_{31} & s_{32} & s_{33} & s_{34} & s_{35} & s_{36} \\ s_{41} & s_{42} & s_{43} & s_{44} & s_{45} & s_{46} \\ s_{51} & s_{52} & s_{53} & s_{54} & s_{55} & s_{56} \\ s_{61} & s_{62} & s_{63} & s_{64} & s_{65} & s_{66} \end{bmatrix} \times \begin{bmatrix} E_x^2 \\ E_y^2 \\ E_z^2 \\ E_y E_x \\ E_z E_x \\ E_x E_y \end{bmatrix}
 \end{aligned} \tag{1.22}$$

1.8.4 Symmetry Properties in Zincblend

As mentioned earlier, the zincblend type crystals belong to the group of point symmetry $\bar{4}3m$. This group has four-fold (90°) rotation axis with inversion symmetry which is, by strict convention, taken as the z-axis, as well as two mutually orthogonal three-fold (120°) rotation axes of symmetry that lie in the plane normal to z. These are designated as the x and y axes. From these two rotation axes,



we can identify the non zero elements in the $[r]$ and $[s]$ tensors. If we consider MQW structures based on III-V material compounds (which have a zincblend type structure), because of the quantum wells, the symmetry is reduced in the z -direction due to the non infinite extent of the crystal lattice in that direction. This reduced symmetry makes the two mutually orthogonal 3-fold rotation axes no longer 3-fold but rather 2-fold (180°) or diad axes, hence, the group will be called $(\bar{4}2m)$ instead of $(\bar{4}3m)$.

If we denote the axes of rotation x , y and z by x_1 , x_2 and x_3 , the 2-fold or diad axes could be x_1 or x_2 and the 4-fold inversion rotation axis is always x_3 .

1.8.5 The Linear Electro-optic Coefficient $[r_{ijk}]$

$$[r] = \begin{bmatrix} r_{11} & r_{12} & r_{13} \\ r_{21} & r_{22} & r_{23} \\ r_{31} & r_{32} & r_{33} \\ r_{41} & r_{42} & r_{43} \\ r_{51} & r_{52} & r_{53} \\ r_{61} & r_{62} & r_{63} \end{bmatrix} = \begin{bmatrix} r_{111} & r_{112} & r_{113} \\ r_{221} & r_{222} & r_{223} \\ r_{331} & r_{332} & r_{333} \\ r_{231} & r_{232} & r_{233} \\ r_{311} & r_{312} & r_{313} \\ r_{121} & r_{122} & r_{123} \end{bmatrix} \quad (1.23)$$

a. Rotation Around the diad axis $\parallel x_1$

Diad means rotation by $\frac{2\pi}{2} = 180^\circ$, it is easy to see that if we rotate by 180° around the axis x_1 , the coordinates of a general point P_{x_1, x_2, x_3} will be $P_{x_1, -x_2, -x_3}$,

$$i. e. x_1 \longrightarrow x_1,$$

$$x_2 \longrightarrow -x_2,$$

$$x_3 \longrightarrow -x_3$$

or simply:

$$1 \longrightarrow 1, 2 \longrightarrow -2, 3 \longrightarrow -3 \quad (1.24)$$

If we use this rule in (1.23) to operate on the subscripts of the linear electrooptic coefficient r_{ijk} , and using the fact that if $r_{ijk} = -r_{ijk}$, then this means that $r_{ijk} = 0$. We have:

$$\begin{aligned} r_{111} &\longrightarrow r_{111} \\ r_{112} &\longrightarrow -r_{112} \longrightarrow r_{112} = 0 \\ r_{113} &\longrightarrow -r_{113} \longrightarrow r_{113} = 0 \\ r_{221} &\longrightarrow r_{221} \\ r_{222} &\longrightarrow -r_{222} \longrightarrow r_{222} = 0 \\ r_{331} &\longrightarrow r_{331} \\ r_{332} &\longrightarrow -r_{332} \longrightarrow r_{332} = 0 \\ r_{333} &\longrightarrow -r_{333} \longrightarrow r_{333} = 0 \\ r_{231} &\longrightarrow r_{231} \\ r_{232} &\longrightarrow -r_{232} \longrightarrow r_{232} = 0 \\ r_{233} &\longrightarrow -r_{233} \longrightarrow r_{233} = 0 \\ r_{311} &\longrightarrow -r_{311} \longrightarrow r_{311} = 0 \\ r_{312} &\longrightarrow r_{312} \\ r_{313} &\longrightarrow r_{313} \\ r_{121} &\longrightarrow -r_{121} \longrightarrow r_{121} = 0 \\ r_{122} &\longrightarrow r_{122} \\ r_{123} &\longrightarrow r_{123} \end{aligned}$$

(i. e.) we are left with 8 non zero elements so far and we have:

$$r = \begin{bmatrix} r_{111} & 0 & 0 \\ r_{221} & 0 & 0 \\ r_{331} & 0 & 0 \\ r_{231} & 0 & 0 \\ 0 & r_{312} & r_{313} \\ 0 & r_{122} & r_{123} \end{bmatrix} \quad (1.25)$$

In the previous part, there was a quicker way to deduce (1.25) from (1.23) by inspection. Since the diad axis was x_1 , then all elements in (1.23) that have either: no 1's or two 1's will be zero elements.

b. Rotation around the 4-fold inversion axis $\parallel x_3$

We use the fact that the 4-fold inversion axis x_3 includes 2-fold or diad axis. We can follow a formal procedure similar to that of the previous section regarding the rotation around the diad axis. Namely, P_{x_1, x_2, x_3} will be $P_{-x_1, -x_2, x_3}$ after 180° rotation around x_3 . Alternatively, we use a quick rule analogous to that of the previous section, all elements that have either no 3's or two 3's will be zero elements. If we look at (1.25) one finds that:

$$r_{111} = r_{221} = r_{331} = r_{313} = r_{122} = 0 \quad (1.26)$$

now we will be left with:

$$r = \begin{bmatrix} 0 & 0 & 0 \\ 0 & 0 & 0 \\ 0 & 0 & 0 \\ r_{231} & 0 & 0 \\ 0 & r_{312} & 0 \\ 0 & 0 & r_{123} \end{bmatrix} \quad (1.27)$$

Furthermore, when the losses are neglected we have $\epsilon_{ij} = \epsilon_{ji}$, this means $r_{ijk} = r_{kij}$, so we have $r_{231} = r_{312}$. In the contracted index notation $23 = 32 = 4$, $31 = 13 = 5$ and $12 = 21 = 6$, so $r_{231} = r_{41}$ and $r_{312} = r_{52}$, and hence we have

$$r_{231} = r_{312} = r_{41} \quad (1.28)$$

$$r = \begin{bmatrix} 0 & 0 & 0 \\ 0 & 0 & 0 \\ 0 & 0 & 0 \\ r_{41} & 0 & 0 \\ 0 & r_{41} & 0 \\ 0 & 0 & r_{63} \end{bmatrix} \quad (1.29)$$

(1.29) differs from the bulk case ($\bar{4}3m$ point group symmetry). In the bulk case, $r_{41} = r_{63}$. In other words, any of the three principal axes can be chosen as the z-axis and the resulting change in the refractive index would be the same. This is obviously not true for quantum well structures. An applied field parallel to the layers would produce results dramatically different from one applied perpendicular to them.

1.8.6 The Quadratic Electro-optic Coefficient $[s_{ijkl}]$

$$\begin{aligned}
 [s] &= \begin{bmatrix} s_{11} & s_{12} & s_{13} & s_{14} & s_{15} & s_{16} \\ s_{21} & s_{22} & s_{23} & s_{24} & s_{25} & s_{26} \\ s_{31} & s_{32} & s_{33} & s_{34} & s_{35} & s_{36} \\ s_{41} & s_{42} & s_{43} & s_{44} & s_{45} & s_{46} \\ s_{51} & s_{52} & s_{53} & s_{54} & s_{55} & s_{56} \\ s_{61} & s_{62} & s_{63} & s_{64} & s_{65} & s_{66} \end{bmatrix} \\
 &= \begin{bmatrix} s_{1111} & s_{1122} & s_{1133} & s_{1123} & s_{1131} & s_{1112} \\ s_{2211} & s_{2222} & s_{2233} & s_{2223} & s_{2231} & s_{2212} \\ s_{3311} & s_{3322} & s_{3333} & s_{3323} & s_{3331} & s_{3312} \\ s_{2311} & s_{2322} & s_{2333} & s_{2323} & s_{2331} & s_{2312} \\ s_{3111} & s_{3122} & s_{3133} & s_{3123} & s_{3131} & s_{3112} \\ s_{1211} & s_{1222} & s_{1233} & s_{1223} & s_{1231} & s_{1212} \end{bmatrix} \quad (1.30)
 \end{aligned}$$

a. Rotation around the diad axis $\parallel x_1$

$$x_1 \longrightarrow x_1, \quad x_2 \longrightarrow -x_2, \quad x_3 \longrightarrow -x_3$$

We can follow the same procedure outlined earlier for determining the $[r_{ij}]$ tensor, however we can use a quicker technique to identify the zero elements by inspection. For the $[s_{ijkl}]$ with diad rotation around x_1 , all terms that have one 1 or three 1's are zero elements so we will end up with

$$[s_{ijkl}] = \begin{bmatrix} s_{1111} & s_{1122} & s_{1133} & s_{1123} & 0 & 0 \\ s_{2211} & s_{2222} & s_{2233} & s_{2223} & 0 & 0 \\ s_{3311} & s_{3322} & s_{3333} & s_{3323} & 0 & 0 \\ s_{2311} & s_{2322} & s_{2333} & s_{2323} & 0 & 0 \\ 0 & 0 & 0 & 0 & s_{3131} & s_{3112} \\ 0 & 0 & 0 & 0 & s_{1231} & s_{1212} \end{bmatrix} \quad (1.31)$$

b. Rotation around the 4-fold inversion axis $\parallel x_3$

Since the 4-fold inversion axis has diad axis included in it, we use the same rule as above: all terms that either have one 3 or three 3's are zero elements, so we will have:

$$[s_{ijkl}] = \begin{bmatrix} s_{1111} & s_{1122} & s_{1133} & 0 & 0 & 0 \\ s_{2211} & s_{2222} & s_{2233} & 0 & 0 & 0 \\ s_{3311} & s_{3322} & s_{3333} & 0 & 0 & 0 \\ 0 & 0 & 0 & s_{2323} & 0 & 0 \\ 0 & 0 & 0 & 0 & s_{3131} & 0 \\ 0 & 0 & 0 & 0 & 0 & s_{1212} \end{bmatrix} \quad (1.32)$$

It is easy to figure out the transformation rule for a point P_{x_1, x_2, x_3} that rotates around a 4-fold inversion axis $\parallel x_3$ as we have done that for a diad axis. We find that:

$$x_1 \longrightarrow -x_2, \quad x_2 \longrightarrow x_1, \quad x_3 \longrightarrow -x_3$$

or simply:

$$1 \rightarrow -2, \quad 2 \rightarrow 1, \quad 3 \rightarrow -3 \quad (1.33)$$

Hence,

$$\begin{array}{lll}
 s_{1111} \rightarrow s_{2222} & \text{call both} & s_{11} \\
 s_{1122} \rightarrow s_{2211} & \text{call both} & s_{12} \\
 s_{1133} \rightarrow s_{2233} & \text{call both} & s_{13} \\
 s_{3311} \rightarrow s_{3322} & \text{call both} & s_{31} \\
 s_{3333} \rightarrow s_{3333} & \text{call it} & s_{33} \\
 s_{2323} \rightarrow s_{1313} = s_{3131} & \text{call both} & s_{44} \\
 s_{1212} \rightarrow s_{2121} = s_{1212} & \text{call it} & s_{66}
 \end{array} \quad (1.34)$$

So finally we end up with $[s_{ij}]$ in the contracted index notation as:

$$[s_{ij}] = \begin{bmatrix} s_{11} & s_{12} & s_{13} & 0 & 0 & 0 \\ s_{12} & s_{11} & s_{13} & 0 & 0 & 0 \\ s_{31} & s_{31} & s_{33} & 0 & 0 & 0 \\ 0 & 0 & 0 & s_{44} & 0 & 0 \\ 0 & 0 & 0 & 0 & s_{44} & 0 \\ 0 & 0 & 0 & 0 & 0 & s_{66} \end{bmatrix} \quad (1.35)$$

Again this differs from the bulk case. It can be shown that in the bulk case we have, $s_{33} = s_{11}$, $s_{66} = s_{44}$, and $s_{13} = s_{31} = s_{12}$.

For a polarizing field perpendicular to the (0,0,1) plane, i. e. $E = E_z$, $E_x = E_y = 0$, we substitute (1.35) and (1.29) into (1.22) we get:

$$\begin{aligned}
\Delta\eta_{11} &= \Delta\eta_1 = s_{13}E_z^2 \\
\Delta\eta_{22} &= \Delta\eta_2 = s_{13}E_z^2 \\
\Delta\eta_{33} &= \Delta\eta_3 = s_{33}E_z^2 \\
\Delta\eta_{23} &= \Delta\eta_4 = 0 \\
\Delta\eta_{31} &= \Delta\eta_5 = 0 \\
\Delta\eta_{12} &= \Delta\eta_6 = r_{63}E_z
\end{aligned} \tag{1.36}$$

Substituting the $\Delta\eta_{ij}$'s (1.36) in (1.21) and the result into (1.19), one gets the following perturbed index ellipsoid equation:

$$(\eta_1 + s_{13}E_z^2)x^2 + (\eta_2 + s_{13}E_z^2)y^2 + (\eta_3 + s_{33}E_z^2)z^2 + 2(r_{63}E_z)xy = 1 \tag{1.37}$$

which can be written as:

$$\frac{x^2}{n_x^2} + \frac{y^2}{n_y^2} + \frac{z^2}{n_z^2} + 2xyr_{63}E_z = 1 \tag{1.38}$$

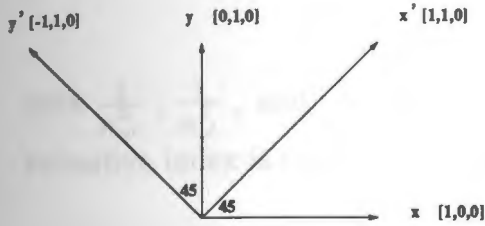
where:

$$\begin{aligned}
\frac{1}{n_x^2} &= \eta_1 + s_{13}E_z^2 = \frac{1}{n_o^2} + s_{13}E_z^2 \\
\frac{1}{n_y^2} &= \eta_2 + s_{13}E_z^2 = \frac{1}{n_o^2} + s_{13}E_z^2 \\
\frac{1}{n_z^2} &= \eta_3 + s_{33}E_z^2 = \frac{1}{n_o^2} + s_{33}E_z^2
\end{aligned} \tag{1.39}$$

where η_1 , η_2 , and η_3 (the principal values of the impermeability tensor) = $\frac{1}{n_o^2}$ since the index ellipsoid is a sphere in the unperturbed zincblend crystal.

Note that $\frac{1}{n_x^2} = \frac{1}{n_y^2}$ so we will call both $\frac{1}{n_x^2}$.

We now need to diagonalize (1.38). Due to the symmetrical appearance of x and y in (1.38) we chose the transform:



$$\begin{aligned}x &= x' \cos \theta - y' \sin \theta \\y &= x' \sin \theta + y' \cos \theta \\z &= z'\end{aligned}\tag{1.40}$$

where $\theta = \frac{\pi}{4}$, substitute (1.40) into (1.38):

$$\frac{(x' - y')^2}{2n_x^2} + \frac{(x' + y')^2}{2n_x^2} + \frac{z'^2}{n_x^2} + (x' - y')(x' + y')(r_{63}E_z) = 1\tag{1.41}$$

$$\text{or } x'^2 \left(\frac{1}{n_x^2} + r_{63}E_z \right) + y'^2 \left(\frac{1}{n_x^2} - r_{63}E_z \right) + \frac{z'^2}{n_x^2} = 1$$

If we put:

$$\begin{aligned}\frac{1}{n_x'^2} &= \frac{1}{n_x^2} + r_{63}E_z \\&= \frac{1}{n_o^2} + s_{13}E_z^2 + r_{63}E_z\end{aligned}$$

$$\text{and } \frac{1}{n_y'^2} = \frac{1}{n_o^2} + s_{13}E_z^2 - r_{63}E_z\tag{1.42}$$

$$\begin{aligned}\text{and } \frac{1}{n_z'^2} &= \frac{1}{n_x^2} \\&= \frac{1}{n_o^2} + s_{33}E_z^2\end{aligned}$$

This means that we have diagonalized (1.38) to the form:

$$\frac{x'^2}{n_{x'}^2} + \frac{y'^2}{n_{y'}^2} + \frac{z'^2}{n_{z'}^2} = 1 \quad (1.43)$$

with $\frac{1}{n_{x'}^2}$, $\frac{1}{n_{y'}^2}$, and $\frac{1}{n_{z'}^2}$, given by (1.42). If we assume that the change in the refractive index is small compared to n_o , we can use the differential relation:

$$d\left(\frac{1}{n^2}\right) = -\frac{2}{n^3} dn \quad (1.44)$$

apply (1.44) to (1.42) we get:

$$\begin{aligned} \Delta n_{x'} &= -\frac{1}{2}n_o^3 r_{63} E_z - \frac{1}{2}n_o^3 s_{13} E_z^2 \\ \Delta n_{y'} &= \frac{1}{2}n_o^3 r_{63} E_z - \frac{1}{2}n_o^3 s_{13} E_z^2 \\ \Delta n_{z'} &= -\frac{1}{2}n_o^3 s_{33} E_z^2 \end{aligned} \quad (1.45)$$

(1.45) are the final results of this analysis. It gives the change in the refractive index when the polarizing electric field is along the z-direction. We need to distinguish between the corresponding changes for different orientations of the crystal optical axes, and different polarizations of the optical electric field vector (TE & TM).

The table below illustrates this when the light is propagating along the $[-1, 1, 0]$ (y' direction) or the $[1, 1, 0]$ (x' direction) for both TE & TM polarizations.

direction of light propagation	optical field polarized along	corresponding Δn
$[-1, 1, 0]$	$[1, 1, 0]$ TE	$\Delta n_{x'}$
	$[0, 0, 1]$ TM	$\Delta n_{z'}$
$[1, 1, 0]$	$[-1, 1, 0]$ TE	$\Delta n_{y'}$
	$[0, 0, 1]$ TM	$\Delta n_{z'}$

where $\Delta n_{x'}$, $\Delta n_{y'}$, $\Delta n_{z'}$ are given by (1.45). In our configuration, for TM polarization, the optical field vector is polarized along the $[0,0,1]$ direction, i.e. normal to the QW layers. Therefore, the corresponding $\Delta n = \Delta n_{z'}$.

Excellent review of the basic material discussed in this appendix can be found in [7], [8], and [9].

References

- [1] S. Namba, "Electro-optical effects of zincblend", *J. Opt. Soc. Am.*, vol. 51, pp. 76-79, 1961.
- [2] W. R. Cook, Jr. and H. Jaffe in *Electro-optic Coefficients*, Vol. 11, New Series, Edited L. Bornstein, Springer, 1979.
- [3] G. T. Valliath, PhD thesis, URI, Dec. 1990.
- [4] J. Manning and R. Olshansky, "The carrier induced index change AlGaAs and 1.3 μm InGaAsP diode lasers", *IEEE J. of Quantum Electronics*, vol. QE-19, pp. 1525-1530, 1983.
- [5] M. A. Afromovitz, "Refractive index of $\text{Ga}_{1-x}\text{Al}_x\text{As}$ ", *Solid State Commun.*, vol. 15, pp. 59-63, 1974.
- [6] G. J. Sonek, J. M. Ballantyne, Y. J. Chen, G. M. Carter, S. W. Brown, E. S. Koteles, and J. P. Salerno, "Dielectric properties of GaAs/AlGaAs multiple quantum well waveguides", *IEEE J. Quantum Electron.*, vol. QE-22, pp. 1015-1018, 1986.
- [7] A. Yariv and P. Yeh, *Optical Waves in Crystals*, Chap. 7, John Wiley, 1984.
- [8] J. F. Nye, *Physical Properties of Crystals*, Oxford University Press, 1957.
- [9] A. Yariv, *Quantum Electronics*, 2nd Ed., Wiley, 1975.

1.9 Figure captions

1.1- Cross section of the waveguide multiple quantum well structure used in measuring the quadratic electro-optic coefficient for TM polarization.

1.2- Block diagram of the experimental setup for measuring the quadratic electro-optic coefficient s_{33} .

1.3- Normalized measured interference pattern "F(V)", and transmitted light intensity "f(V)" for [-1,1,0] oriented device at 850 nm.

1.4- Normalized measured interference pattern "F(V)", and transmitted light intensity "f(V)" for [-1,1,0] oriented device at 875 nm.

1.5- Calculated quadratic electro-optic coefficient s_{33} versus wavelength. Solid line is for [-1,1,0] orientation, and dotted line is for [1,1,0] oriented device.

1.6- Comparison between the quadratic electro-optic coefficients s_{31} (TE) solid line and s_{33} (TM) dotted line, as a function of the detuning from the exciton absorption edge for the [-1,1,0] orientation.

1.7- Calculated change in refractive index Δn as a function of applied electric field for different values of wavelengths for the [-1,1,0] orientation.

Figure 1.1: Cross section of the waveguide multiple quantum well sample.

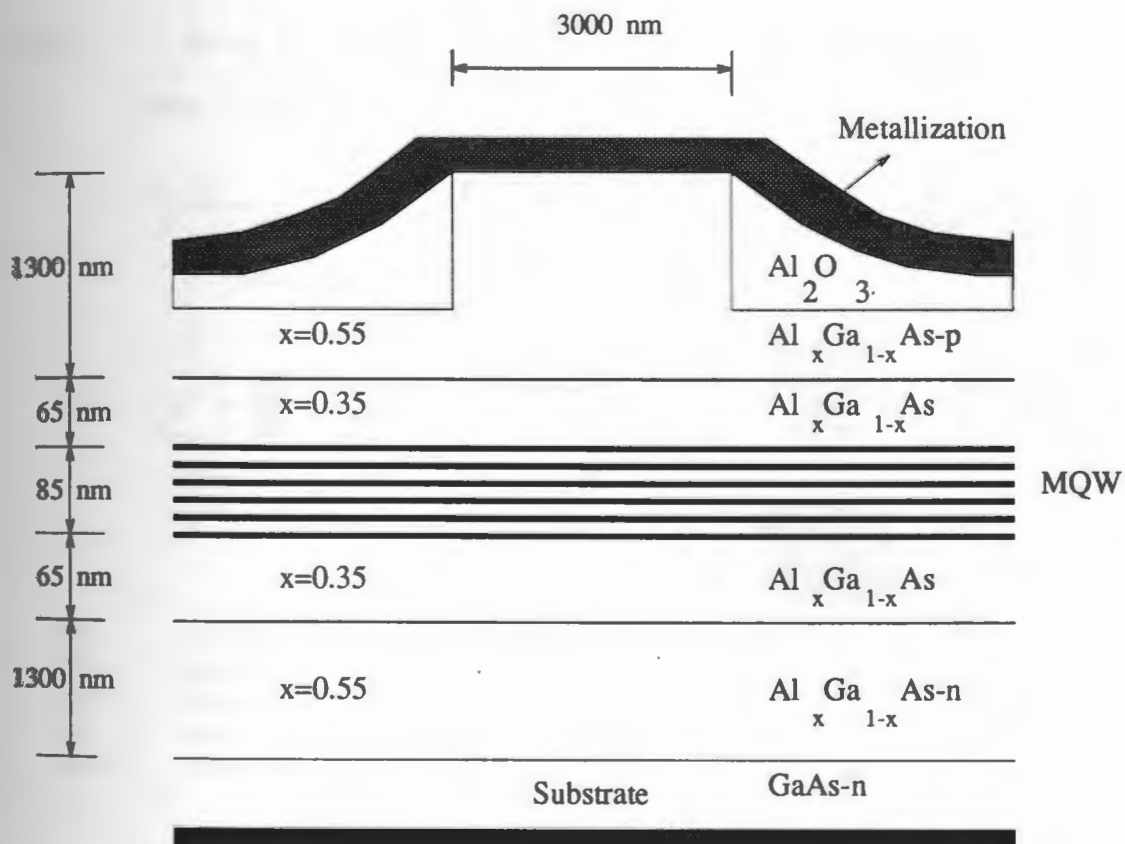


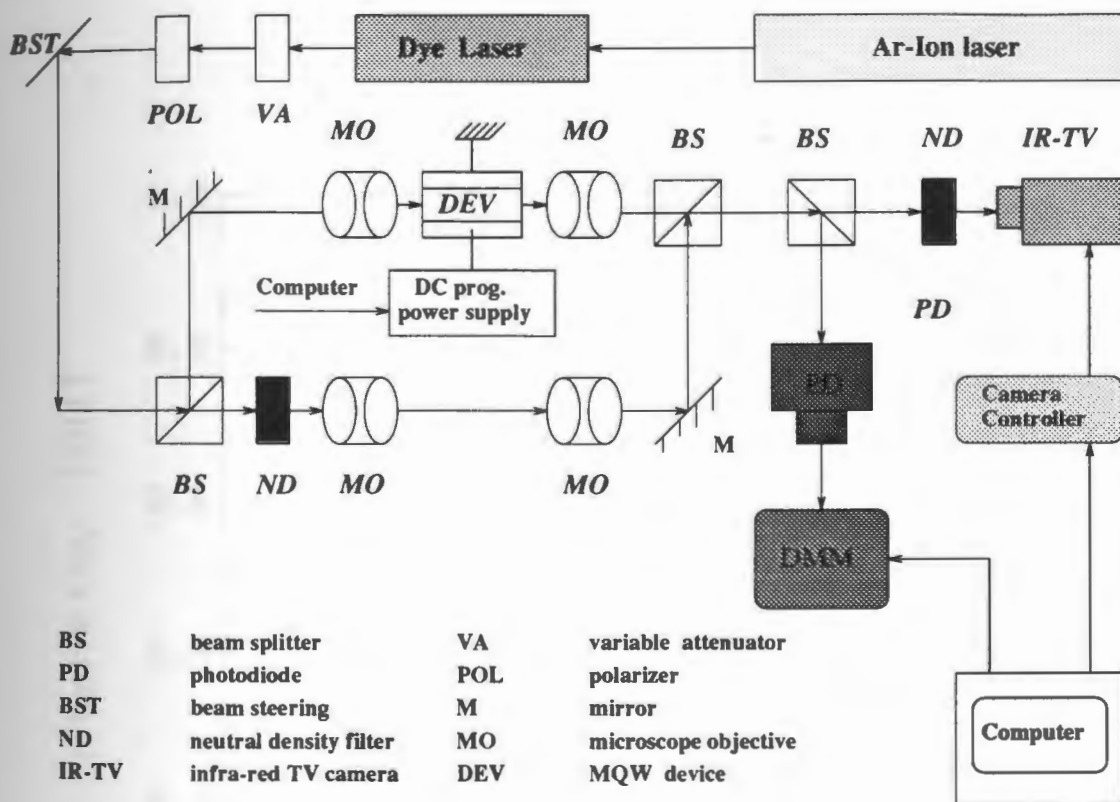
Figure 1.2: Block diagram of the experimental setup for measuring s_{33} .

Figure 1.3: Normalized measured interference pattern " $F(V)$ ", and transmitted light intensity " $f(V)$ " at 850 nm.

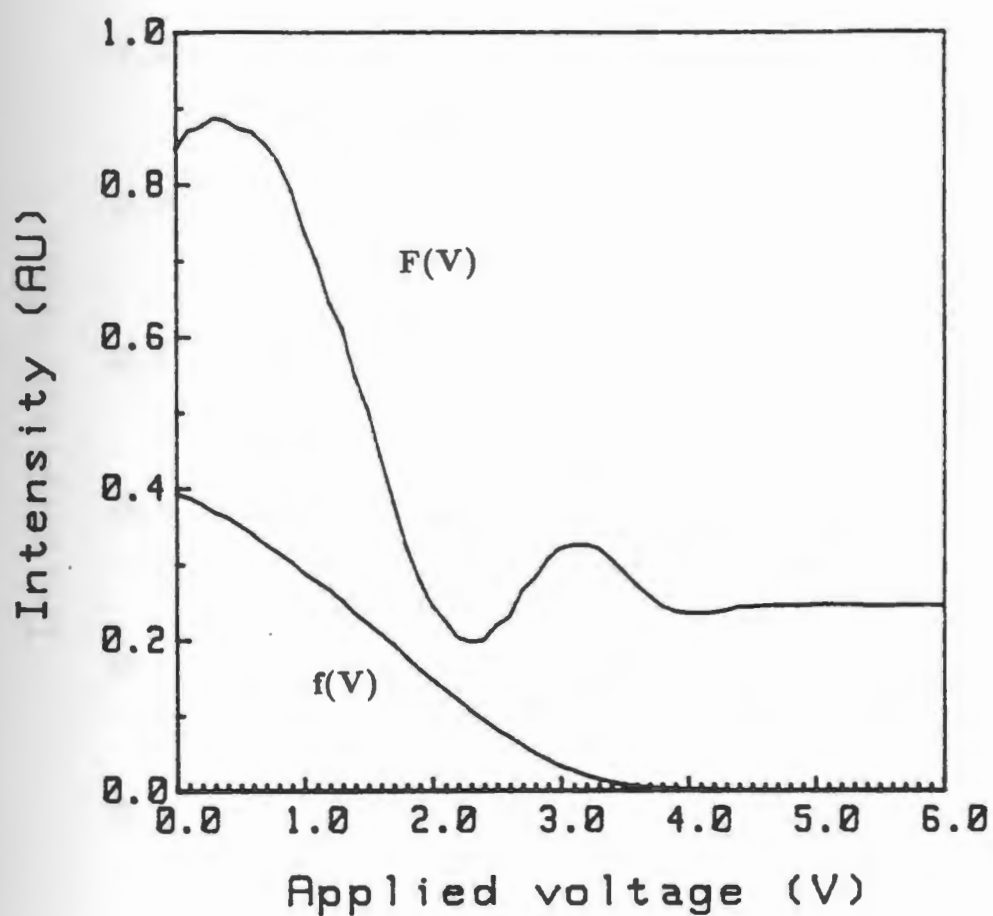


Figure 1.4: Normalized measured interference pattern " $F(V)$ ", and transmitted light intensity " $f(V)$ " at 875 nm.

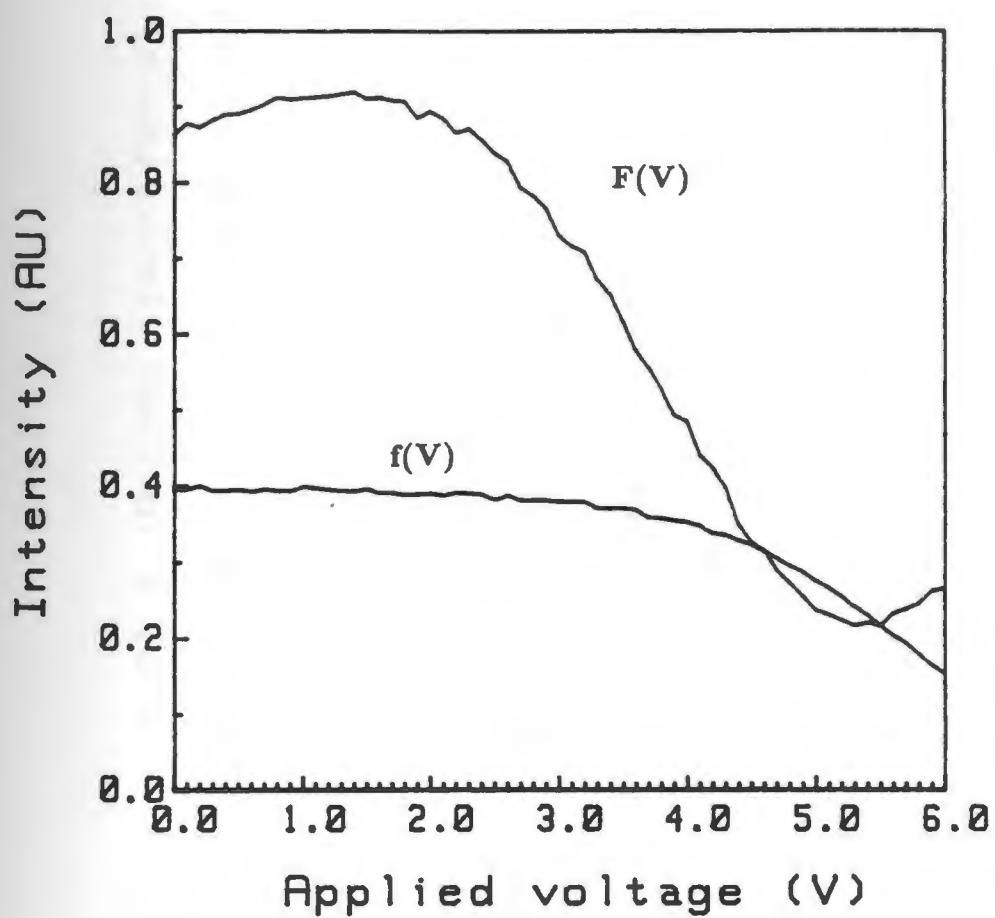


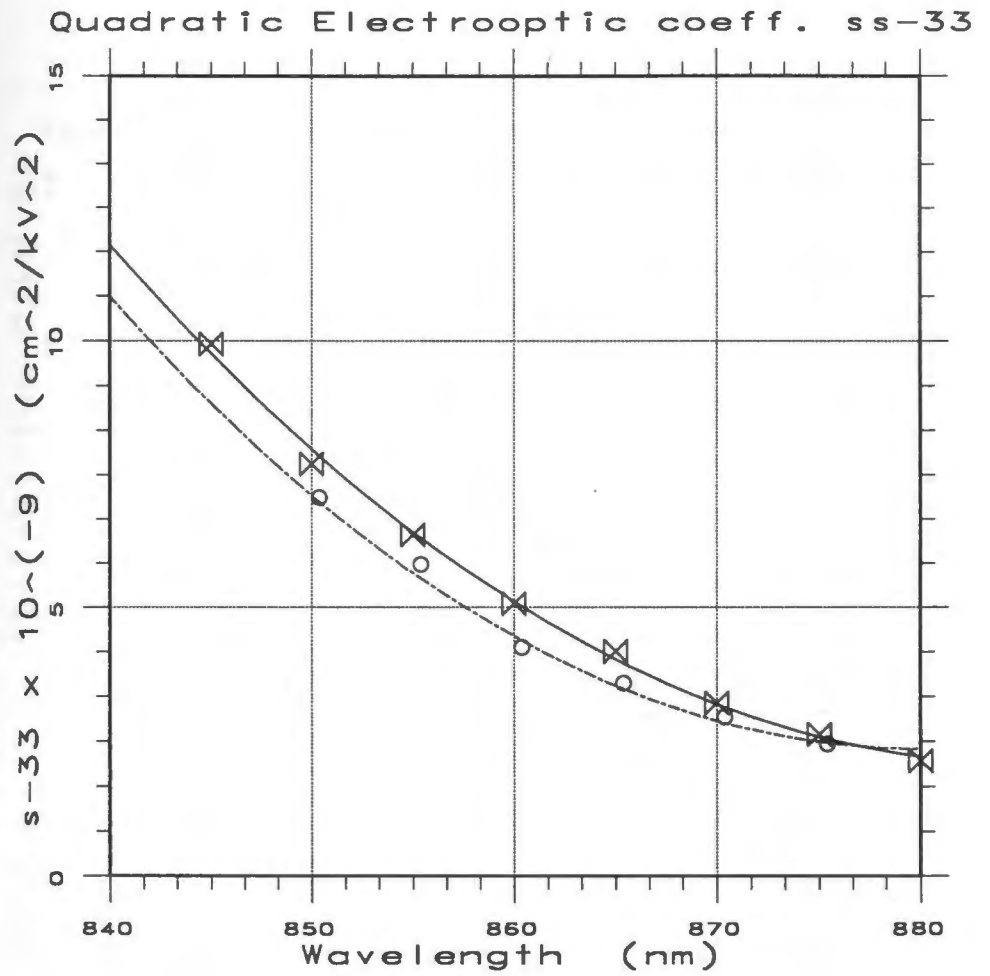
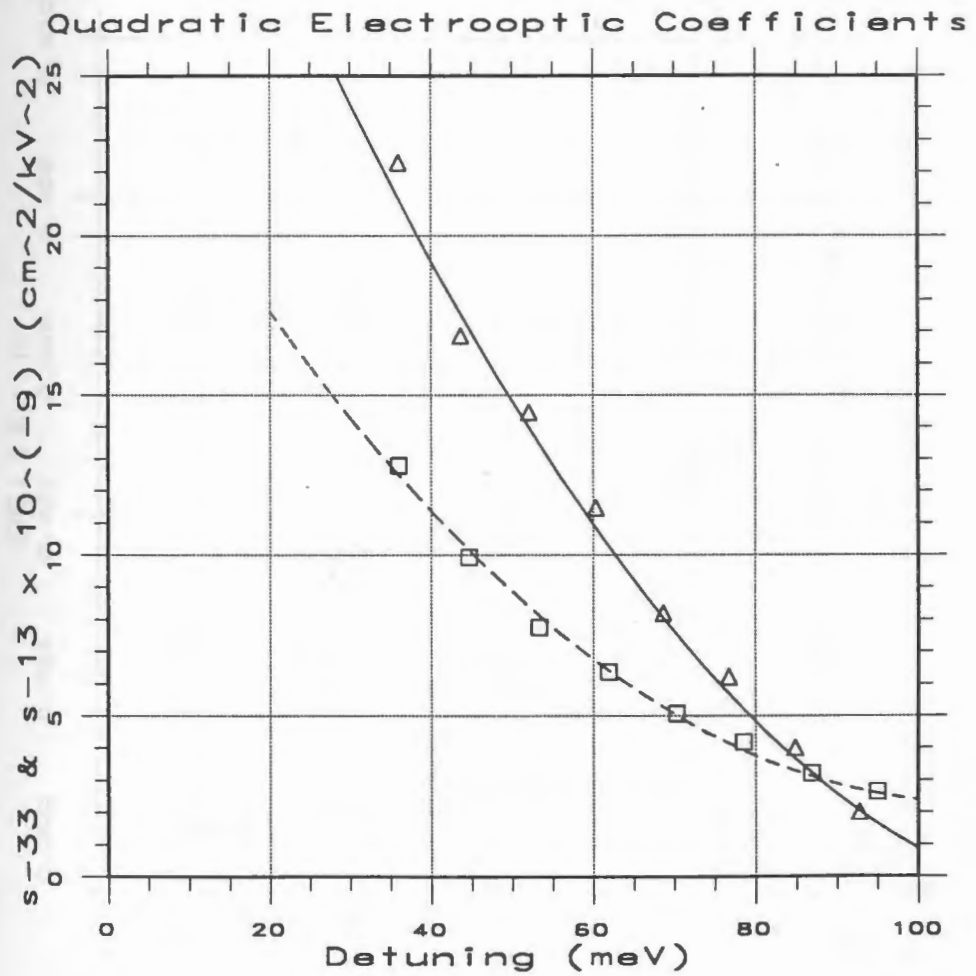
Figure 1.5: Calculated quadratic electro-optic coefficient s_{33} versus wavelength.

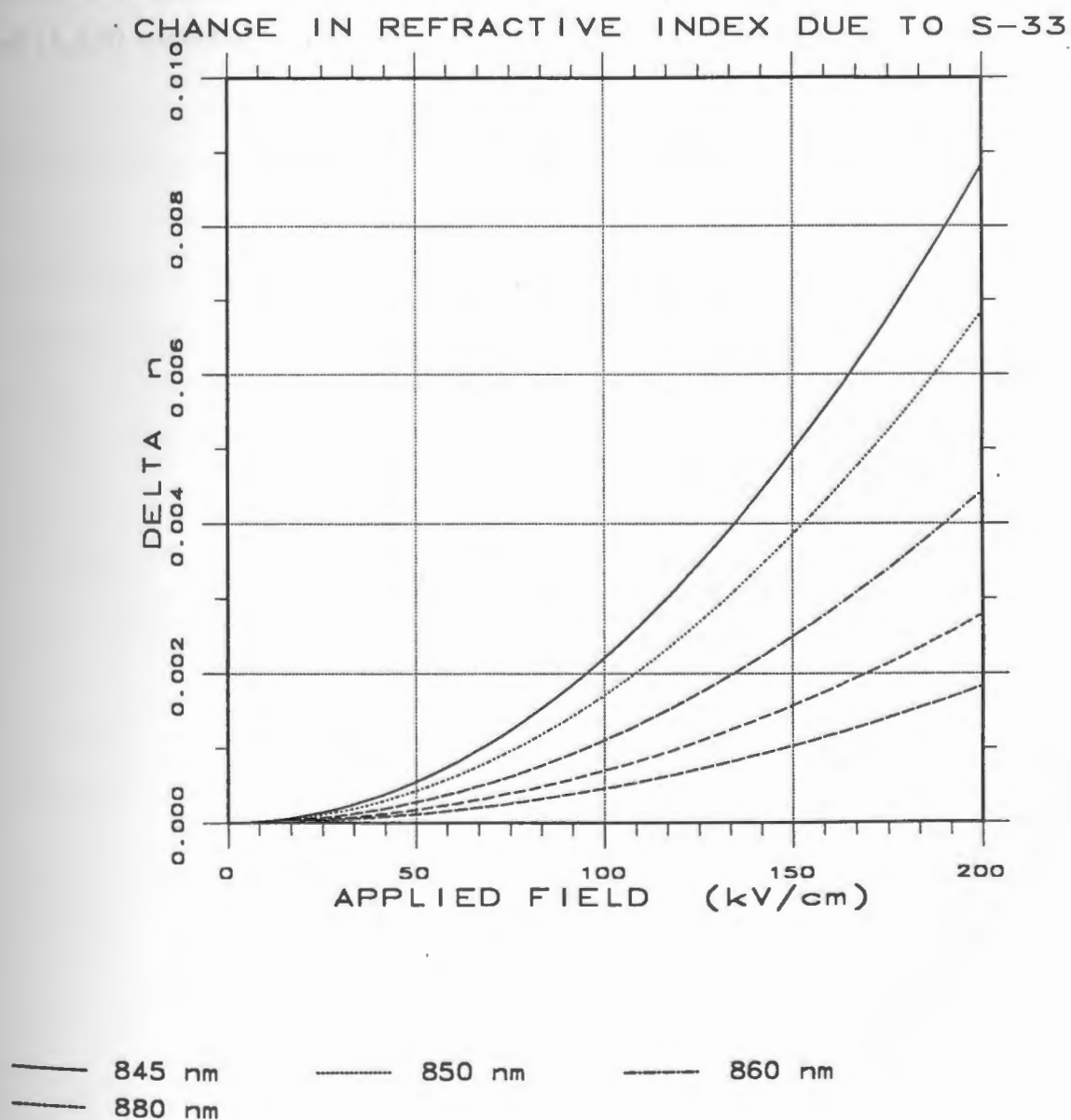
Figure 1.6: Comparison between the quadratic electro-optic coefficients s_{31} (TE) solid line and s_{33} (TM) dotted line as a function of the detuning from the exciton absorption edge for the $[-1,1,0]$ orientation.



□ □ □ s_{33}

△ △ △ s_{31}

Figure 1.7: Calculated change in refractive index Δn as a function of applied field for the $[-1,1,0]$ orientation.



Manuscript 2

Orientation dependence in the change of electroabsorption for [-1,1,0] and [1,1,0] oriented GaAs/AlGaAs multiple quantum well structures

ABSTRACT

We report on the

orientation dependence

of the electroabsorption

in the TM polarization

TITLE :

Orientation dependence in the change of electroabsorption for $[-1,1,0]$ and $[1,1,0]$ oriented GaAs/AlGaAs multiple quantum well structures

ABSTRACT :

We report experimental observation of orientation dependence in the change of electroabsorption (as much as a factor of 2 near the band edge) between $[-1,1,0]$ and $[1,1,0]$ oriented GaAs/AlGaAs MQW waveguide modulators for both TE and TM polarizations.

2.1 Introduction

In recent years the optical properties of multiple quantum wells (MQW) have been the subject of increasing interest. Because the excitonic absorption resonances are retained at room temperature in a QW, they have the potential for practical applications in electrooptic devices.

When an electric field is applied perpendicularly to the quantum well layers, the band edge shifts to lower photon energies while still retaining their excitonic features. This electroabsorptive effect has been called the Quantum Confined Stark effect [1], it is therefore particularly interesting both from a practical and fundamental viewpoint as it forms the basis of a variety of modulators and optical switching devices.

In the theoretical analysis of multiple quantum well structures (MQW's) [2], the wavefunction is usually separated into a Z-dependent and a transverse part, with the Z-part containing the features of the potential well and its modification by the applied electric field.

A loss in the oscillator strength of interband absorption is observed as the electric field is increased. In the simplest approximation [3], if one may neglect any perturbation of the electron and hole wavefunctions in the plane of the layers by the electric field; the oscillator strength, and hence interband absorption, is proportional to the overlap integral of the wavefunctions normal to the layers. This overlap integral decreases as the electrons and holes are pulled to opposite

sides of the well by the electric field leading to an increase in the change in electroabsorption.

In many device applications, it is desirable to achieve the largest change in absorption with the smallest possible applied voltage. Our measurements show that at a given wavelength and applied voltage, the change in absorption is larger in the $[-1,1,0]$ oriented devices than in the $[1,1,0]$ ones for both TE and TM polarizations.

2.2 Test samples

The samples were grown by metallo-organic vapor phase epitaxy (MOVPE) on a (001) substrate of n-doped GaAs at Siemens FL in Munich, Germany. The active region contained six GaAs QW's each 75 Å thick, separated by five 80 Å thick $Al_{.35}Ga_{.65}As$ barrier layers. Figure (2.1) shows a cross section of the MQW sample used.

The MQW layers and the index grading layers in the QW device were not intentionally doped. The residual doping in these layers was found to lie in the middle 10^{16} cm^{-3} range. The doping of the cover layers ranged between 2 and $5 \times 10^{17} \text{ cm}^{-3}$ leading to a p-i-n sequence in the doping profile.

A stripe 3 μm width was then formed by sputter etching a ridge into the top AlGaAs cover layer to form the ridge waveguide. The height of the ridge was

designed to assume single lateral mode operation. The etched surface was passivated with a $.3 \mu\text{m}$ sputtered Al_2O_3 and finally the metal contact was evaporated on the finished wafer.

The samples were identical except for the orientation of the waveguides, where the optical axis of the guide was oriented along the $[-1,1,0]$ direction in some samples while along the $[1,1,0]$ in others. Figure (2.2) is a schematic illustration of how both the $[-1,1,0]$ and $[1,1,0]$ samples were cut from the same wafer which was grown on a (001) plane. The length of the QW waveguide modulator was 1 mm. Both facets were AR-coated to improve transmission and to reduce Fabry-Perot resonances. The preparation of the $[-1,1,0]$ and the $[1,1,0]$ samples were identical.

2.3 Measurements and results

A tunable dye laser, using the Dye Styryl 9M, was employed as the light source. The light was chopped at a reference frequency, launched into and collected from the device using a pair of microscope objectives. The light out from the device was imaged on the IR TV camera as well as the photodiode. The camera helped in the alignment by looking at the fundamental mode profile and insuring that it was guided under the ridge. The photodiode was used in the actual measurements of the transmitted light intensity.

A DC programmable power supply applied the reverse bias to the device, from 0 to 6 volts in steps of 0.1 volts, while two computer controlled lock-in amplifiers

measured both the transmitted light intensity and photocurrent. The photocurrent (electron hole pairs generated due to the absorption of light photons) and the current of the photodiode were converted to voltage using two transimpedance amplifiers. The transimpedance amplifiers were made up of a dual operational amplifier chip and feed back resistance that defined the current to a voltage gain. Figure (2.3) shows the experimental set-up used.

Figure (2.4-a), solid curves, show the normalized transmitted light intensity for TE polarization at 850 nm as a function of the applied voltage for the $[-1,1,0]$ orientation. Figure (2.4-b) shows the same for the $[1,1,0]$ orientation. It is clear that the dynamic range of change in electroabsorption is larger for the $[-1,1,0]$ orientation. Figure (2.5-a,b) show the same but for TM polarization.

If $P_t(V, \lambda)$ is the transmitted light intensity through the device at a given wavelength and applied voltage, then we can write

$$P_t(V, \lambda) = P_{ic} e^{-\alpha(V, \lambda) \Gamma L} \quad (2.1)$$

Where P_{ic} is the coupled power in the device, Γ is the confinement factor and L is the device length, hence one can write the change in absorption $\Delta\alpha(V, \lambda) = \alpha(V, \lambda) - \alpha(0, \lambda)$ as,

$$\Delta\alpha(V, \lambda) = \frac{1}{\Gamma L} \ln \frac{P_t(0, \lambda)}{P_t(V, \lambda)} \quad (2.2)$$

The voltage independent part of the detected light, which we shall call P_{leak} , should be subtracted from the measured light intensity by the lock-in amplifier.

So equation (2.2) is modified to

$$\Delta\alpha(V, \lambda) = \frac{1}{\Gamma L} \ln \frac{P_t(0, \lambda) - P_{leak}}{P_t(V, \lambda) - P_{leak}} \quad (2.3)$$

Figure (2.6-a) shows plots of the logarithmic term in equation (2.3) vs. applied voltage (i.e. $\Delta\alpha(V, \lambda)$ in arbitrary units A.U.) for TE polarization at 850 nm. Figure (2.6-b) is for TM polarization. As these plots indicate, $\Delta\alpha(V, \lambda)$ is always larger for the $[-1,1,0]$ orientation than the $[1,1,0]$ orientation. This implies that the $[-1,1,0]$ orientation is more suited for intensity modulator or switch applications since it provides a larger change in absorption at a given applied voltage.

We have repeated these measurements on several $[-1,1,0]$ and $[1,1,0]$ oriented devices prepared from the same wafer and this confirmed the previous observations: the $[-1,1,0]$ oriented samples always showed larger changes in electroabsorption than the $[1,1,0]$ oriented ones.

These results were confirmed by measurement of the photocurrent (I_{ph}). As shown in Figure (2.4-a) and (2.4-b) the relative change in photocurrent is also larger for the $[-1,1,0]$ samples (2.4-a) than for the $[1,1,0]$ (2.4-b), though the difference is not as pronounced as in the transmitted intensity. This can be due to the reduced accuracy of photocurrent measurement because a part of the photocurrent is generated in the substrate which is not subject to the Quantum Confined Stark Effect. Furthermore, the collection efficiency of photoelectrons affect the photocurrent which could not be independently determined. It was found, however, that the relative change in photocurrent was always larger for the $[-1,1,0]$ samples than in the $[1,1,0]$ case.

We have also carried out the same measurements, $\Delta\alpha(V, \lambda)$, for double heterostructure (DH) waveguide modulators. Figure (2.7) shows a cross section of the double heterostructure sample used. Figure (2.8) shows the results from

transmitted light intensity measurements for TE polarization in the same arbitrary units. It is clear that the difference in $\Delta\alpha(V, \lambda)$ between the two orientations for the DH structures is small compared to the changes in the QW structures. This suggests that the change in electroabsorption in QW's is enhanced by quantization and excitonic effects.

2.4 Results and explanation

We believe that the orientation dependence in the electroabsorption is attributed to the anisotropy [4] of the valence subband structure of the two dimensional hole system in the QW. This is equivalent to different hole effective masses in different directions.

The conduction- and valence subband energies and the binding energies of the excitons in the GaAs/AlGaAs MQW structures in the presence of an electric field has been calculated by several groups [2]. In these calculations, it is assumed that the heavy and light hole subbands are decoupled and hence Dingle's [5] simple particle in a box model is valid. The results of these calculations are in qualitative agreement with the experimental results.

Recently, it has been pointed out [6] [7] that the valence subband states are more complicated and far from being trivially parabolic even at the Brillouin-zone center. This is because the QW periodic potential mixes the bulk heavy hole and light hole states of both parities giving rise to dipole allowed transitions between all pairs of valence and conduction subbands. This in turn affects

the energy versus momentum dispersion curves and the optical matrix elements, i.e. the electronic and optical properties of the semiconductor QW. Strong exciton structures corresponding to "forbidden" transitions have been observed in luminescence studies [8] and have been reproduced in theoretically calculated absorption spectra taking valence band hybridization into account [9].

It is clear that if one wants to account for this electroabsorption orientation dependence, one has to start from first principles to calculate the absorption coefficient as the simple particle in a box model will not be adequate.

The free carrier (electron, hole) states are to be solved within the effective mass approximation, where the CB and VB states are expressed in terms of the zone center Bloch functions for bulk GaAs. Unlike the case for the conduction band, the valence band in bulk GaAs, in the limit of infinite spin-orbit splitting, is four fold degenerate at the band edge with total spin of $J=3/2$. The heavy hole ($J_z = 3/2, -3/2$) and the light hole ($J_z = 1/2, -1/2$) subband states are thus strongly hybridized and hence the effective mass hole Hamiltonian will be a matrix (4 x 4). This matrix Hamiltonian is a function of $k_{//}$ (k_x and k_y). Due to the lack of inversion symmetry in the appearance of (k_x and k_y) as entries to hole matrix Hamiltonian in the off diagonal terms, it is orientation dependent as we will shortly show (Appendix A).

The implication of this orientation dependence in the hole matrix Hamiltonian is the anisotropy of the hole subband in plane dispersion which has been recognized by several groups. For every k_x and k_y , the solution of the hole multiband matrix Hamiltonian will render a different $E(k_{//})$ and a different hole eigenstate. These

$E(k_{//})$ and the electron/ hole states can then be used to calculate the optical matrix element and then the value of the absorption coefficient. Consequently, the absorption coefficient, which is an explicit function of the electron/hole energies and the optical matrix element (see Appendix A), will be different along different orientations.

2.5 Transverse sample measurements

We have done the same measurements on a transverse probe as opposed to the waveguide sample we measured earlier. Figure (2.9) shows a schematic of the MQW transverse structure used for the measurement with layer thicknesses, material composition and doping profiles indicated. The i-MQW layers of the p-i-n structure were grown by molecular beam epitaxy (MBE) at Siemens RTL in Princeton, NJ (as opposed to MOCVD in the waveguide samples). The i-MQW layers consisted of an alternate layers of GaAs and $Al_{.32}Ga_{.68}As$ (50 wells 105Å, and 51 barriers 95Å). The residual doping in the i- layer is approximately $10^{-14}cm^{-3}$ and around $10^{-17}cm^{-3}$ in the P and N layers so that the applied voltage was dropped entirely across the i-layer. The input face (P-AlGaAs) was AR coated using an etch-tuning method to prevent unwanted Fabry-Perot interference effects.

The light was incident normal to the quantum well layers and the electric field vector was rotated using a polarizer and a half wave plate. In this configuration, one can not investigate of course the TM polarization. We were not able to see any significant change in the electroabsorption as the electric field vector was

rotated in that particular arrangement. The reason for that might be the short interaction length between the incident optical radiation and the quantum wells ($0.525 \mu\text{m}$) for this transverse sample.

To elaborate more on that, from the geometry one can write for the transmitted light intensity $P_t(\lambda, V)$ in terms of the incident power P_{in} :

$$P_t(\lambda, V) = P_{in}(1 - R)e^{-\alpha(\lambda, V)d} \quad (2.4)$$

where R is the reflection coefficient of the output facet (the AlGaAs/air interface) and d is the sum over the GaAs well widths ($.525 \mu\text{m}$), hence

$$\alpha(\lambda, V) = \frac{-1}{d} \text{Ln} \frac{P_t(\lambda, V)/P_{in}}{1 - R} \quad (2.5)$$

and the change in the absorption coefficient is

$$\Delta\alpha_{transverse}(V, \lambda) = \frac{1}{d} \text{Ln} \frac{P_t(0, \lambda)}{P_t(V, \lambda)} \quad (2.6)$$

It is known that in quantum wells the absorption coefficient at a given applied voltage and operating wavelength depends on the quantum well material composition and thickness, consequently the change in the absorption coefficient which we define as $\Delta\alpha(V, \lambda) = \alpha(V, \lambda) - \alpha(0, \lambda)$, is also a function of the quantum well thickness and material composition. If we assume that both the waveguide and transverse samples had the same quantum well material composition and thickness, then $\Delta\alpha_{transverse}(V, \lambda) = \Delta\alpha_{waveguide}(V, \lambda)$, hence

$$\frac{1}{d} \text{Ln} \frac{P_{t-transverse}(0, \lambda)}{P_{t-transverse}(V, \lambda)} = \frac{1}{\Gamma L} \text{Ln} \frac{P_{t-waveguide}(0, \lambda) - P_{leak}}{P_{t-waveguide}(V, \lambda) - P_{leak}} \quad (2.7)$$

If $\Gamma = 0.85$, $L = 0.1 \text{ cm}$, and the logarithmic term value for the waveguide sample oriented along $[-1, 1, 0]$ for TE polarization is roughly 4.5 at $V=5$ volts (see figure 2.6-a), then $\left(\frac{P_t(0, \lambda)}{P_t(V, \lambda)}\right)_{transverse} = 1.0027$. Similarly, one would get 1.0015 for the

[1,1,0] orientation if we take the logarithmic term for the waveguide sample to be 2.5 at $V=5$ volts (see figure 2.6-a).

It is clear that ratios between the transmitted light intensity at an applied voltage of 5 volts and at zero voltage are almost one for both orientations (this means that the transverse sample's interaction length is not big enough to see an appreciable change in the transmitted light intensity). Also, the difference between the two orientations is very small to resolve considering the inherent background polarization sensitivity in the optics involved in the setup (lenses, half wave plate). This explains why it was not possible to see any significant change in the electroabsorption as we rotated the electric field vector in the transverse sample measurements arrangement.

2.6 Effect of stress/strain on the QW electronic states and optical properties

The introduction of stress in a solid produces changes in the lattice parameter and in some cases, in the symmetry of the material. These in turn produce significant changes in the electronic band structure. All configuration of stress can be divided into two classes: the isotropic class, which give rise to a volume change without disturbing the crystal symmetry, and the anisotropic class, which in general reduces the symmetry present in the strain free lattice, alter the electronic states and energy gaps, and in some cases, remove the degeneracies. Also, effective masses will be affected by the variations in energy gaps as well as by variations in the interband optical matrix elements.

Lattice mismatch between quantum well layers grown along the [001] direction creates stress which introduces strain with a uniaxial component along that direction. The relative lattice mismatch $\frac{\delta a_0}{a_0}$ between the host materials of heterolayers varies from almost zero in (*GaAs/Al_{0.3}Ga_{0.7}As*) to values as large as several percentages (7 per cent between InAs and GaAs, for example). This fact makes us believe that the possibility of unintentionally introducing stress/strain in the wafer from which the samples were made is a rather slim one.

It is still possible that these stresses might have been introduced externally during the phase of preparation/mounting of the devices. If this was the case, we wonder why did the [-1,1,0] and the [1,1,0] oriented devices showed consistently the same behavior when measurements were performed on several devices ?

Furthermore, the effects of external stress along several directions on the electronic structure and optical properties of various III-V based quantum wells have been investigated both experimentally [13] and theoretically [14] for example. In [13] the stress dependence of the heavy/light -hole to conduction subband transitions of several *GaAs/Al_{0.3}Ga_{0.7}As* multiple quantum wells of different thicknesses (40, 110, 220 Å) was experimentally studied. The stress was perpendicular to the growth axis. As the external stress was increased from 0 to 1 Kbar, the fundamental heavy hole to conduction subband transition energy increased by 1.8 meV for the 110 Å thick MQW. To put that change in perspective, it represents about 0.0586 of the total shift (- 30.717 meV) of the fundamental exciton absorption edge at an applied electric field of 200 kV/cm for that particular waveguide sample.

2.7 Effect of refractive index change due to the linear electrooptic effect on the confinement factor Γ

One last point remains to be addressed so as to complete the picture. From (2.3) we see that $\Delta\alpha(V, \lambda)$ depends on the confinement factor Γ . If for example we consider a $[-1,1,0]$ oriented device subject to an electric field normal to the layers, for TE polarization, the change in the refractive index $\Delta n(E)$ due to the applied electric field E is given by [15]

$$\Delta n = -\frac{1}{2}n^3 r_{63}E - \frac{1}{2}n^3 s_{13}E^2 \quad (2.8)$$

where r_{63} and s_{13} are the linear and quadratic electrooptic coefficients respectively. On the other hand, for a $[1,1,0]$ oriented device $\Delta n(E)$ would be expressed as

$$\Delta n = +\frac{1}{2}n^3 r_{63}E - \frac{1}{2}n^3 s_{13}E^2 \quad (2.9)$$

One might argue that the Δn 's are different in both orientations, consequently, that explains the difference in $\Delta\alpha$'s for both orientations. First, it is difficult to imagine that the contribution of the linear electrooptic effect alone in the change in refractive index would double the value of the confinement factor Γ (since we experimentally saw a factor of 2 difference in the change in electroabsorption between both orientations near the band edge for example). Second, we still saw a difference in the change in electroabsorption between both orientations even for a TM polarized light as figure (2.6-b) indicates. It is well known that for a TM polarized light, due to symmetry considerations, the linear electrooptic coefficient (which is the cause of the difference in Δn in both orientations) vanishes and

hence the expression for the change in the refractive index can be written as

$$\Delta n = -\frac{1}{2}n^3 s_{33} E^2 \quad (2.10)$$

Where s_{33} is the quadratic electrooptic coefficient when the light is TM polarized. (As our measurements of s_{33} in the previous part indicated, s_{33} is slightly different for the two orientations, but this would not create such a big difference in Δn so as to change Γ by a factor of two). As a result if that argument was correct, one would not have seen a change in the electroabsorption for a TM polarized light, which did not happen as figure (2.6-b) indicated.

2.8 Summary and conclusion

We have studied experimentally the change in electroabsorption in $[-1,1,0]$ and $[1,1,0]$ oriented 75 Å GaAs/AlGaAs MQW waveguide modulators near the band edge for both TE and TM polarizations by measuring absorption as a function of the applied voltage and also by measuring the photocurrent. The results show that the change in electroabsorption is larger in the $[-1,1,0]$ orientation by as much as a factor of 2 than in the $[1,1,0]$ orientation near the band edge for TE polarization. This makes the $[-1,1,0]$ orientation more suitable even for electroabsorptive device applications. To our knowledge, orientation dependence in the change in electroabsorption for MQW's has not been reported to date. We also gave a qualitative explanation to support our observations and correlate them with quantization and excitonic effects in quantum wells.

2.9 Appendix A

This appendix is intended to give a qualitative explanation of the orientation dependence in electroabsorption between the $[-1,1,0]$ and $[1,1,0]$ oriented devices which we have experimentally observed. In order to do that, one has to start from first principles to calculate the absorption coefficient in MQW structures with band mixing and excitonic effects considered. This has to be done so as to realistically calculate the electronic states, and hence the energy versus momentum dispersion curves, in MQW structures. They both appear explicitly in the expression to be derived for the absorption coefficient, and also affect the calculated value of the optical matrix element which appears explicitly in the expression for the absorption coefficient as well.

In what follows, we calculate the absorption coefficient in MQW structures using envelope function description of electronic states within the frame of the multiband effective mass scheme.

2.9.1 Absorption coefficient calculation

Absorption can be described by the interaction between elementary excitations of the solid (electrons and holes) and the quanta of the electromagnetic field (the photons). Absorption of light by a solid is strongly dependent on :

1. Where the initial and final states lie in the Brillouin- zone,
2. how large the densities of states are,
3. whether the transitions are allowed or forbidden by the symmetry of the states concerned,

4. the polarization of the incident photon.

The absorption coefficient is defined as the energy absorbed per unit volume per unit time divided by the incident energy per unit area per unit time.

Let us represent the incident light by the vector potential $\mathbf{A}(\mathbf{r}, t)$

$$\mathbf{A}(\mathbf{r}, t) = A_0 \hat{e} \exp [i(\mathbf{q} \cdot \mathbf{r} - \omega t)] + c.c. \quad (2.11)$$

Where c.c. stands for the complex conjugate. Using Maxwell's equations one can write

$$\nabla \times \left(\mathbf{E} + \frac{\partial \mathbf{A}}{\partial t} \right) = 0 \quad (2.12)$$

or

$$\mathbf{E} + \frac{\partial \mathbf{A}}{\partial t} = -\nabla \Phi \quad (2.13)$$

The vector potential \mathbf{A} and the scalar potential Φ may be chosen such that $\Phi = 0$, i.e.

$$\mathbf{E} = -\frac{\partial \mathbf{A}}{\partial t} \quad (2.14)$$

Let $W(\omega)$ be the number of photons absorbed per unit volume per unit time, so the energy absorbed/unit volume/unit time is

$$\text{Energy/vol./time} = \hbar\omega.W(\omega) \quad (2.15)$$

The incident energy per unit area per unit time is given by the Poynting vector \mathbf{S} .

$$\mathbf{S} = \frac{1}{2} \text{Re} \int_s \mathbf{E} \times \mathbf{H}^* . ds \quad (2.16)$$

Without any loss of generality, for a TEM wave traveling in positive z-direction and polarized along the x-direction for example, one can write

$$\mathbf{E}(z, t) = E_0 \hat{e}_x \exp [i(-qz + \omega t)] \quad (2.17)$$

and

$$\mathbf{H}(z, t) = E_0 \frac{q}{\omega \mu_0} \hat{e}_y \exp [i(-qz + \omega t)] \quad (2.18)$$

so

$$S = \frac{1}{2} \frac{E_0^2 q}{\mu_0 \omega} \quad (2.19)$$

using the facts that $c^2 = 1/\mu_0 \epsilon_0$, $q = n\omega/c$, and $|E|^2 = E_0^2 = \omega^2 A_0^2$, one can write

$$\dot{S} = \frac{1}{2} \omega^2 A_0^2 n c \epsilon_0 \quad (2.20)$$

hence, the absorption coefficient is

$$\alpha = \frac{2\hbar}{\epsilon_0 n c \omega A_0^2} W(\omega) \quad (2.21)$$

To determine $W(\omega)$, we need to solve the Schrödinger wave equation for an electron in the presence of the perturbing potential due to the optical radiation represented by the vector potential \mathbf{A}

$$\left[\frac{1}{2m_0} (\mathbf{p} + e\mathbf{A})^2 + V(\mathbf{r}) \right] \Psi = i\hbar \dot{\Psi} \quad (2.22)$$

or

$$\left[\frac{p^2}{2m_0} + V(\mathbf{r}) + \frac{e}{m_0} \mathbf{p} \cdot \mathbf{A} + \frac{e^2}{2m_0} A^2 \right] \Psi = i\hbar \dot{\Psi} \quad (2.23)$$

or

$$[H_0 + \hat{H}] \Psi = i\hbar \dot{\Psi} \quad (2.24)$$

Where $H_0 = \frac{p^2}{2m_0} + V(\mathbf{r})$ is the Hamiltonian in the absence of the perturbing optical radiation, $V(\mathbf{r})$ is the lattice periodic potential, and $\hat{H} = \frac{e}{m_0} \mathbf{p} \cdot \mathbf{A}$ represents the perturbing Hamiltonian. The A^2 term was neglected and considered as second order. Let Ψ_0 be the solution of

$$H_0 \Psi_0 = i\hbar \dot{\Psi}_0 \quad (2.25)$$

$$\Psi_0 = e^{-\frac{i}{\hbar} E_n(\mathbf{k})t} |n, \mathbf{k}\rangle \quad (2.26)$$

and $|n, \mathbf{k}\rangle$ are the Bloch functions which form a complete orthonormal basis

$$|n, \mathbf{k}\rangle = e^{-i(\mathbf{k}\cdot\mathbf{r})} u_n(\mathbf{k}, \mathbf{r}) \quad (2.27)$$

We now expand Ψ in terms of Ψ_0

$$\Psi = \sum_{n, \mathbf{k}} a_n(\mathbf{k}, t) e^{-\frac{i}{\hbar} E_n(\mathbf{k})t} |n, \mathbf{k}\rangle \quad (2.28)$$

Substituting (2.27) (2.28) into (2.23) and multiplying by the bra $\langle m, \mathbf{k}'|$ both sides and using the orthonormality of the Bloch functions we get

$$a_m(\mathbf{k}', t) = \frac{1}{i\hbar} \sum_{n, \mathbf{k}} a_n(\mathbf{k}, t) \cdot \text{Exp}\left[\frac{i}{\hbar} (E_m(\mathbf{k}') - E_n(\mathbf{k}))t\right] \cdot \langle m, \mathbf{k}' | \hat{H} | n, \mathbf{k} \rangle \quad (2.29)$$

Let $a_j(\mathbf{k}, t=0) = 1$ and all other $a_n(\mathbf{k}, t \neq 0) = 0$, i.e. we assume that at $t=0$ the electron described by (2.23) is in the state \mathbf{k} and in the j th band, so we can write the previous equation as

$$\dot{a}_j(\mathbf{k}', t) = \frac{1}{i\hbar} \text{Exp}\left[\frac{i}{\hbar} (E_j(\mathbf{k}') - E_j(\mathbf{k}))t\right] \cdot \langle j, \mathbf{k}' | \hat{H} | j, \mathbf{k} \rangle \quad (2.30)$$

The probability $W(j, \mathbf{k}, \dot{j}, \mathbf{k}', \omega, t)$ that the electron at a time t will be in the state $|\dot{j}, \mathbf{k}'\rangle$ is then equal to $|a_j(\mathbf{k}', t)|^2$, so

$$W(j, \mathbf{k}, \dot{j}, \mathbf{k}', \omega, t) = \frac{-1}{\hbar^2} \left| \int_0^t \text{Exp}\left[\frac{i}{\hbar} [E_j(\mathbf{k}') - E_j(\mathbf{k})] \dot{t}\right] \cdot \langle j, \mathbf{k}' | \hat{H} | j, \mathbf{k} \rangle d\dot{t} \right|^2 \quad (2.31)$$

Let us examine the matrix element $\langle \dot{j}, \mathbf{k}' | \hat{H} | j, \mathbf{k} \rangle$ that appears in (2.31), using the definition of \hat{H} , (2.23), (2.11), and the fact that in direct gap semiconductors, the extrema of the valence band and the conduction band occur at the same wave vector \mathbf{k} , i.e. the electron momentum change in direct transitions is almost zero or $\mathbf{k}=\mathbf{k}'$ (conservation of momentum) so one can write

$$\langle \dot{j}, \mathbf{k}' | \hat{H} | j, \mathbf{k} \rangle = \frac{eA_0\hbar}{im_0} \text{Exp}(-i\omega t) \langle \dot{j}, \mathbf{k} | \hat{\epsilon} \cdot \nabla | j, \mathbf{k} \rangle \quad (2.32)$$

Substitute (2.32) into (2.31) we get

$$W(j, \mathbf{k}, \dot{j}, \mathbf{k}', \omega, t) = \frac{e^2 A_0^2}{m_0^2} |M_{jj}(\mathbf{k})|^2 \cdot \left| \int_0^t \text{Exp}\left[\frac{i}{\hbar} [E_j(\mathbf{k}') - E_j(\mathbf{k}) - \hbar\omega] \dot{t}\right] \cdot d\dot{t} \right|^2 \quad (2.33)$$

Where $M_{j\dot{j}}(\mathbf{k}) = \langle \dot{j}, \mathbf{k} | \hat{e} \cdot \nabla | j, \mathbf{k} \rangle$. Using Fermi's golden rule

$$\left| \int_0^t \text{Exp} \left[\frac{i}{\hbar} [E_j(\dot{\mathbf{k}}) - E_j(\mathbf{k}) - \hbar\omega] t \right] dt \right|^2 = 2\pi \hbar t \delta [E_j(\dot{\mathbf{k}}) - E_j(\mathbf{k}) - \hbar\omega] \quad (2.34)$$

Substitute (2.34) in (2.33) we get

$$W(j, \mathbf{k}, \dot{j}, \omega, t) = \frac{2\pi \hbar t e^2 A_0^2}{m_0^2} |M_{j\dot{j}}(\mathbf{k})|^2 \cdot \delta [E_j(\dot{\mathbf{k}}) - E_j(\mathbf{k}) - \hbar\omega] \quad (2.35)$$

To find the total number of transitions per unit volume per unit time from (2.35), we divide by t , sum over all j occupied bands and \dot{j} unoccupied bands and integrate over the Brillouin-zone to account for all possible transitions between electrons in different bands with different states that might contribute to the absorption of a photon polarized along \hat{e} . After doing that and substituting the result in (3.4) for $\alpha(\hbar\omega)$ we get

$$\alpha(\hbar\omega, \hat{e}) = \frac{\pi \hbar e^2}{n c m_0^2 \omega \epsilon_0 \hbar \omega} \frac{1}{\hbar \omega} \sum_{\mathbf{k}} \sum_{j, \dot{j}} |\hat{e} \cdot p_{j\dot{j}}(\mathbf{k})|^2 \cdot \delta [E_j(\dot{\mathbf{k}}) - E_j(\mathbf{k}) - \hbar\omega] \quad (2.36)$$

Where $p_{j\dot{j}}(\mathbf{k})$ is the optical matrix element

$$p_{j\dot{j}}(\mathbf{k}) = \langle \dot{j}, \mathbf{k} | P | j, \mathbf{k} \rangle \quad (2.37)$$

In the above expression it was assumed that all states in the j th band are occupied and all states in the \dot{j} are empty. If this was not so, the occupational probabilities of the states have to be included.

So the calculation of α actually amounts to the calculation of the electron and hole states and their associated energies as a function of the \mathbf{k} . We will point out how to calculate them using the effective mass envelope scheme.

2.9.2 Envelope function description of electronic states in the multiband effective mass scheme

There are some rather stringent requirements for a satisfactory procedure to compute electronic states in heterostructures:

1. it should be able to handle heterojunctions and quantum wells,
2. it must be able to deal with realistic description of the bulk band structures of the constituent materials especially degeneracies,
3. it is highly desirable to have a method that can incorporate external fields (electric/magnetic).

A semi-empirical nearest neighbor tight binding model has been used [6] to calculate electronic states. It showed that heavy and light hole subbands mix to build up a hybrid hole state. This leads to a number of interesting phenomena not predicted by the simple particle in a box model. Most important among these is the prediction of many "forbidden" transitions which violate the $\Delta j=0$ selection rule and the discovery of the "negative" hole masses for subbands which are strongly interacting at the Brillouin-zone center. However, it is not easy to see how such a model could be used when external fields (electric or magnetic) are present. Furthermore, if one wants to keep the number of orbitals and range of interaction limited, it is not always possible to describe the band edges accurately. The envelope function approximation in its multiband version fulfills all the above requirements and is intermediate in complexity between the particle in a box and the tight binding models. Using this rather efficient and flexible method, the electric field induced changes in the conduction and valence subband structures, exciton binding energies, exciton oscillator strengths of both allowed

and forbidden transitions and the total absorption spectra can be calculated.

In the envelope function approximation, the wave function in each layer of the heterostructure is expressed by the product of one or more slowly varying envelope functions and the $k=0$ Bloch functions of the corresponding bulk semiconductor. The envelope functions satisfy an effective mass like equation and are joined at each interface with the appropriate boundary conditions, which must be derived from the smoothness conditions for the total wavefunction.

The envelope function scheme takes advantage of two considerations

1. Most of the materials forming the heterostructure display similar band structures. Moreover, the periodic part of the Bloch functions of the relevant band edges do not differ very much from one material to the other.
2. The relevant electronic states of the actual heterostructure are often close to the band extrema; thus only a small fraction of the host Brillouin zone participates in the building of the heterostructure state.

In the envelope function approximation, the free electron and hole states respectively are

$$\Psi_n^e(k_{//}) = \sum_{\sigma} f_n^{\sigma}(z_e) u_0^{\sigma}(r) e^{ik_{//} \cdot \rho} \quad (2.38)$$

$$\Psi_m^h(k_{//}) = \sum_{\nu} g_m^{\nu}(k_{//}, z_h) u_0^{\nu}(r) e^{ik_{//} \cdot \rho} \quad (2.39)$$

Where the index n and m label the subband, the index σ and ν label the z component of the spin, e and h refer to electrons and holes, $u_0(r)$ is the zone center periodic part of the Bloch functions (we will discuss this further shortly),

$k_{//} = k_x \hat{x} + k_y \hat{y}$, $\rho = x \hat{x} + y \hat{y}$, and $f_n^\sigma(z_e)$ and $g_m^\nu(k_{//}, z_h)$ are the envelope functions for electrons and holes respectively. the parallel wave vector $k_{//}$ is a good quantum number because of the translational symmetry along the x and y directions (the plane of the quantum well layers).

In many III-V based heterostructures, the band edges relevant to optical and transport properties have the symmetries of the Γ_6 (electron bands), Γ_8 (degenerate heavy hole and light hole bands), and Γ_7 valence band which is split by the spin orbit coupling Δ from the Γ_8 edge. In GaAs, $\Delta = 340$ meV, it is a fair approximation to take only the Γ_6 and Γ_8 edges into consideration when building up a quantum well state from a bulk state. This is the infinite spin orbit splitting approximation and is exploited to limit the sum to 2 bands (Γ_6 , up and down spins) for electrons in (2.38), (indeed the two bands are identical as they are decoupled since the electron Hamiltonian is diagonal) and to limit the sum to 4 bands (Γ_8 heavy and light holes, up and down spins) for holes (2.39). This translates to a 4 x 4 matrix Hamiltonian for holes.

Let H_0 be the Hamiltonian of an electron/hole in a periodic potential (due to the lattice), and let U be an additional potential (due to the confining potential $V_{e,h}(z_{e,h})$ and the applied electric field $\pm V_F(z_{e,h})$). U should be slowly varying or almost constant over a unit cell which is the condition for the validity of the effective mass theory. The eigenfunctions of H_0 (the Bloch functions) are denoted by $|n, k\rangle$ and the corresponding eigen values by $E_n(k)$, n labeling the band and k wandering through the first Brillouin- zone of the crystal. Thus

$$H_0 |n, k\rangle = E_n(k) |n, k\rangle \quad (2.40)$$

In the effective mass scheme, to find an electron/hole state wavefunction $\Psi_{n,m}^{e,h}$ we must solve the Schrödinger equation

$$(H_o + U)\Psi_{n,m}^{e,h} = E_{n,m}^{e,h}(k)\Psi_{n,m}^{e,h} \quad (2.41)$$

Rather than using the usual Bloch functions $|n, k\rangle$ corresponding to H_o ,

$$|n, k\rangle = e^{i(k \cdot r)} u_{n,k}(r) \quad (2.42)$$

The scheme uses a slightly modified Bloch functions to expand $\Psi_{n,m}^{e,h}$.

$$|n, k\rangle = e^{i(k \cdot r)} u_{n,0}(r) \quad (2.43)$$

$u_{n,0}(r)$ is the periodic part of the Bloch functions calculated at the zone center. We assert that these modified basis functions form a complete orthonormal set if the Bloch functions do [10].

The reason for this choice of basis is to avoid the difficulties associated with the variation the $u_{n,k}(r)$ with wave vector k from one band to another when building up a hybrid hole state. Unfortunately, an added complication arises when we evaluate the matrix elements of H_o . The matrix representation of H_o is no longer diagonal, since the modified basis functions are not eigen functions of H_o unlike the Bloch functions. The matrix representation of H_o , $\langle \hat{n}, \hat{k} | H_o | n, k \rangle$, surfaces when we substitute the $\Psi_{n,m}^{e,h}$ in its expanded form (using the modified basis functions) in the Schrödinger equation to solve for the envelope wavefunctions and the subband structure for electrons and holes.

The effective mass model treats electrons and holes separately, the electron subband structure $E_n^e(k_{//})$ and the envelope wavefunction $f_n^\sigma(z_e)$ are obtained by solving

$$H_{\sigma\delta} f_n^\sigma(z_e) = E_0^n f_n^\sigma(z_e) \quad (2.44)$$

where

$$E_n^e(k_{//}) = E_0^n + \frac{\hbar^2 k_{//}^2}{2m_e^*} \quad (2.45)$$

and

$$H_{\sigma\sigma} = \left[\frac{p^2}{2m_e^*} + V_e(z_e) - V_F(z_e) \right] \delta_{\sigma\sigma} \quad (2.46)$$

σ labels the electron spin ($\sigma = \pm 1/2$), m_e^* is the effective mass of the electron taken to be $0.067 m_0$, $V_e(z_e)$ is the confining square potential whose height is taken to be 0.6 of the band gap mismatch between the GaAs and the AlGaAs and $V_F(z_e)$ is the potential due to the applied electric field. $V_F(z_e) = -eFz_e\Theta(W/2 - |z_e|)$, where e is the electronic charge, F is the electric field strength, and $\Theta(x)$ is a unit step function which cuts off the electric field potential at the edge of the well of width W . The cutoff is necessary in order to obtain a variational solution since in the absence of the cutoff there are no true bound states. Indeed if the field strength is not too large the states will have a long lifetime and can be considered quasibound.

Similarly, the hole subband structure $E_m^h(k_{//})$ and the envelope wavefunction $g_m^\nu(k_{//}, z_h)$ are obtained by solving

$$\sum_{\nu'} H_{\nu\nu'}(k_{//}, k_x) g_m^{\nu'}(k_{//}, z_h) = E_m^h(k_{//}) g_m^\nu(k_{//}, z_h) \quad (2.47)$$

where

$$H_{\nu\nu'}(k_{//}, k_x) = T_{\nu\nu'} + [V_h(z_h) + V_F(z_h)] \delta_{\nu\nu'} \quad (2.48)$$

ν labels the z -component of the hole spin ($\nu = -3/2, -1/2, 1/2, 3/2$), $V_h(z_h)$ is the confining hole potential and is taken to be 0.4 of the band gap mismatch between the GaAs and the AlGaAs and $V_F(z_h)$ is the potential due to the applied electric field, and $T_{\nu\nu'}$ is the kinetic energy matrix given in the limit of infinite spin-orbit splitting by the $k \cdot p$ expression of Luttinger and Kohn [10] with k_x replaced by

the operator $-i\frac{\partial}{\partial z}$

$$T_{\nu\nu} = \frac{\hbar^2}{2m_o} \begin{bmatrix} \frac{1}{2}P & L & M & 0 \\ L^* & \frac{1}{6}P + \frac{2}{3}Q & 0 & M \\ M^* & 0 & \frac{1}{6}P + \frac{2}{3}Q & -L \\ 0 & M^* & -L^* & \frac{1}{2}P \end{bmatrix}$$

Where

$$\begin{aligned} \frac{1}{2}P &= (\gamma_1 + \gamma_2)(k_x^2 + k_y^2) + (\gamma_1 - 2\gamma_2)k_z^2, \\ \frac{1}{6}P + \frac{2}{3}Q &= (\gamma_1 - \gamma_2)(k_x^2 + k_y^2) + (\gamma_1 + 2\gamma_2)k_z^2, \\ L &= -2\sqrt{3}\gamma_3(k_x - ik_y)k_z, \\ M &= \sqrt{3}\gamma_2(k_x^2 - k_y^2) - i2\sqrt{3}\gamma_3k_xk_y \end{aligned}$$

For GaAs we adopt here the values $\gamma_1=6.93$, $\gamma_2=2.15$, and $\gamma_3=2.81$ which are called the Luttinger parameters. (Each of the matrix elements $H_{\nu\nu}(\mathbf{k})$ is written as a second order polynomial in \mathbf{k} , the the Luttinger parameters (γ 's) are the fitting coefficients to this polynomial such that the eigen values of the matrix $H(\mathbf{k})$ reproduce the correct energy dispersion relations for the bands). It is a sensible approximation to neglect the difference between the γ parameters of GaAs and AlGaAs due to the similarity of their band structure.

When $k_x = k_y = 0$, the off diagonal terms in $T_{\nu\nu}$ vanish, consequently (2.48) will be diagonal, and (2.47) will split into two sets of single component equations. In other words, the valence subbands would decouple into a purely heavy hole ($J_z = \pm 3/2$) subband with effective mass in the z-direction $= \frac{m_o}{\gamma_1 - 2\gamma_2}$ and a purely light hole ($J_z = \pm 1/2$) subband with effective mass in the z-direction $= \frac{m_o}{\gamma_1 + 2\gamma_2}$. When $k_{//} \neq 0$, the notion of heavy/light hole character at finite $k_{//}$ has little or no physical meaning as the off diagonal terms in the hole matrix Hamiltonian (L

and M) very effectively mix heavy and light hole states of both spins and produce a hybrid hole state.

The solution of (3.7) and (2.47) can be obtained variationally [9] by expanding $f_n(z_e)$ and $g_m^\nu(k_{//}, z_h)$ as sums of 10 even and 10 odd Gaussian type orbitals of the form $e^{-\beta x^2}$ and $ze^{-\beta x^2}$, where the exponents β are chosen to cover a broad physical range. Substituting these expansions for the envelope functions into the effective mass equations (3.7) and (2.47), reduces the problem to a generalized eigenvalue problem to be solved for the subband energies $E_n^e(k_{//})$ and $E_m^h(k_{//})$ and the envelope function expansion coefficients.

Remains the calculation of the optical matrix element $p_{nm}(k_{//})$ as defined in (2.37) to completely determine $\alpha(\hbar\omega)$, we have

$$p_{nm}(k_{//}) = \langle \Psi_m^h(k_{//}) | P | \Psi_n^e(k_{//}) \rangle \quad (2.49)$$

This can be written as

$$p_{nm}(k_{//}) = \sum_{\nu, \sigma} \int dr u_0^{\nu*}(r) P u_0^\sigma(r) \int_{-\infty}^{\infty} dz g_m^\nu(k_{//}, z) f_n^\sigma(z) \quad (2.50)$$

The functions $u_0^{\nu, \sigma}(r)$ can be expressed in terms of the functions $|S\rangle$, $|X\rangle$, $|Y\rangle$, and $|Z\rangle$ which have the following symmetry properties:

$|S\rangle$ is completely symmetric in x, y , and z like $\sqrt{x^2 + y^2 + z^2}$, $|X\rangle$ is antisymmetric in x but symmetric in y and z like $x\sqrt{x^2 + y^2 + z^2}$, $|Y\rangle$ is antisymmetric in y but symmetric in x and z like $y\sqrt{x^2 + y^2 + z^2}$, $|Z\rangle$ is antisymmetric in z but symmetric in x and y like $z\sqrt{x^2 + y^2 + z^2}$. Electrons in the conduction band have completely symmetric wavefunctions $|S\rangle$. The spin up and spin down $u_0^{\sigma=\pm 1/2}(r)$ are written as a two component spinor

$$u_0^{\sigma=1/2} = \begin{pmatrix} |S\rangle \\ 0 \end{pmatrix}$$

$$u_0^{\sigma=-1/2} = \begin{pmatrix} 0 \\ |S\rangle \end{pmatrix}$$

For the valence band, the situation is more complex. An electron moving in a strong electric field sees an effective magnetic field due to relativistic effects even if there were no external magnetic fields. This is known as the spin orbit interaction. It modifies the spin up and spin down $u_0^\nu(\mathbf{r})$ in a non trivial way as follows [11]

$$u_0^{\nu=3/2} = \frac{1}{\sqrt{2}} \begin{pmatrix} |X\rangle + i|Y\rangle \\ 0 \end{pmatrix}$$

$$u_0^{\nu=-3/2} = \frac{1}{\sqrt{2}} \begin{pmatrix} 0 \\ |X\rangle - i|Y\rangle \end{pmatrix}$$

$$u_0^{\nu=1/2} = \frac{1}{\sqrt{6}} \begin{pmatrix} -2|Z\rangle \\ |X\rangle + i|Y\rangle \end{pmatrix}$$

$$u_0^{\nu=-1/2} = \frac{1}{\sqrt{6}} \begin{pmatrix} |X\rangle - i|Y\rangle \\ 2|Z\rangle \end{pmatrix}$$

It can be shown that due to the symmetry of the functions $|S\rangle$, $|X\rangle$, $|Y\rangle$, and $|Z\rangle$ mentioned earlier, only the following integrals are non zero $\langle S|P_x|X\rangle = \langle S|P_y|Y\rangle = \langle S|P_z|Z\rangle = P_0$, where P_0 is a constant and can be estimated [12] using

$$P_0^2 = \frac{m_0 E_g}{2} \left(\frac{m_0}{m_c^*} - 1 \right) \frac{3E_g + 3\Delta}{3E_g + 2\Delta} \quad (2.51)$$

It has been pointed out [6] that for quantum wells, the approximation $p_{nm}(k_{//}) = p_{nm}(0)$ is a very poor one. $p_{nm}(k_{//})$ is rapidly varying even for small values of $k_{//}$ because of the strong mixing of heavy and light hole states by the off diagonal

terms in the valence band Hamiltonian. Thus, it is necessary to retain the $k_{//}$ dependence of $p_{nm}(k_{//})$ in the absorption coefficient calculation.

The energy conservation delta function in (2.36) is replaced by $\Delta_{nm}[E_m^h(k_{//}) - E_n^e(k_{//}) - \hbar\omega]$, where $\Delta(E) = \frac{\Gamma_{nm}}{\pi} \frac{1}{E^2} \Gamma_{nm}^2$ is a Lorentzian line shape that mimics the effects of inhomogeneous broadening in MQW structures due to the variations in the individual well size.

Finally, to include the first order excitonic effects, (Coulomb attraction forces between the electron and hole pair forming the exciton). To include this effect on the computed band to band absorption, one multiply by the two dimensional Coulomb enhancement factor of Shinada and Sugano [16] who calculated the absorption coefficient including excitonic effects in two-dimensional systems.

The summation over $k_{//}$ in the expression for $\alpha(\hbar\omega)$ (2.36) is converted to an integral. The value of this integral is not the same in different directions since both the valence subband dispersion $E_m^h(k_{//})$ and the optical matrix element $p_{nm}(k_{//})$ values are direction dependent as clearly seen from the multiband hole Hamiltonian which lacks the inversion symmetry in k_x and k_y in the off diagonal terms due to band mixing. In our case, we are interested in the $[-1,1,0]$ and the $[1,1,0]$ directions. Looking back to the 4×4 matrix $(T_{\nu\nu})$ of the multiband hole Hamiltonian, we see that the entry $L = -2\sqrt{3}\gamma_3(k_x - ik_y)k_x$ is going to be different for both orientations considered. For the $[-1,1,0]$ orientation, it reads as $L = -2\sqrt{3}\gamma_3(-k_x - ik_y)k_x$ instead. Obviously, that will make the energy vs momentum, the hole electronic states, and the optical matrix elements different for both directions. Consequently, the absorption coefficient will also differ for

both orientations.

In other words, if one wants to accurately assess the orientation dependence of the absorption coefficient, the isotropic approximation, (used by some people for the sake of simplicity), can not be used due to the anisotropy of the valence subband dispersion, (which have been reported by several groups as previously indicated), and direction dependence of the optical matrix element $p_{nm}(k_{//})$. Both appear explicitly in the expression for the absorption coefficient. This makes the integration over k not a simple 1-D integration.

References

- [1] D. Miller, D. Chemla, T. Damen, A. Gossard, W. Wiegman, T. Wood, and C. Burrus, "Band edge electroabsorption in quantum well structures: The quantum confined stark effect.", *Phys. Rev. letters*, Vol 53, No. (22), 1984, P. 2173
- [2] D. Miller, D. Chemla, T. Damen, A. Gossard, W. Wiegman, T. Wood, and C. Burrus, "Electric field dependence of optical absorption near the band edge of quantum well structures." *Phys. Rev.*, Vol B32, 1985, P. 1043
- [3] D. Miller, D. Chemla, T. Damen, A. Gossard, W. Wiegman, T. Wood, and C. Burrus, "Electric field dependence of linear optical properties in Quantum well structures: Waveguide electroabsorption and sum rules." *J. of Quantum Electronics*, Vol 22 , no(9), 1986, P.1826
- [4] Tsuneya Ando, "Hole subband at GaAs/AlGaAs heterojunctions and quantum wells.", *J. of the physical society of Japan*, Vol 54, 1985, PP 1528-1536
- [5] R. Dingle, in *Festkoerperprobleme*, edited by H. J. Queisser, (Pergamon, New York, 1975), Vol. 15, P. 21
- [6] J. N. Schulman, Yia-Chung Chang, "Band mixing in semiconductor superlattices.", *Physical review B*, Vol 31, 1985, PP 2056-2068

- [7] M. Altarelli, "Band structure, Impurities, and Excitons in superlattices.", *Heterojunction and semiconductor superlattices*, edited by G. Allan, G. Bastard, N. Boccara, M. Lannoo and M. Voos, Springer Verlag. PP 12-37
- [8] R. C. Miller, D. A. Kleinman, W. A. Nordland, and A. C. Gossard, *Physical review B*, Vol 22, 1980, P863
- [9] G. D. Sanders, Yia-Chung Chang, "Optical properties in modulation-doped GaAs-GaAlAs quantum wells.", *Physical review B*, Vol 31, 1985, PP 6892-6895
- [10] J. M. Luttinger and W. Kohn, "Motion of electrons and holes in perturbed periodic fields.", *Physical review*, Vol 97, 1955, PP 869-883
- [11] G. Bastard, and A. Brum "Electronic states in semiconductor heterostructures." *J. of Quantum Electronics*, Vol 22 , no(9), 1986, P.1625
- [12] S. Datta, "Quantum phenomena.", *Modular series on solid state devices*, edited by R. Pierret, and G. Neudeck, Vol VIII Addison-Wesley publishing company, 1989, PP 201
- [13] C. Jagannath, E. Koteles, J. Lee, J. chen, B. Elman, and Y. Chi , *Physical review B*, Vol 34, 1986, P 7027
- [14] G. D. Sanders, Yia-Chung Chang, *Physical review B*, Vol 32, 1985, P 4282
- [15] J. Faist, F. K. Reinhart, D. Martin and E. Tuncel, "Orientation dependence of phase modulation in P-N junction GaAs/AlGaAs waveguides.", *Appl. Phys. lett.*, Vol 50, 1987, PP 68-70
- [16] M. Shinada, and M. Sugano *J. of the Physical society of Japan*, Vol 21, 1966, P 1396

2.10 Figure captions

2.1- Cross section of the Multiple Quantum Well waveguide sample used.

2.2- Schematic illustration of how both $[-1,1,0]$ and $[1,1,0]$ samples were cut from the same wafer which was grown on a (001) plane.

2.3- Experimental setup for measuring the change in electroabsorption.

2.4- Normalized transmitted light intensity (—) and photocurrent (- - -) versus applied voltage for TE polarization at 850 nm, heavy hole exciton position is at 830 nm. a) $[-1,1,0]$ orientation, b) $[1,1,0]$ orientation.

2.5- Normalized transmitted light intensity (—) and photocurrent (- - -) versus applied voltage for TM polarization at 850 nm, light hole exciton position is at 820 nm. a) $[-1,1,0]$ orientation, b) $[1,1,0]$ orientation.

2.6- Change in the absorption coefficient in A.U. for $[-1,1,0]$ orientation (—) and $[1,1,0]$ orientation (- - -) versus applied voltage at 850 nm for both polarizations. a) TE polarization, heavy hole exciton is at 830 nm, b) TM polarization, light hole exciton is at 820 nm.

2.7- Cross section of the Double heterostructure sample used.

2.8- Change in the absorption coefficient in A.U. for $[-1,1,0]$ orientation (- - -)

and $[1,1,0]$ orientation (—) versus applied voltage in DH structures at 800 nm for TE polarization.

2.9- Cross section of the Multiple Quantum Well transverse sample used.



Figure 2.1: Cross section of the Multiple Quantum Well waveguide sample.

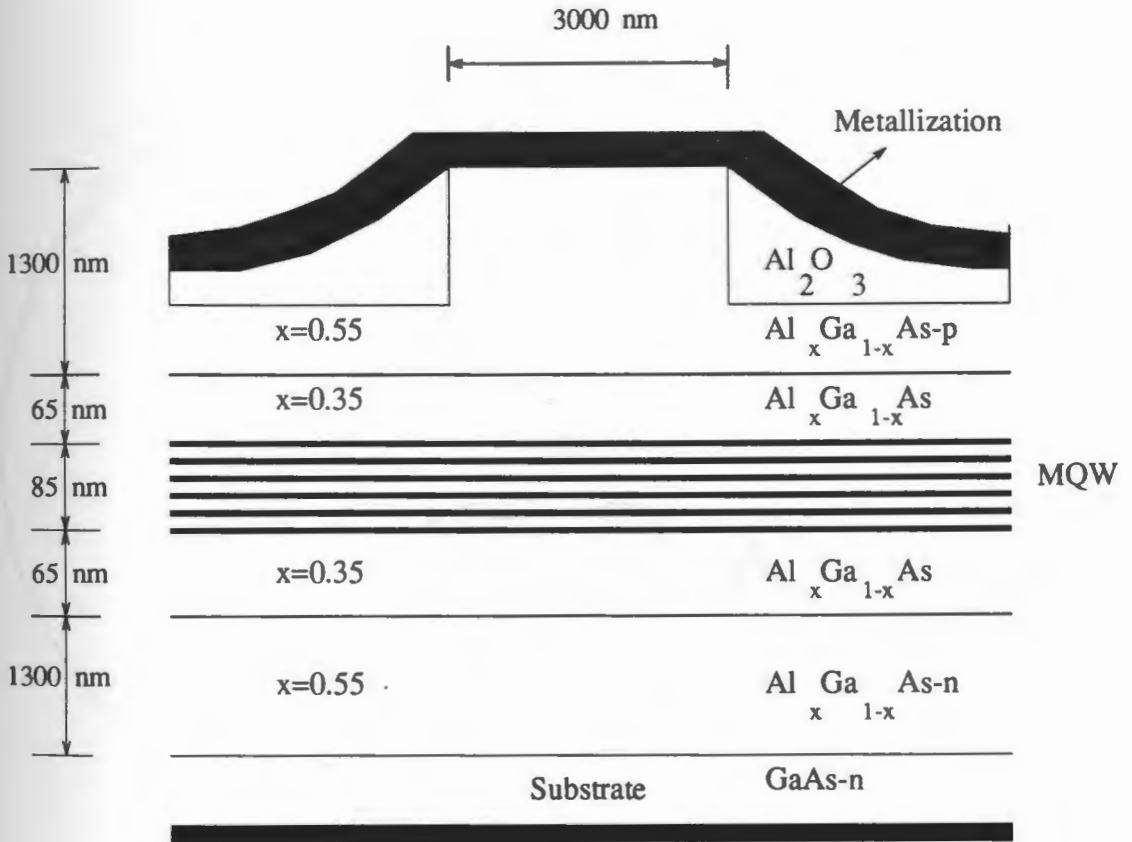


Figure 2.2: Schematic illustration of how both $[-1,1,0]$ and $[1,1,0]$ samples were cut from the same wafer which was grown on a (001) plane.

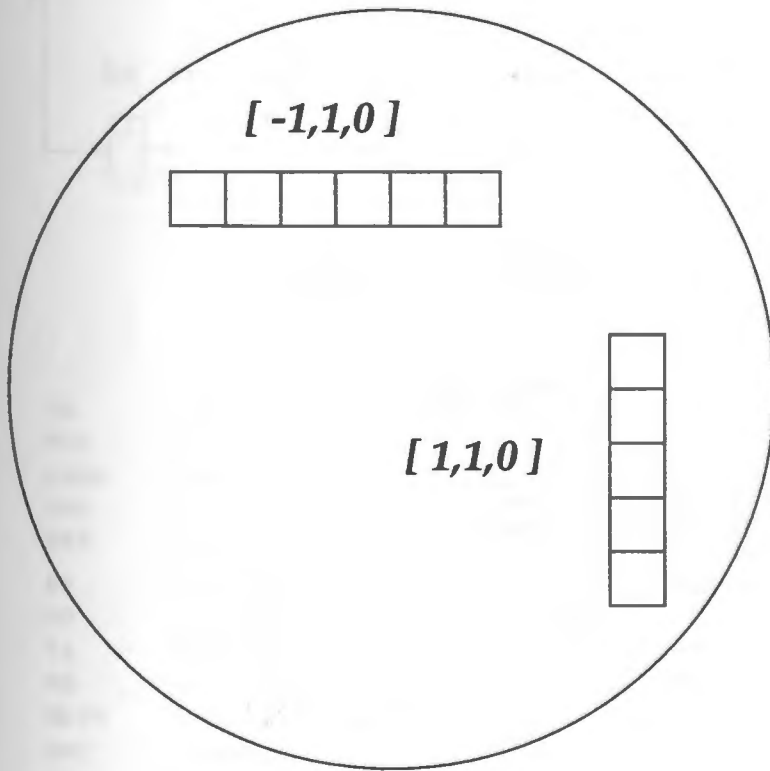


Figure 2.3: Experimental setup for measuring the change in electroabsorption.

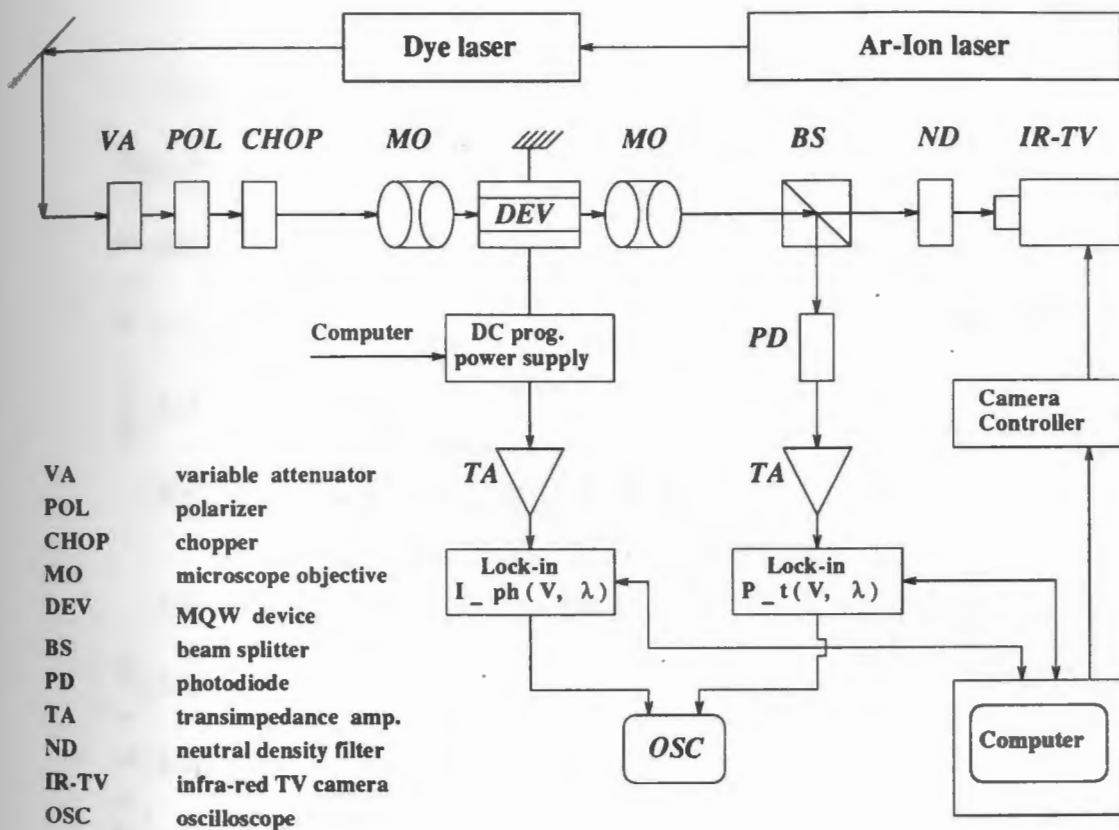
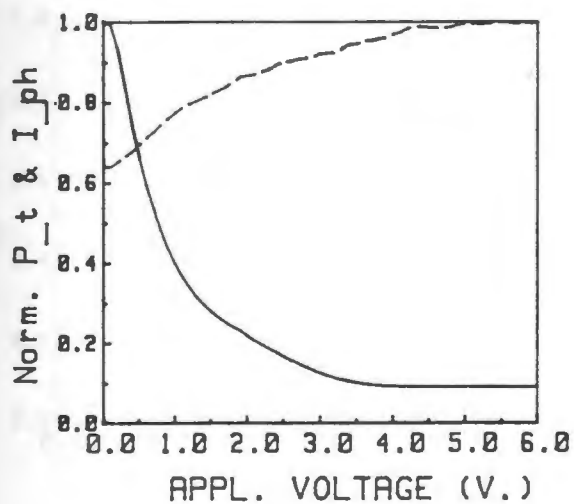
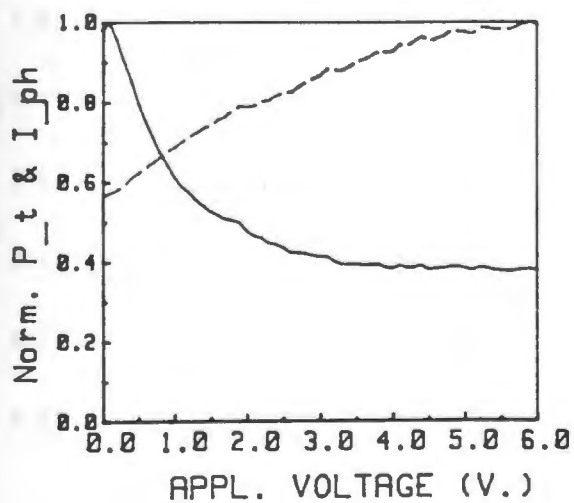


Figure 2.4: Normalized P_t and I_{ph} vs. applied voltage for TE polarization at 850 nm, a) $[-1,1,0]$ orientation, b) $[1,1,0]$ orientation.

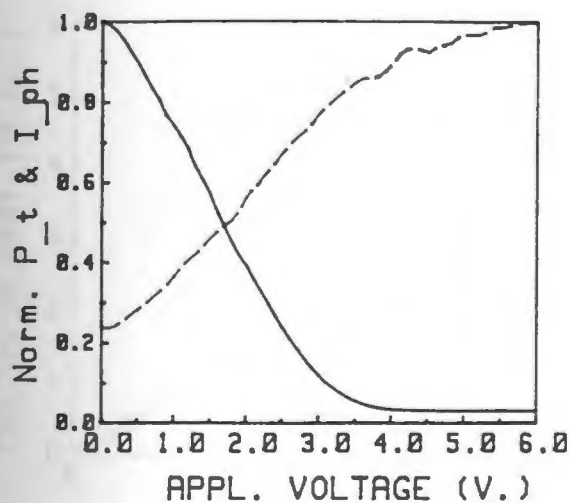


a. $[-1,1,0]$

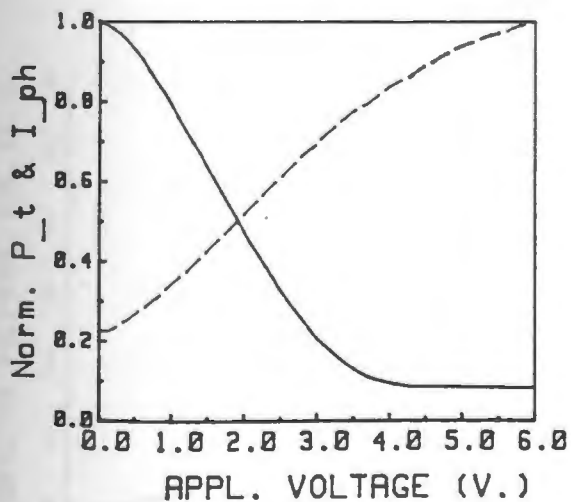


b. $[1,1,0]$

Figure 2.5: Normalized P_t and I_{ph} vs. applied voltage for TM polarization at 850 nm, a) $[-1,1,0]$ orientation, b) $[1,1,0]$ orientation.

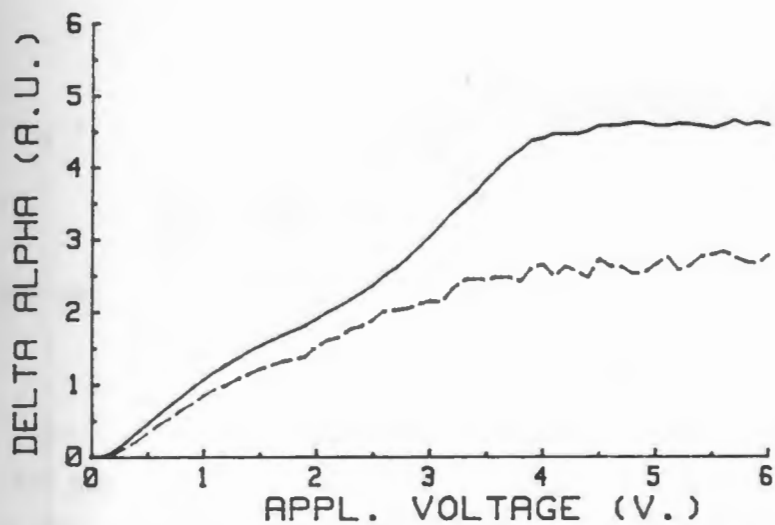


a. $[-1,1,0]$

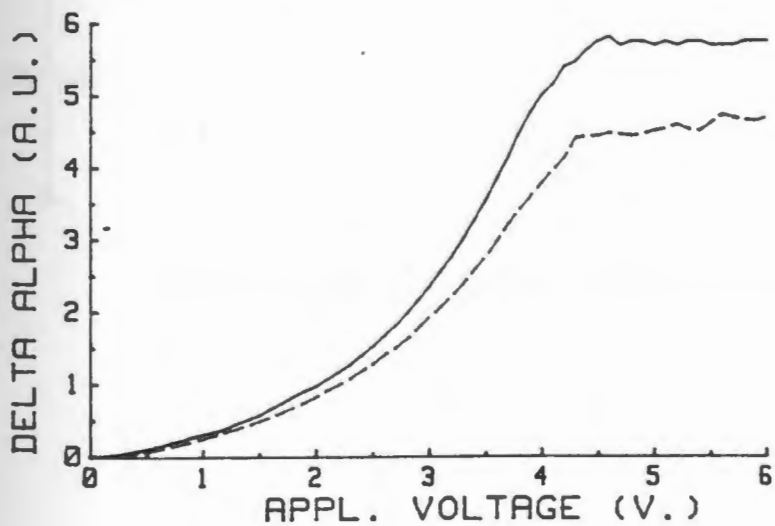


b. $[1,1,0]$

Figure 2.6: Change in the absorption coefficient in A.U. vs. applied voltage at 850 nm (hh exciton is at 830 nm, lh exciton is at 820 nm). a) TE polarization, b) TM polarization.



a. TE



b. TM

Figure 2.7: Cross section of the Double heterostructure sample used.

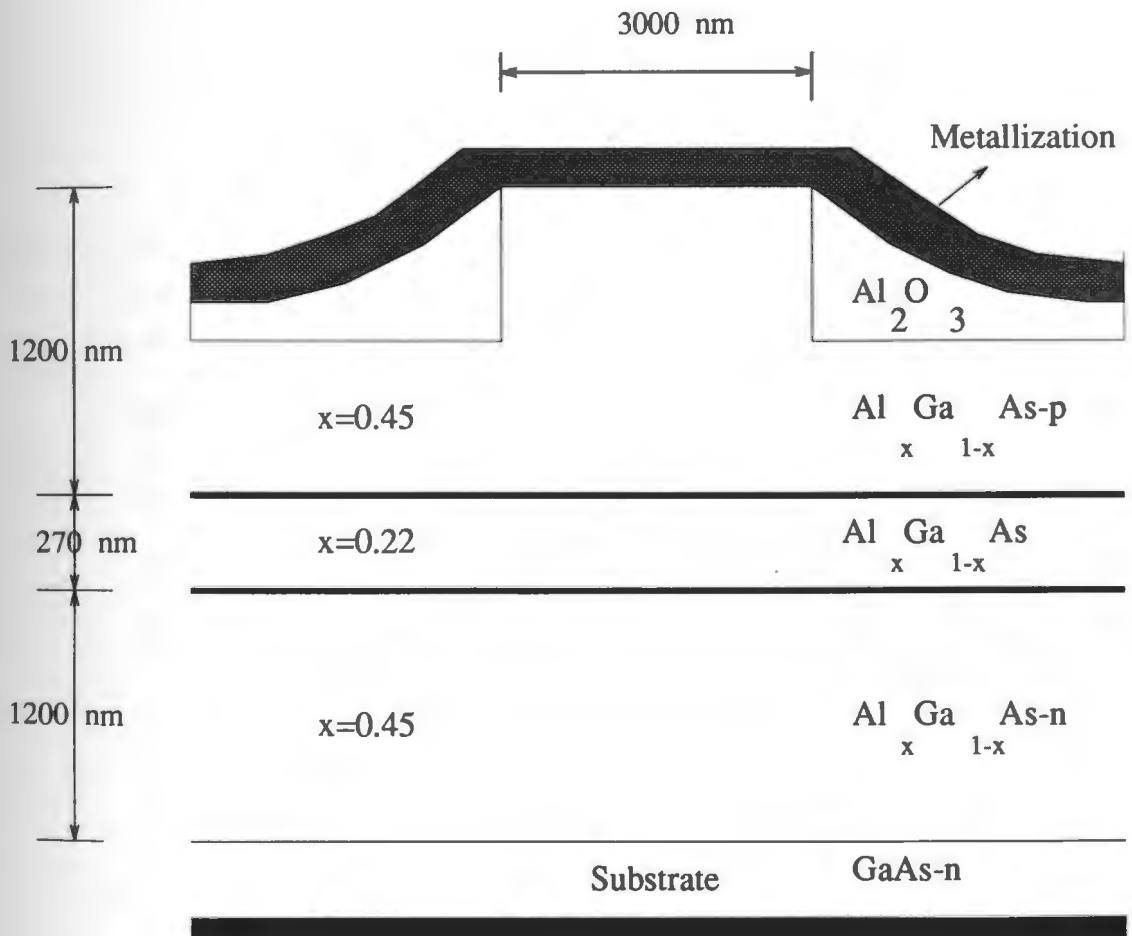
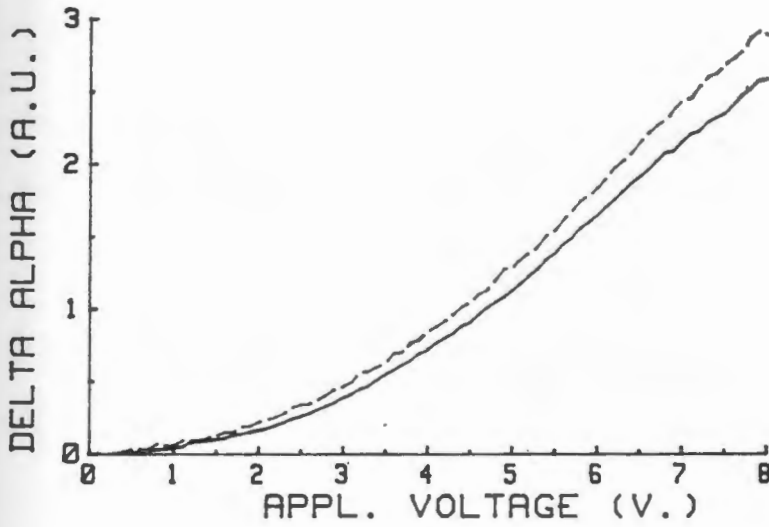
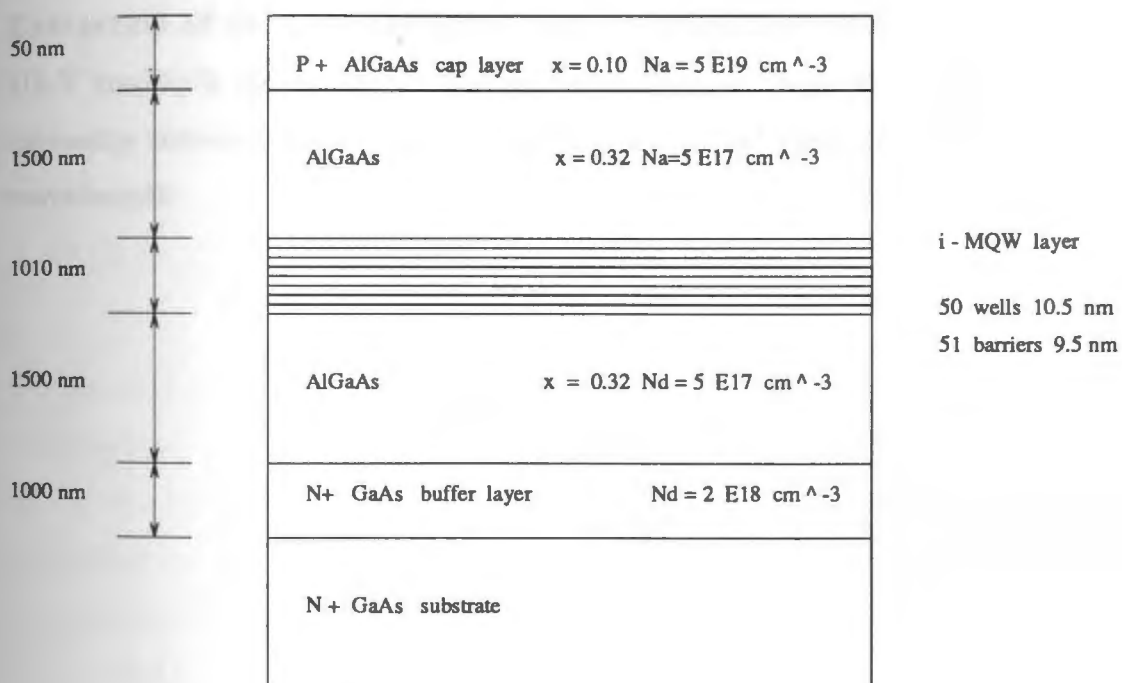


Figure 2.8: Change in the absorption coefficient in A.U. vs. applied voltage in DH structures at 800 nm for TE polarization.



(*absorption edge is at 730 nm*)

Figure 2.9: Cross section of the Multiple Quantum Well transverse sample.



Manuscript 3

Extraction of the spectral dependence of the absorption coefficient in III-V multiple quantum well structures from transmitted light intensity measurements as a function of applied field at a single wavelength

ABSTRACT

[Faint, illegible text in the abstract section]

TITLE:

Extraction of the spectral dependence of the absorption coefficient in III-V multiple quantum well structures from transmitted light intensity measurements as a function of applied field at a single wavelength

ABSTRACT:

We report, for the first time, the development of a useful and a rather simple experimental technique that can be used to determine the wavelength dependence of the absorption coefficient as a function of electric field in III-V compound based Multiple Quantum Well (MQW) devices. In this technique, the absorption coefficient $\alpha(F, \lambda)$ [cm^{-1}] at some wavelength λ [nm] and applied electric field F (kV/cm), is extracted from measurement of the transmitted light intensity through the device at a fixed wavelength λ_z as a function of the applied electric field. Results show good agreement with direct measurements of $\alpha(F, \lambda)$.

3.1 Introduction

When an electric field is applied perpendicularly to the layers of a MQW structure, the band edge shifts to lower photon energies while still retaining its excitonic features. This effect is referred to as the Quantum Confined Stark Effect (QCSE) [1]. It is this steep rise of the absorption edge, coupled with the very high excitonic peak, and its shift with the applied field, that make this effect particularly interesting both from a practical and fundamental viewpoint as it forms the basis of a variety of modulators and optical switching devices.

For the design and development of optical light modulators utilizing the QCSE, one needs to know the value of absorption for the electron-heavy hole (e-hh) fundamental edge as a function of wavelength and applied electric field. The value of $\alpha(F, \lambda)$ can be experimentally measured for a given material composition and device geometry. This measurement requires a spectrally variable light source which can be scanned over a relatively wide range of wavelengths. Furthermore, this range of wavelengths needs to be scanned for each value of the applied electric field.

In the method we describe shortly, we use a source emitting at a properly chosen wavelength λ_x , and measure the transmitted light intensity as a function of the applied electric field F . From this measurement we can deduce $\alpha(F, \lambda)$ at any λ shorter than λ_x , and any value of F .

The structure of this paper is as follows: In section II we describe the sample used, the experimental setup, and show results of the measurement. In section

III we outline the technique used in processing the measured data. Section IV discusses the results, we then conclude with a summary in section V.

3.2 Sample, experimental setup and measurements

Figure (3.1) shows a schematic of the MQW transverse structure used for the measurement with layer thicknesses, material composition and doping profiles indicated. The i-MQW layers of the p-i-n structure were grown by molecular beam epitaxy (MBE) of alternate layers of GaAs and $Al_{.32}Ga_{.68}As$ (50 wells 105Å, and 51 barriers 95Å). The residual doping in the i-layer is approximately $10^{-14}cm^{-3}$ and around $10^{-17}cm^{-3}$ in the P and N layers so that the applied voltage was dropped entirely across the i-layer. The input face (P-AlGaAs) was AR coated using an etch-tuning method to prevent unwanted Fabry-Perot interference effects. The electric field in the wells was determined from the applied voltage with known doping profile by solving Poisson's equation. The built-in potential was found to be about 1 V.

Figure (3.2) shows the experimental setup used. A dye laser, using the dye Styryl 9M, was employed as the light source (although source tunability is not needed). The light was chopped at a reference frequency and then launched into and collected from the device using a pair of microscope objectives. Light was incident perpendicularly to the layers, i.e. the optical electric field vector was parallel to the MQW layers (TE polarization). A DC programmable power supply applied the reverse bias to the device while two computer controlled lock-in amplifiers

measured both the transmitted light intensity $P_t(\lambda_z, V)$, and the generated photocurrent $I_{ph}(\lambda_z, V)$. The latter is shown here for convenience and was not used in the evaluation.

Figure(3.3) shows the normalized P_t and I_{ph} at $\lambda_z = 860$ nm. We note that a dip in the measured P_t corresponds to a peak in the I_{ph} . The two features seen in Figure (3.3) correspond to the e-hh and the e-lh excitons. Those features occur when the e-hh and e-lh transition energy decreases due to the applied electric field until it matches the incident photon energy. If λ_z was higher, those features would have occurred at higher voltages. This is because the incident photon energy will be smaller and one needs more applied electric field to decrease the e-hh (or e-lh) transition energy so as to match the photon energy.

Before we explain the proposed technique, let us quickly verify the position of the e-hh exciton peak. For the particular sample used, calculations and measurements [2] indicate that the e-hh exciton peak at zero applied electric field occurs around 1465 meV. If $\lambda_z = 860$ nm (i.e. $E_z = 1441.9$ meV), then the energy difference between the heavy hole exciton energy at zero field $E_{hh}(0)$ and the incident photon energy E_z is 23.1 meV. The electric field F that will cause $E_{hh}(0)$ to decrease by that very same difference (i.e. 23.1 meV) can be readily calculated and is found to be about 103 kV/cm which corresponds to an applied voltage of about 9.3 V for this particular sample. Looking at Figure (3.3) it is clearly seen that the e-hh exciton peak truly occurs at 9.3 V.

3.3 Technique

From the geometry of the sample one can write for the transmitted light intensity $P_t(\lambda, V)$ in terms of the input coupled power P_c as :

$$P_t(\lambda, V) = P_c(1 - R)e^{-\alpha(\lambda, V)d} \quad (3.1)$$

where R is the reflection coefficient of the output facet (the AlGaAs/air interface) and d is the sum over the GaAs well widths ($.525 \mu m$), hence

$$\alpha(\lambda, V) = \frac{-1}{d} Ln \frac{P_t(\lambda, V)/P_c}{1 - R} \quad (3.2)$$

The coupled power can be written as $P_c = \eta_c P_{in}$, where η_c is the coupling efficiency and P_{in} is the incident power. η_c was assumed to be one since the light was sharply focused onto the sample which had a large aperture. Alternatively, one may use optical fibers to couple the light in and out of the sample. The input fiber should have a small diameter to insure that all the light is coupled into the fiber, and the output fiber should have a bigger diameter to insure that all the light emerging from the output face of the device was collected.

Figure (3.4) shows the absolute value of $\alpha(\lambda_x = 860 \text{ nm}, F)$ in cm^{-1} using equation (3.2) with the solution of Poisson's equation employed to convert the horizontal axes from voltage to electric field.

The optical absorption coefficient can be written as a product of the excitonic absorption peak α_{hh} and a line shape function [3]. Optical light modulators operate on the long wavelength side of the fundamental absorption edge which fits extremely well a Lorentzian line shape [4], so $\alpha(F, h\nu)$ can be written as :

$$\alpha(F, h\nu) = \frac{\alpha_{hh}(F)}{1 + \left[\frac{E_{hh}(F) - h\nu}{\Gamma_{hh}(F)} \right]^2} \quad (3.3)$$

Where $\alpha_{hh}(F)$ is the heavy hole absorption peak, $E_{hh}(F)$ is the heavy hole exciton energy, $\Gamma_{hh}(F)$ is the half width half maximum (HWHM) of the Lorentzian line shape, $h\nu$ is the incident photon energy and “n” is the Lorentzian line shape exponent which theoretically equals 2. We, however, found that a better fit is achieved with $n=2.5$. $\alpha_{hh}(F)$ is a measure of the e-hh interband absorption strength referred to as the “oscillator strength” which is proportional to the overlap between the electron and the hole wavefunctions. This overlap decreases as the applied field increases as the electrons and holes are pulled apart from each other to opposite sides of the quantum well, therefore one can write:

$$\alpha_{hh}(F) = constant \times \int_{-\infty}^{+\infty} |\Psi_e(z, F) * \Psi_h^*(z, F) dz|^2 \quad (3.4)$$

This constant of proportionality is easily calculated using the measured value of $\alpha_{hh}(F)$ and the calculated value of the overlap integral between the electron and hole wavefunctions at the same field F .

$E_{hh}(F)$ is the sum of the electron and hole energies in the z-direction minus the binding energy of the electron hole pair which has two components: the electron hole pair kinetic energy in the plane of the QW layers, and the potential energy due to their Coulomb interaction. We have used perturbation methods [4] to calculate the electron and heavy hole energy as well as the perturbed wavefunctions as a function of the applied field F . Details of the computation of the perturbed wavefunctions, (using perturbation methods), and the exciton binding energy, (using variational methods), as a function of the applied electric field is outlined in Appendix A.

We differ from [5] in the method used to calculate the exciton binding energy. We did not use variational techniques to calculate the perturbed electron and hole

wavefunctions, we instead used perturbation techniques which rendered more realistic electron and hole wavefunctions of finite penetration into the barriers as opposed to using an effective well thickness beyond which the electron and hole wavefunctions identically vanish. Figure (3.5) and (3.6) show the calculated $E_{hh}(F)$ and the oscillator strength $OSC_{str}(F)$ versus the applied electric field F in kV/cm respectively.

Now the HWHM of the exciton line shape $\Gamma_{hh}(F)$ in meV remains to be determined. This line shape is Lorentzian, it broadens as the electric field is increased. To determine this field dependence of $\Gamma_{hh}(F)$ we use equation (3.3) where $h\nu = E_x = 1441.9$ meV, $\alpha(F, h\nu)$ corresponds to an $\alpha(V, \lambda_x)$ is experimentally measured, $\alpha_{hh}(F)$ and $E_{hh}(F)$ are calculated numerically as indicated earlier, hence one can calculate for each value of the applied electric field F the corresponding $\Gamma_{hh}(F)$. Figure (3.7) shows $\Gamma_{hh}(F)$ using equation (3.3). The dots are the calculated $\Gamma_{hh}(F)$ using the measured data of $\alpha(F, 860$ nm) and the solid line is the fit in the least mean square error sense.

Figure (3.8) a and b schematically illustrates the technique we propose to measure the spectral dependence of electroabsorption in MQW structures. The usual technique, Figure 3.8 (a), of measuring the spectral dependence of electroabsorption $\alpha_a(F, \lambda)$ is to apply an electric field F_a to the device and sweep with the variable photon energy $h\nu_a$, then change the applied field and redo the $h\nu_a$ sweep again to obtain a family of curves each corresponding to a value of an applied field. However, in our technique Figure 3.8 (b), we keep the incident photon energy fixed at some properly chosen E_x and sweep the applied electric field increasing it from zero to get the $E_{hh}(0)$ to decrease and get closer and closer to

the photon energy E_x . The correspondence between the two techniques can be thought of as a one to one mapping from the energy domain to the electric field domain where increasing the photon energy $h\nu_a$ from E_x to $E_x + \Delta$ corresponds to finding the electric field F_b that will decrease $E_{hh}(0)$ by the same amount Δ , i.e. causing $E_{hh}(0)$ to decrease to $E_{hhb}(F_b) = E_{hh}(0) - \Delta$. Since we are interested in the long wavelength side of the fundamental absorption edge, the range over which $h\nu_a$ is scanned is from E_x to $E_{hha}(F_a)$, where F_a is the field at which we want to calculate α . This corresponds to decreasing $E_{hh}(0)$ until it reaches the value of $E_{hh}(0) - (E_{hha}(F_a) - E_x)$. Notice that the maximum decrease in $E_{hh}(0)$ is $\Delta_{max} = E_{hh}(0) - E_x$. Note also that the $h\nu_a$ sweep range decreases as F_a increases which is a manifestation of the shift of the e-hh exciton peak to lower energies as the applied field increases. Using equation (3.3) and (3.4) one may write α_a and α_b as :

$$\alpha_a(F_a, h\nu_a) = \frac{\alpha_{hha}(F_a)}{1 + \left[\frac{E_{hha}(F_a) - h\nu_a}{\Gamma_{hha}(F_a)} \right]^n} \quad (3.5)$$

and

$$\alpha_b(F_b, h\nu_b = E_x) = \frac{\alpha_{hhb}(F_b)}{1 + \left[\frac{E_{hhb}(F_b) - E_x}{\Gamma_{hhb}(F_b)} \right]^n} \quad (3.6)$$

or

$$\alpha_a(F_a, h\nu_a) = \alpha_b(F_b, E_x) \cdot \frac{osc_{str}(F_a)}{osc_{str}(F_b)} \cdot \frac{1 + \left[\frac{E_{hhb}(F_b) - E_x}{\Gamma_{hhb}(F_b)} \right]^n}{1 + \left[\frac{E_{hha}(F_a) - h\nu_a}{\Gamma_{hha}(F_a)} \right]^n} \quad (3.7)$$

Equation (3.7) was the formula used to deduce the α at a field F_a and photon energy $h\nu_a$. F_b is the applied field required to decrease $E_{hh}(0)$ by the amount $h\nu_a - E_x$. $\alpha_b(F_b, E_x)$ and $\Gamma_{hha,b}$ are measured quantities while $E_{hha,b}$ and the oscillator strengths are calculated numerically.

3.4 Results

Figure (3.9) shows the final result for the wavelength dependence of absorption coefficient for electric fields from 0 to 70 kV/cm. The family of curves are based on equation (3.7) for processing the measured data $P_t(V, 860 \text{ nm})$. The $\alpha(F, h\nu)$ measured by varying the wavelength is shown in figure (3.10). It is clear that the results of our technique as shown in figure (3.9) are in very good agreement with the spectral measurement of α .

One remaining point we would like to address is the proper choice of λ_z or the wavelength at which the measurement is performed. Clearly as λ_z increases one covers more range of the spectral dependence of α . The contrast between maxima and minima in $P_t(\lambda_z, V)$ decreases however as λ_z increases, since one moves away from the absorption edge. Consequently, performing the measurement at a long wavelength might affect the accuracy of the results. Nevertheless, this inconvenience can be taken care of by increasing the number of quantum wells in the transverse probe or sample to obtain a larger contrast in P_t .

At this point, we would like to elaborate on the practical significance of the technique we proposed. One might argue that for transverse probes a tunable coherent source is not really needed for the absorption coefficient measurement since one can use a white light source and a monochromator instead, which seems to be simpler and more direct. Apart from the fact that using a non coherent light source for electroabsorption measurement is susceptible to noise and can not be used for waveguide type samples. For some III-V materials $\alpha_{hh}(0)$ is not as high as that of GaAs/AlGaAs based devices and hence one needs a large number of QW layers to obtain a large enough contrast in the measured transmitted

light intensity P_t as a function of the applied voltage. This very large number of QW's may lead to non-uniformity in the thickness of the wells and consequently less meaningful data. Furthermore, transverse probes are not suitable if electroabsorption was to be measured for TM polarized light. The solution to the above problems is to use waveguide probes where fewer QW layers are enough to obtain an acceptable contrast in P_t . Indeed a proper choice of the waveguide probe length (L) can lead to a better contrast in P_t compared to transverse probes. Also waveguide probes support both TE and TM light polarizations. For waveguide type probes, one definitely needs a tunable coherent light source which is expensive, and may not be readily available in every lab. Here comes the strength and practical significance of the method we proposed, which uses a fixed wavelength coherent source and a programmable DC power supply which are more readily available in practically every lab, hence can be used at an advantage to measure the spectral dependence of α in waveguide structures made up of any material composition. Of course, for waveguide structures one will need to determine the confinement factor in both the transverse and lateral directions which can be easily calculated for a given device material and geometry.

3.5 Conclusion

We have proposed, for the first time, a useful and a rather simple technique that can be used to calculate the spectral dependence of electroabsorption in MQW based structures by measuring the transmitted light intensity as a function of the applied electric field. The technique does not require a tunable light source to characterize the device but rather a readily available programmable power supply. This technique can be used for MQW devices of any material composition, and

provides a useful tool for optical modulator design and development.

3.6 Acknowledgement

We would like to thank Mr. K. Jelly of MOTOROLA INC, Schaumburg, IL, for providing the transverse probe and the measured $\alpha(F, \lambda)$ shown in figure (3.10). That sample was produced at the Siemens Research and Technology Laboratories in Princeton, NJ.

3.7 Appendix A

In this appendix we describe in detail how we computed the electron-heavy hole exciton binding energy as a function of the applied electric field in GaAs/AlGaAs Multiple Quantum Well structures.

Within the effective mass approximation, the electron-hole Hamiltonian can be written as:

$$\begin{aligned}
 H &= H_{ez} + H_{hz} + H_{eh} \\
 &= H_{KEZe} + V_e(z_e) + eFz_e + H_{KEZh} + V_h(z_h) - eFz_h - H_{KEreh} - V_{eh}(r, z_e, z_h)
 \end{aligned} \tag{3.8}$$

where we have the following:

1. z_e and z_h are the coordinates perpendicular to the plane QW layers for the electrons and holes respectively.
2. "r" is the relative position of the electron and the hole in the plane of the QW layer.

3.

$$\begin{aligned}
 H_{KEZe} &= -\frac{\hbar^2}{2m_{e\perp}^*} \frac{\partial^2}{\partial z_e^2} \\
 H_{KEZh} &= -\frac{\hbar^2}{2m_{h\perp}^*} \frac{\partial^2}{\partial z_h^2}
 \end{aligned} \tag{3.9}$$

are the kinetic energy operators for the electron and hole respectively in the z direction, with $m_{e\perp}^*$ and $m_{h\perp}^*$ being the effective masses of the electron and hole respectively in the z direction.

4. $V_e(z_e)$ and $V_h(z_h)$ are the built-in rectangular quantum-well potentials for the electron and hole respectively.

5. F is the applied electric field normal to the QW layers.

6.

$$H_{KErch} = -\frac{\hbar^2}{2\mu} \frac{\partial^2}{\partial r^2} \quad (3.10)$$

is the kinetic energy operator of the relative motion of the electron and hole with

$$\mu = \frac{m_{e\parallel}^* m_{h\parallel}^*}{m_{e\parallel}^* + m_{h\parallel}^*}$$

being the reduced effective mass in the plane of the layers ($m_{e\parallel}^*$ and $m_{h\parallel}^*$ are the effective masses of the electron and hole, respectively, in the plane of the layers).

7.

$$V_{eh}(r, z_e, z_h) = -\frac{e^2}{4\pi\epsilon[|z_e - z_h|^2 + r^2]^{1/2}} \quad (3.11)$$

is the Coulomb potential energy due to the electron-hole attraction.

To attempt a full solution of $H\psi = E\psi$, where H is given by (3.8), we use a mix of perturbational and variational methods with the separable trial function:

$$\psi(r, z_e, z_h) = \psi_e(z_e) \psi_h(z_h) \phi_{eh}(r) \quad (3.12)$$

where $\psi_e(z_e)$ and $\psi_h(z_h)$ are the exact wavefunctions of the individual electrons and holes in the one-dimensional quantum wells with the applied field F [i. e. , the lowest eigenfunctions of $H_{KEZe} + V_e(z_e) - eFz_e$ and the equivalent for holes], and

$$\phi_{eh}(r) = \sqrt{\frac{2}{\pi}} \frac{1}{\lambda} e^{-\frac{r}{\lambda}} \quad (3.13)$$

(i. e. , we chose a simple 1-s like orbital for the in-plane radial motion) with λ , the amplitude diameter of the exciton orbit as a variational parameter.

Formally evaluating the expectation value of H we obtain:

$$\langle \psi | H | \psi \rangle = E_{ez} + E_{hz} + E_b \quad (3.14)$$

where E_{ez} , E_{hz} and E_b are the energies of the individual electrons and holes kinetic energy in the z direction and E_b is the exciton binding energy we are interested in and is given by:

$$E_b = E_{KEr} + E_{PEr} \quad (3.15)$$

where E_{KEr} is the kinetic energy of the relative electron-hole motion in the QW layer plane and is given by:

$$E_{KEr} = \langle \phi_{eh} | H_{KEr} | \phi_{eh} \rangle \quad (3.16)$$

and E_{PEr} is the Coulomb potential energy of the electron-hole relative motion, is given by:

$$E_{PEr} = \langle \psi | V_{eh} | \psi \rangle \quad (3.17)$$

E_{PEr} is of course dependent on the variational parameter λ . The calculation of (3.16) is straight forward

$$\begin{aligned} E_{KEr} &= \langle \phi_{eh} | -\frac{\hbar^2}{2\mu} \frac{\partial^2}{\partial r^2} | \phi_{eh} \rangle \\ &= -\frac{\hbar^2}{2\mu} \frac{2}{\pi} \frac{1}{\lambda^4} \int_{\theta=0}^{2\pi} \int_{r=0}^{\infty} r e^{-\frac{2r}{\lambda}} dr d\theta \end{aligned}$$

or

$$E_{KEr} = \frac{\hbar^2}{2\mu\lambda^2} \quad (3.18)$$

The evaluation of the integrals in (3.17) are more involved. The fact that the wavefunction ψ is separable is of less importance here because the potential V_{eh} couples all variables. This integral in 3.17) will be carried out partly analytically (the integration over r) and partly numerically (the integration over z_e and z_h). Using (3.11), (3.12), (3.13) and (3.17) we have:

$$E_{PEr} = -\frac{e^2}{2\pi^2\epsilon\lambda^2} \int_{\theta=0}^{2\pi} \int_{z_e=-\infty}^{+\infty} \int_{z_h=-\infty}^{+\infty} \psi_e^2(z_e)\psi_h^2(z_h) \int_{r=0}^{\infty} \frac{r e^{-\frac{2r}{\lambda}}}{[(z_e - z_h)^2 + r^2]^{1/2}} dr dz_e dz_h d\theta \quad (3.19)$$

The integral over θ in (3.19) is trivial and the integral over r can be performed using integration tables, yielding:

$$\begin{aligned} G(\gamma) &= \frac{2}{\lambda} \int_{r=0}^{\infty} \frac{r e^{-\frac{2r}{\lambda}}}{\sqrt{\gamma^2 + r^2}} dr \\ &= \frac{2|\gamma|}{\lambda} \frac{\pi}{2} [H_1\left(\frac{2|\gamma|}{\lambda}\right) - Y_1\left(\frac{2|\gamma|}{\lambda}\right)] - 1 \end{aligned} \quad (3.20)$$

where $H_1(u)$ is the first-order Struve function and Y_1 is the first order Bessel function of the second kind (Neumann function) and $\gamma = z_e - z_h$.

$\psi_e(z_e)$, $\psi_h(z_h)$ in (3.19) and E_{ez} , E_{hz} in (3.14) are obtained by solving:

$$(H_{KEze} + V_e(z_e) - eFz_e) \psi_e(z_e) = E_{ez} \psi_e(z_e) \quad (3.21)$$

and the equivalent for holes. We use perturbation methods to solve (3.21). In this method, the potential of the applied field (eFz) is considered as a perturbation

to the Hamiltonian and the perturbed wavefunctions ($\psi_e(z_e)$ and $\psi_h(z_h)$) are expressed as a linear combination of the unperturbed wavefunctions ($\psi_e^0(z_e)$ and $\psi_h^0(z_h)$), i.e. the bound states of the electrons and holes with no applied electric field (actually they are not truly bound states due to the finite height of the potential barriers), so we can write:

$$\psi_{e,h}(Z) = \sum_i a_{i e,h} \psi_{i e,h}(Z) \quad (3.22)$$

substituting (3.22) into (3.21) the problem is transformed into an eigen value problem with the following matrix to diagonalize:

$$\begin{bmatrix} \Delta E_0 & & p_{ij} \\ & E_1 - E_0 - \Delta E_0 & \\ p_{ij} & & E_i - E_0 - \Delta E_0 \end{bmatrix} (a_i) = 0 \quad (3.23)$$

where

$$\begin{aligned} p_{ij} &= \pm eF \int_{-\infty}^{\infty} \psi_i^0(z_{e,h}) z_{e,h} \psi_j^0(z_{e,h}) dz_{e,h} && \text{for } (i+j) \text{ odd} \\ &= 0 && \text{for } (i+j) \text{ even} \end{aligned} \quad (3.24)$$

Figure (3.11) shows the perturbed electron and hole wavefunctions for different applied electric fields.

The double integral over z_e , z_h :

$$E_{PEr} = -\frac{e^2}{2\pi\epsilon\lambda} \int_{z_e=-\infty}^{\infty} \int_{z_h=-\infty}^{\infty} \psi_e^2(z_e) \psi_h^2(z_h) G(r) dz_e dz_h \quad (3.25)$$

is then evaluated numerically for every given λ and applied electric field.

The limits of integration for $z_{e,h}$ was taken from $-2d$ to $+2d$, where d is the quantum well thickness. These limits were found adequate since the penetration of the electron and hole wavefunctions in the barrier layers becomes insignificant beyond that. The value of λ that minimizes E_b given by (3.15) is the exciton diameter and corresponding E_b is the exciton binding energy.

The exciton binding energy decreases as the electric field is increased since the electron and the hole are pushed apart from each other and hence their Coulomb attraction forces are decreased. The decrease in the exciton binding energy as the electric field was increased from $0 \rightarrow 100\text{kV/cm}$ is 1.48mev . Figure (3.12) shows the calculated exciton binding energy as a function of the applied electric field.

References

- [1] D. Miller, D. Chemla, T. Damen, A. Gossard, W. Weigman, T. Wood, and C. Burrus, "Band edge electroabsorption in quantum well structures: The quantum confined Stark effect", *Phys. rev. letters*, Vol. 53, pp 2173-2176, 1984.
- [2] K. Jelly, K. Alavi, and R. Engelman, "Experimental determination of electroabsorption in GaAs/AlGaAs Multiple Quantum Wells as a function of well width", *Electronics Letters*, Vol. 24, pp 1555-1557, 1988.
- [3] K. Nishi and T. Hiroshima, "Enhancement of quantum confined Stark effect in a graded gap quantum well." *Appl. Phys. Lett.*, vol 51, pp.320-322, 1987
- [4] G. Lengyel, K. Jelly, and R. Engelmann, "A semi-empirical model for Electroabsorption in GaAs/AlGaAs Multiple Quantum Well modulator structures". *J. of Quantum Electronics*, vol 26, 1990, pp 296-304
- [5] D. Miller, D. Chemla, T. Damen, A. Gossard, W. Weigman, T. Wood, and C. Burrus, "Electric field dependence of optical absorption near the band edge of quantum well structures." *Phys. Rev.*, Vol B32, pp 1043-1060, 1985.

3.8 Figure captions

3.1- Cross section of the transverse MQW structure used in experiment showing thicknesses, material compositions, and doping profiles.

3.2- Experimental setup used to measure the transmitted light intensity P_t and the generated photocurrent I_{ph} .

3.3- Measured transmitted light intensity P_t (solid line), and generated photocurrent I_{ph} (broken line) at $\lambda=860$ nm as a function of applied voltage.

3.4- Absolute value of absorption coefficient at 860 nm as a function of the applied electric field in kV/cm.

3.5- Heavy hole exciton energy $E_{hh}(F)$ as a function of the applied electric field.

3.6- Normalized oscillator strength for the heavy hole exciton as function of the applied electric field.

3.7- Half width half maximum (HWHM) of the heavy hole Lorentzian line shape as a function of the applied electric field.

3.8- Schematic illustration of the technique used to deduce the spectral dependence of electroabsorption. a) describes the traditional technique while b) describes the technique we propose.

3.9- Calculated spectral dependence of absorption coefficient shown for electric fields from 0 to 70 kV/cm, extracted from measurement of transmitted light intensity at 860 nm as a function of applied voltage.

3.10- Measured spectral dependence of absorption coefficient for the 10.5 nm transverse probe at different values of the applied voltage/field.

3.11- Perturbed electron and hole wavefunctions for different values of the applied electric field. a) for electrons, b) for holes.

3.12- Calculated exciton binding energy as a function of applied electric field.

Figure 3.1: Cross section of the transverse MQW structure.

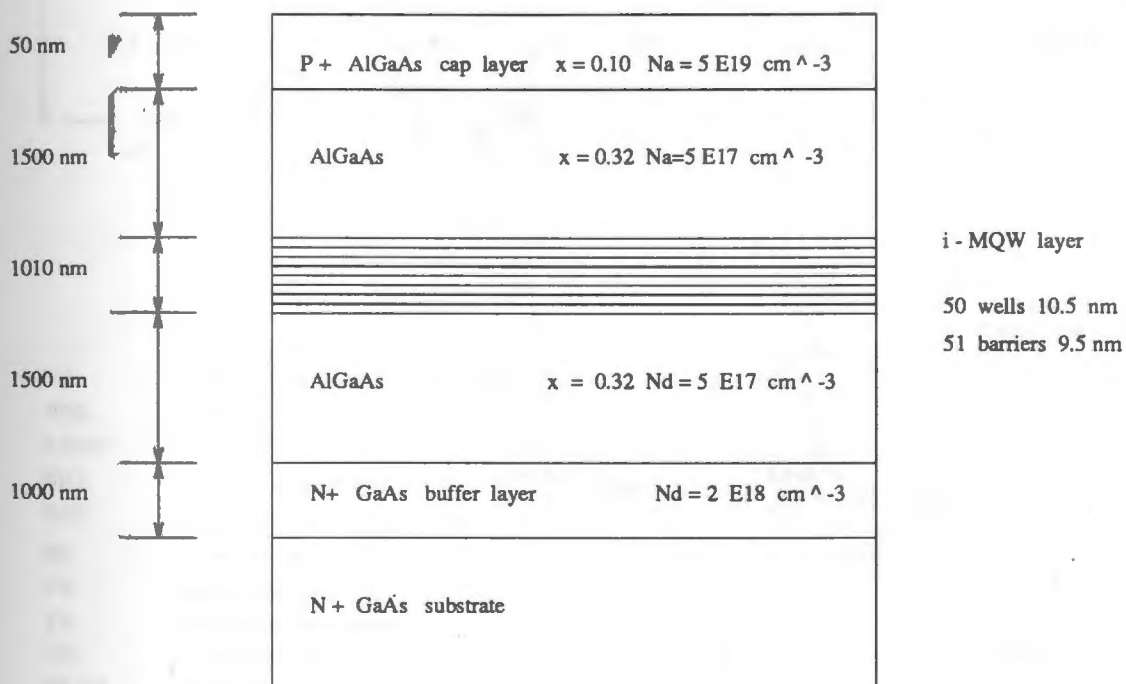


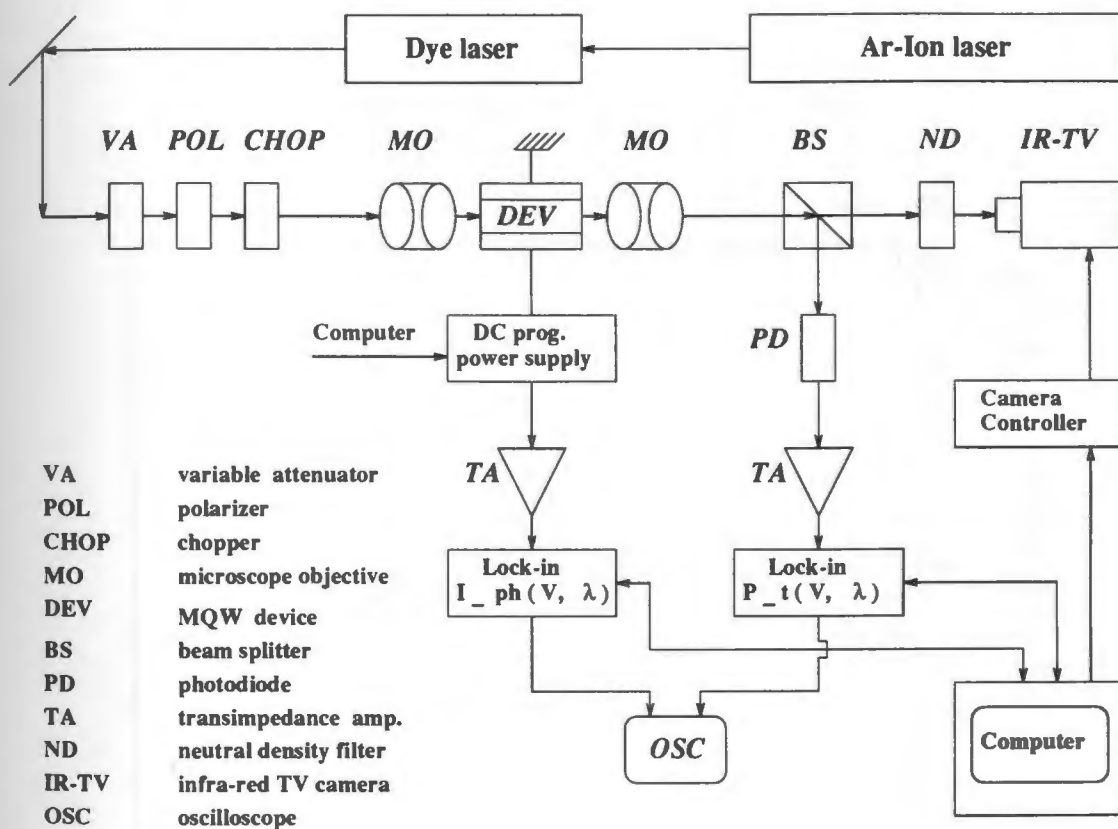
Figure 3.2: Experimental setup used to measure P_t and I_{ph} .

Figure 3.3: Measured P_t , and I_{ph} at $\lambda=860$ nm as a function of voltage.

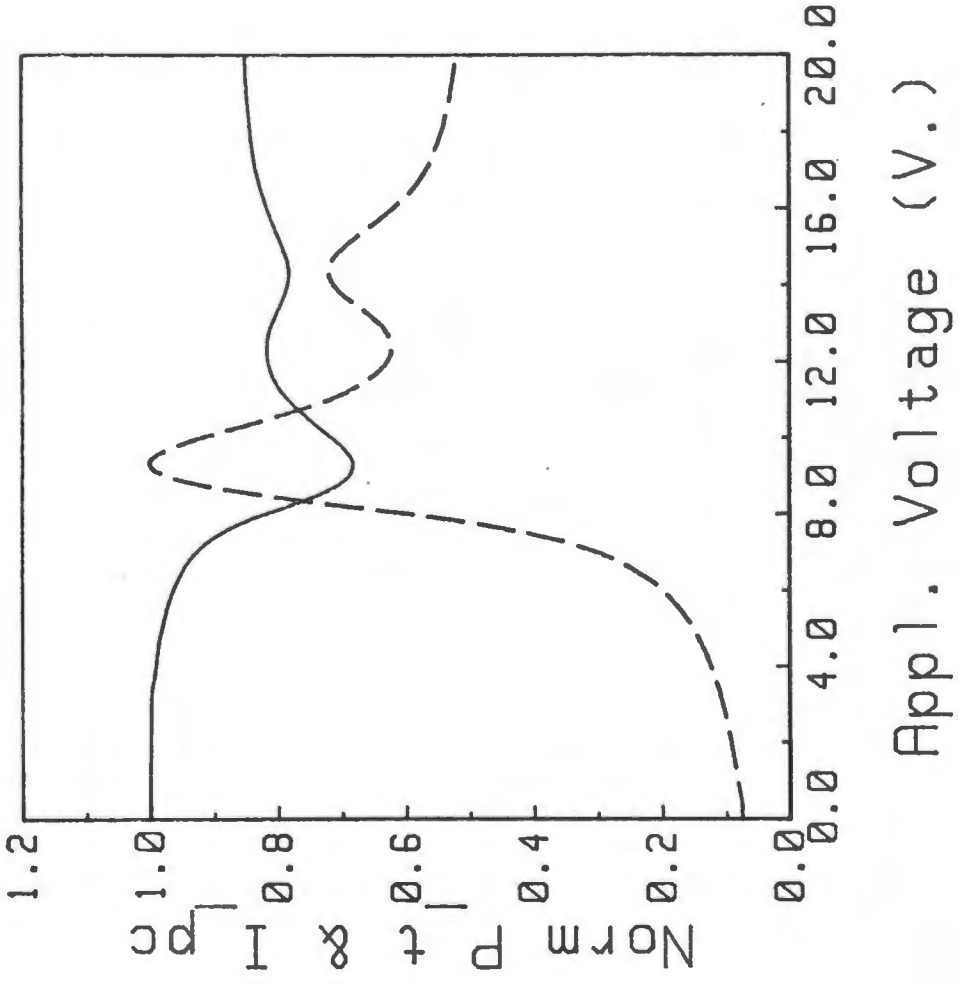


Figure 3.4: Absorption coefficient at 860 nm as a function of applied electric field.

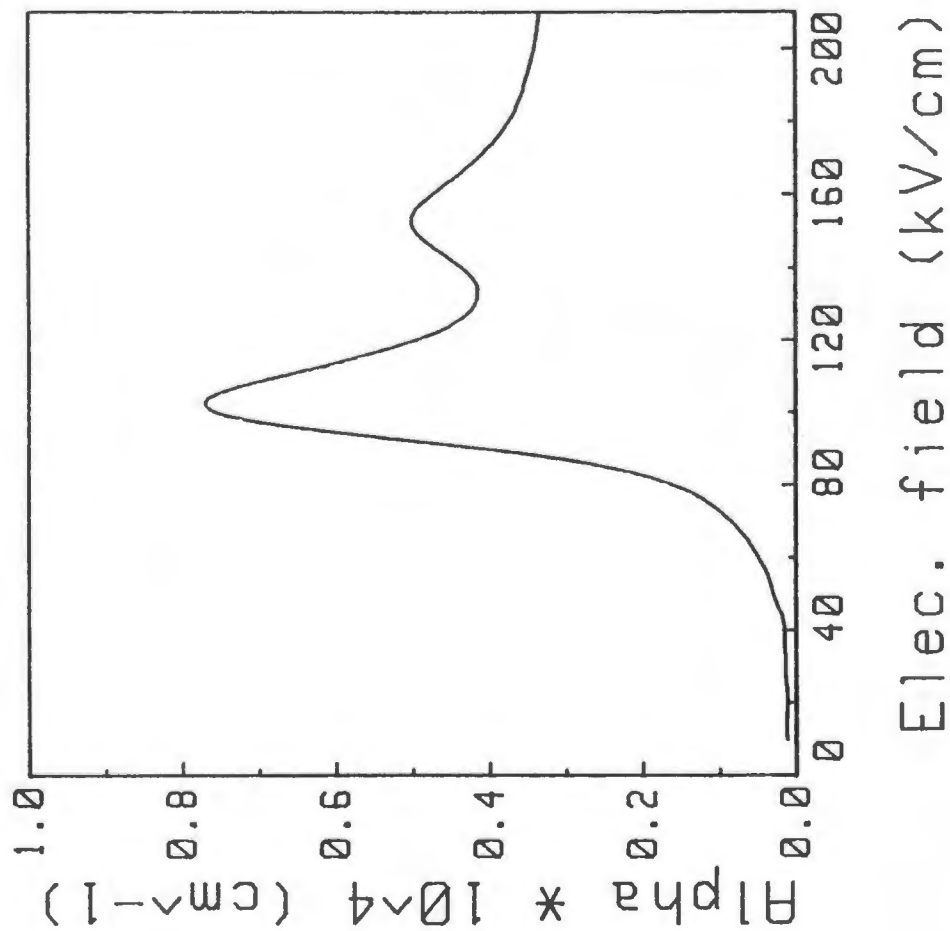


Figure 3.5: Heavy hole exciton energy $E_{hh}(F)$ as a function of applied electric field.

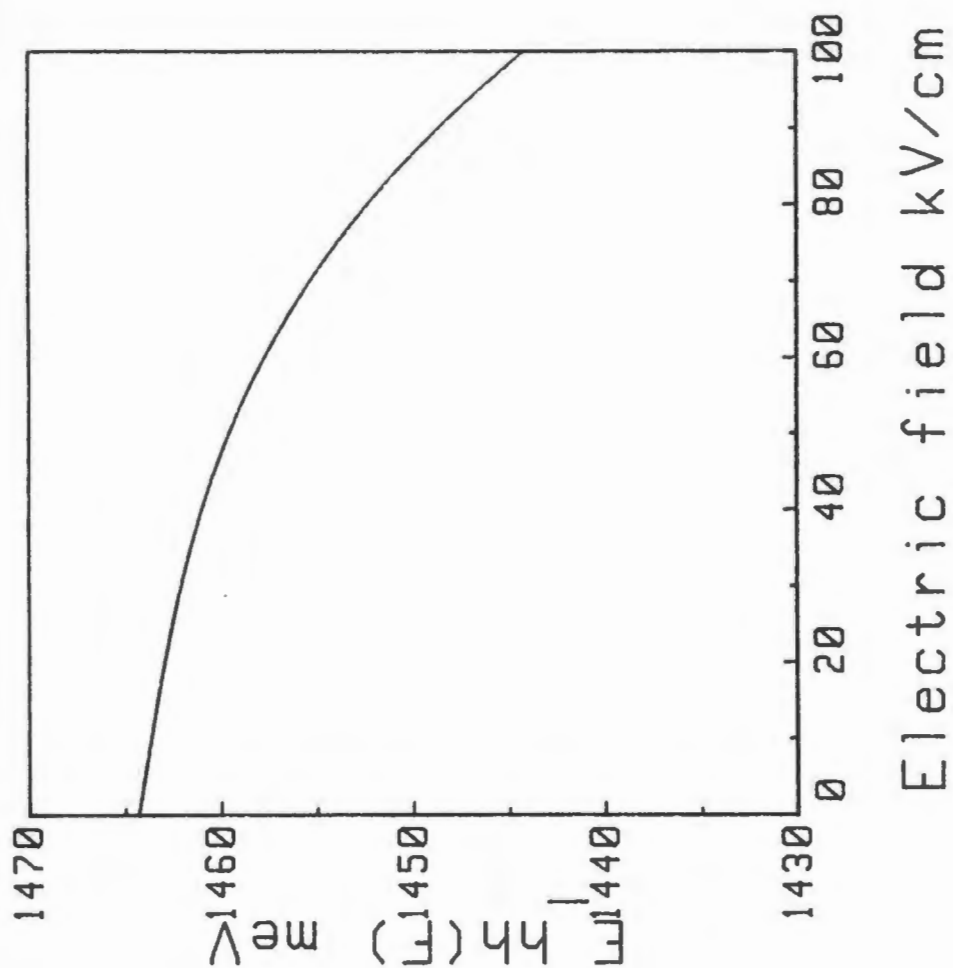


Figure 3.6: Normalized oscillator strength for the heavy hole exciton as function of applied electric field.

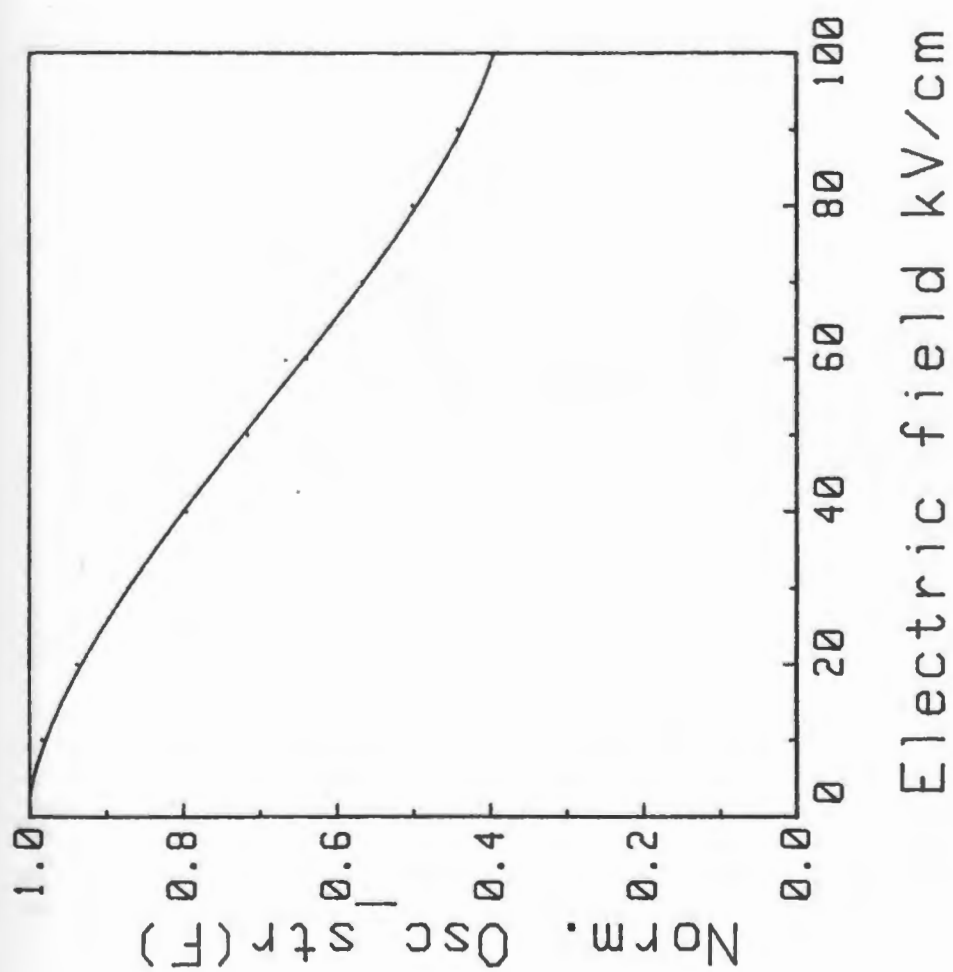


Figure 3.7: HWHM of the heavy hole Lorentzian line shape as a function of applied electric field.

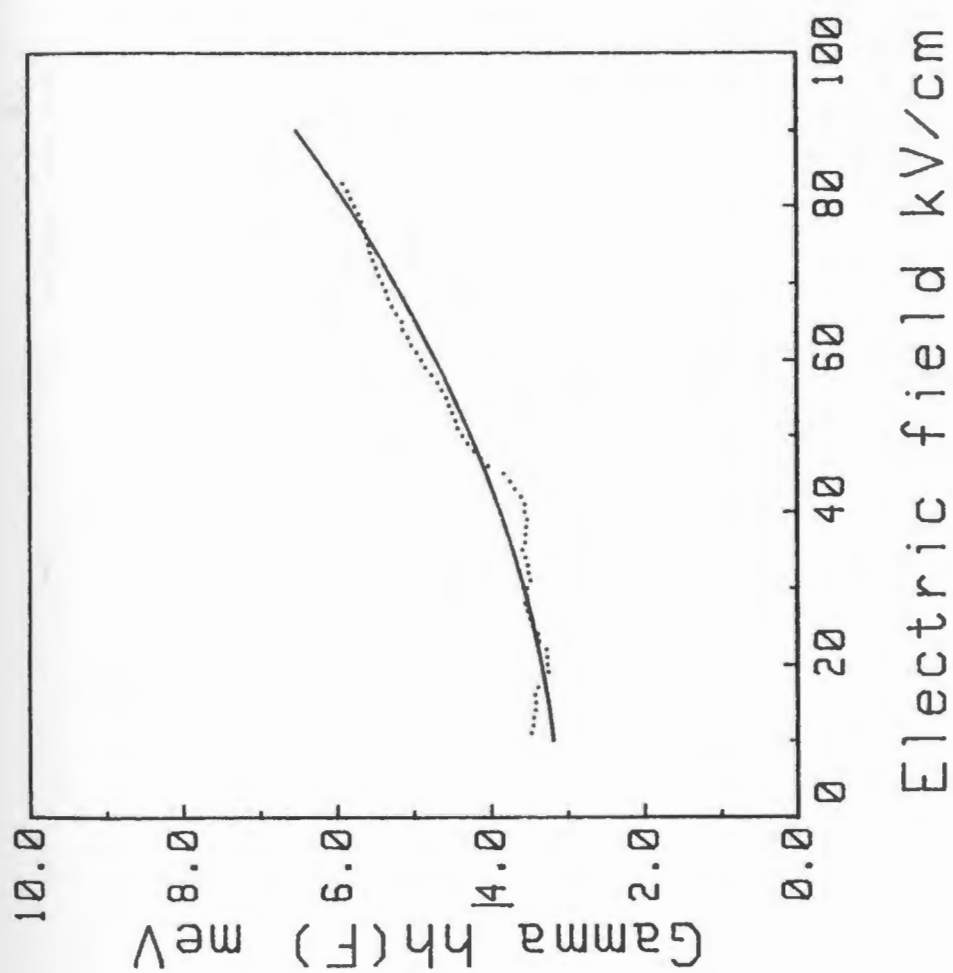


Figure 3.8: Schematic illustration of the technique used to deduce the spectral dependence of electroabsorption.

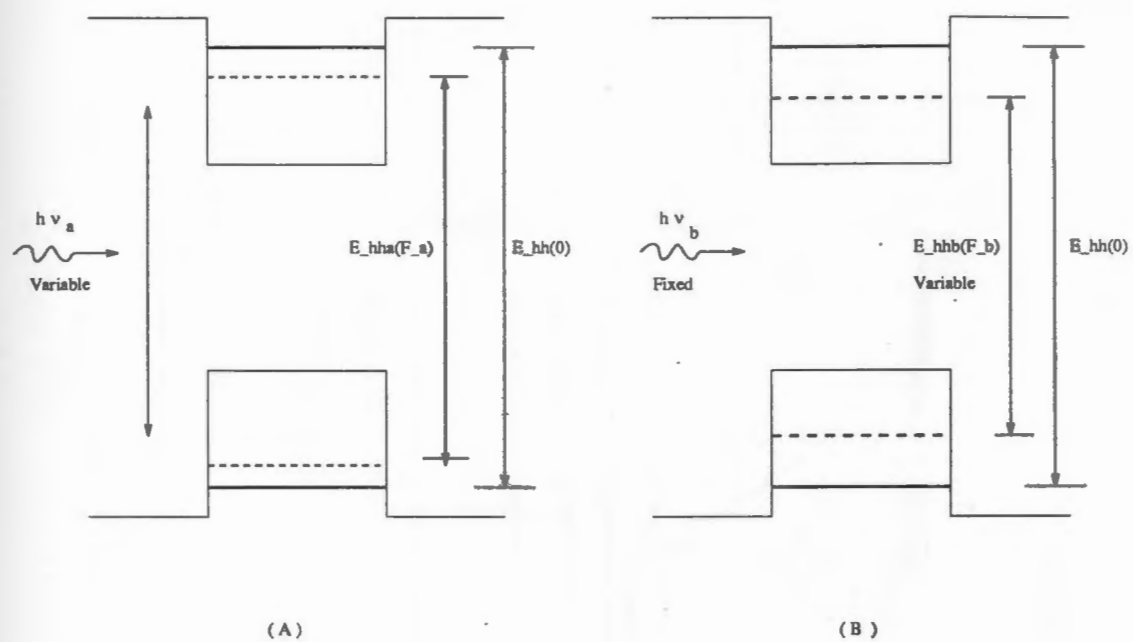


Figure 3.9: Calculated spectral dependence of the absorption coefficient for different values of applied field.

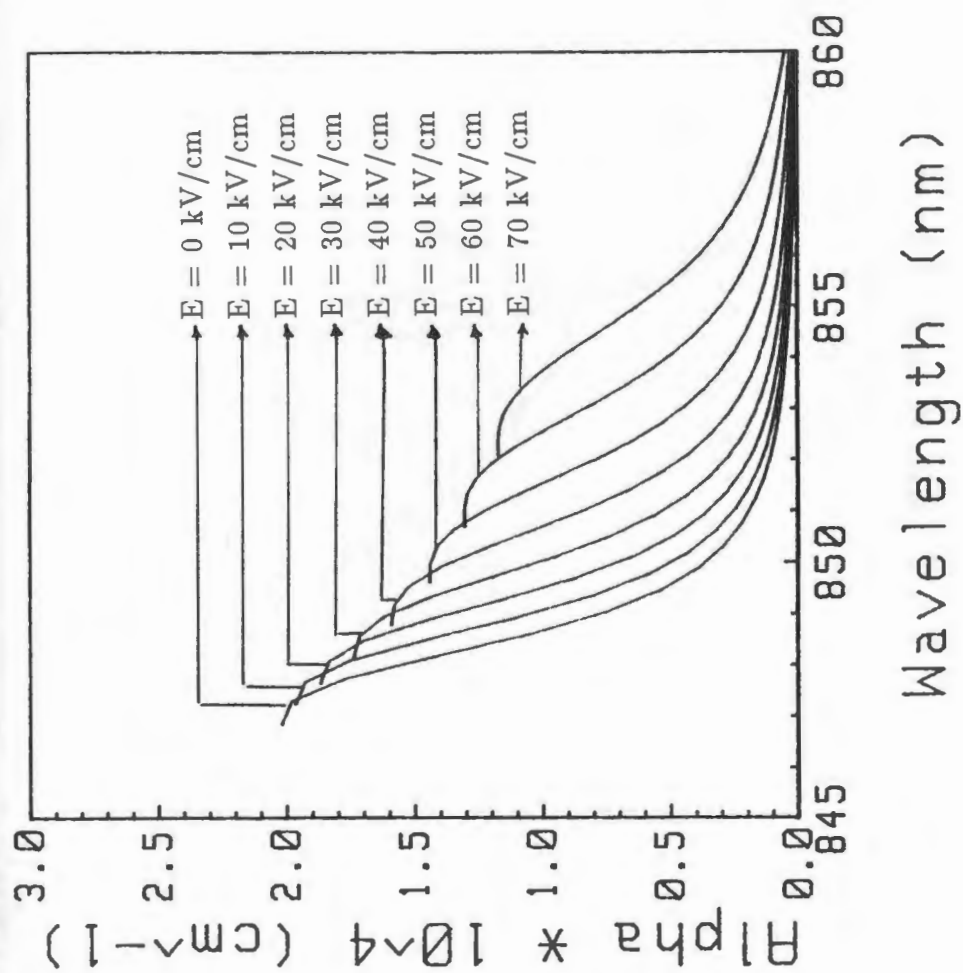


Figure 3.10: Measured spectral dependence of absorption coefficient for different values of applied voltage/field.

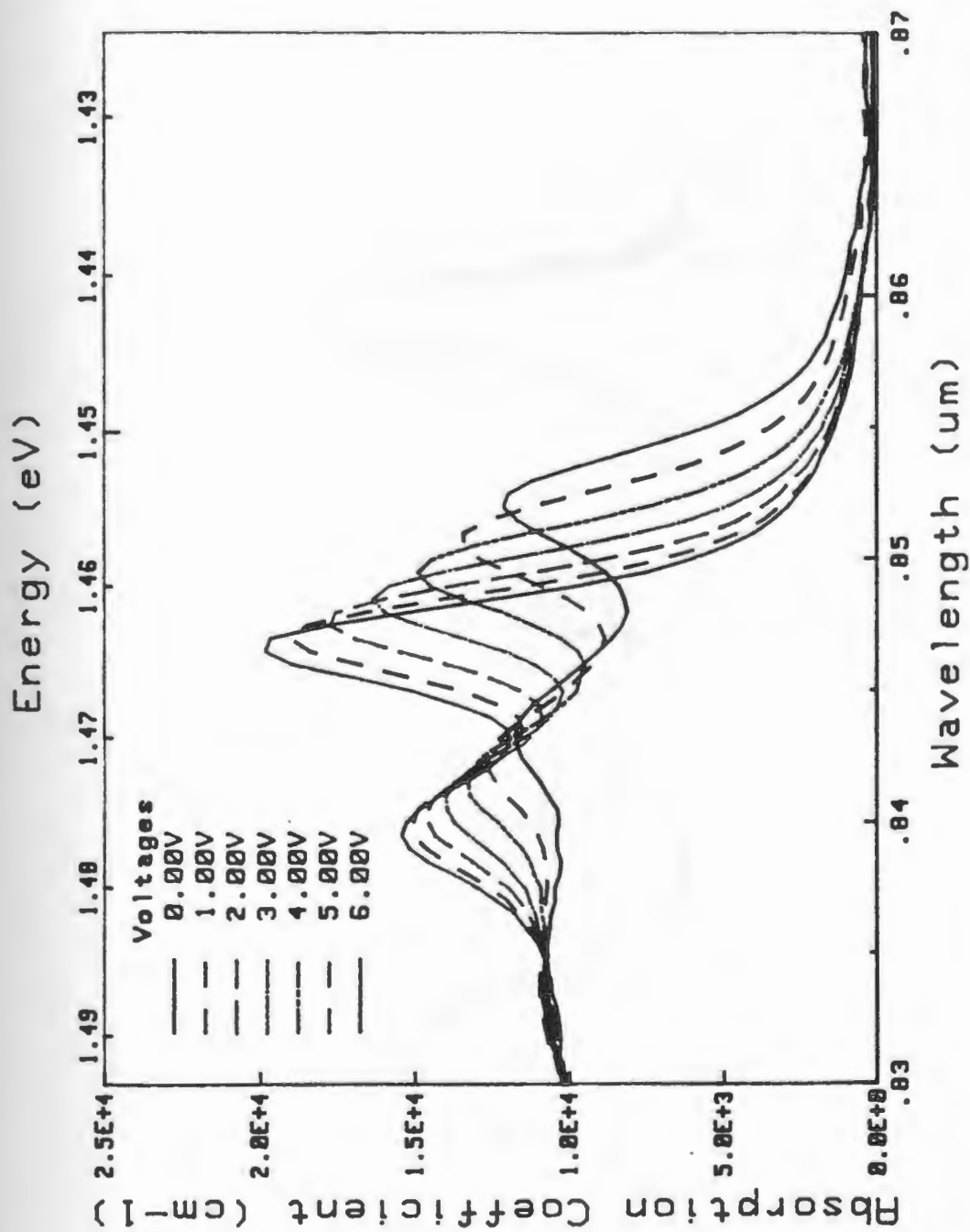


Figure 3.11: Perturbed electron and hole wavefunctions for different values of applied field. a) for electrons, b) for holes.

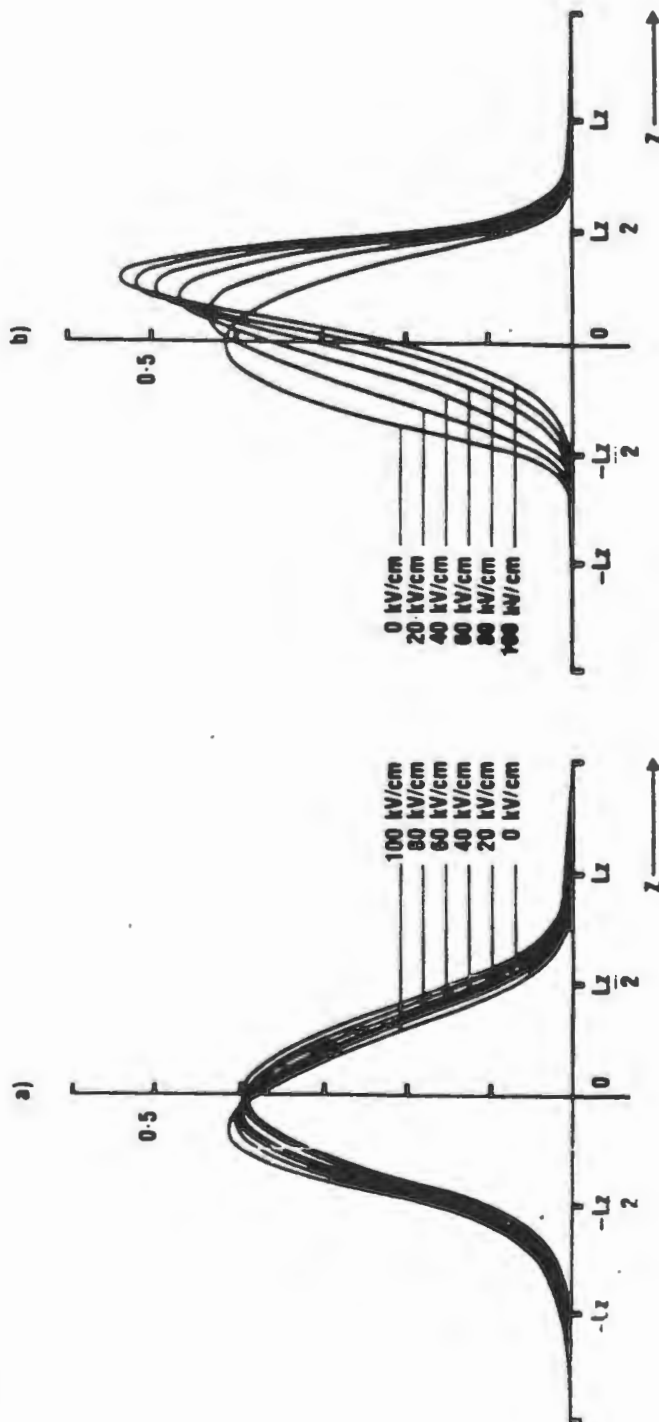
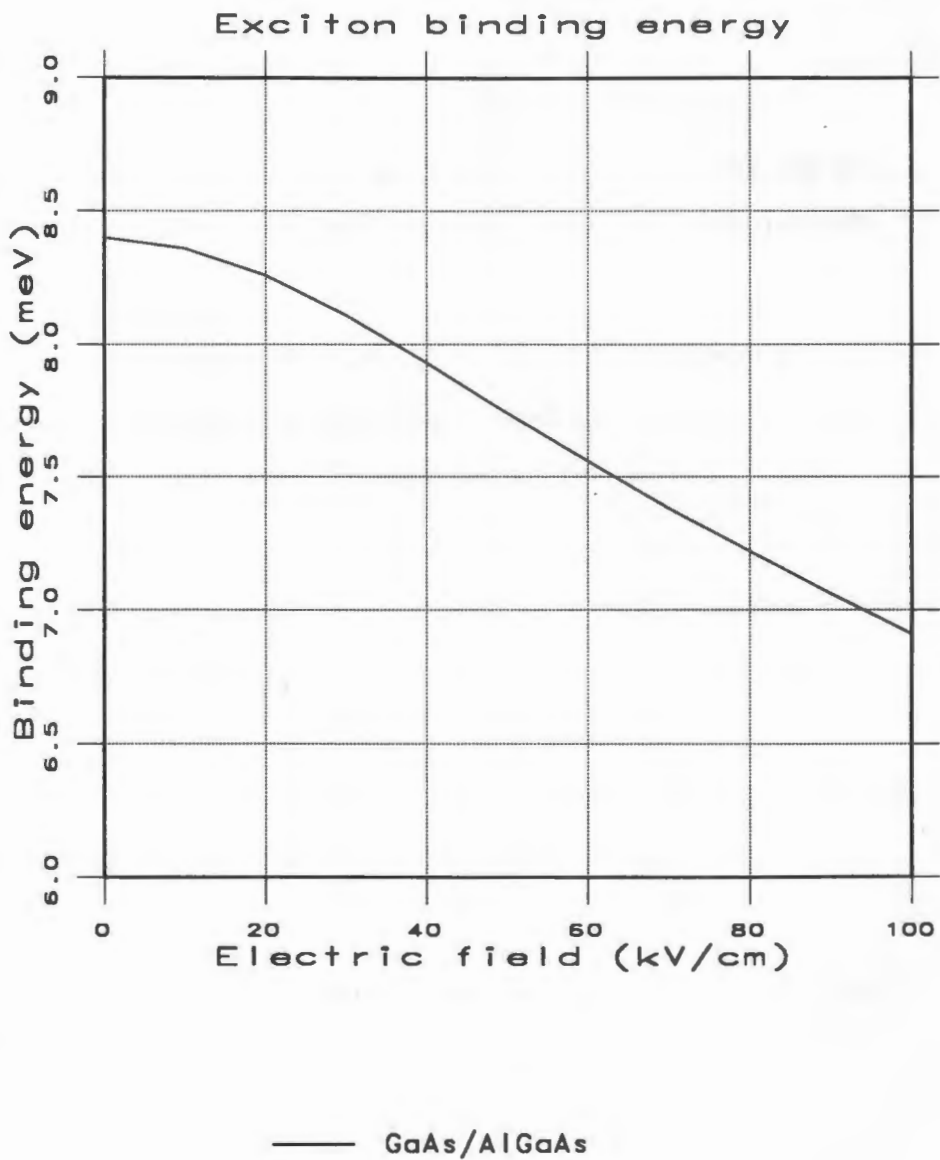


Figure 3.12: Calculated exciton binding energy as a function of applied field.



BIBLIOGRAPHY

Afromovitz, M. A., "Refractive index of $\text{Ga}_{1-x}\text{Al}_x\text{As}$ ", *Solid State Communication*, volume 15, pp. 59-63, 1974.

Tsuneya Ando, "Hole subband at GaAs/AlGaAs heterojunctions and quantum wells.", *Journal of the physical society of Japan*, volume 54, 1985, pp 1528-1536.

M. Altarelli, "Band structure, Impurities, and Excitons in superlattices.", *Heterojunction and semiconductor superlattices*, edited by G. Allan, G. Bastard, N. Boccara, M. Lannoo and M.Voos, Springer Verlag, pp 12-37.

Arfken, G. , *Mathematical Methods for Physicists*, p. 421, Academic Press, Orlando, 1985.

G. Bastard, and A. Brum "Electronic states in semiconductor heterostructures." *Journal of Quantum Electronics*, volume 22 , no(9), 1986, p. 1625.

Casey, H. C., and Panish, M. B., *Heterostructure Lasers*, (Academic Press, New York, 1978), Part A, p. 193.

Cook, Jr., W. R., and Jaffe, H., in *Electro-optic Coefficients*, edited by L. Bornstein, (Springer, 1979), volume 11, New Series.

S. Datta, "Quantum phenomena.", Modular series on solid state devices, edited by R. Pierret, and G. Neudeck, volume VIII Addison-Wesley publishing company, 1989, PP 201.

R. Dingle, in *Festkoerperprobleme*, edited by H. J. Queisser, (Pergamon, New York, 1975), volume 15, p. 21.

Erman, M., Vodjdani, N., Jarry, P., Graziani, D., and Pinhas, H., "Optical and electrooptical analysis of GaAs inverted rib phase modulators grown by vapor phase epitaxy", *IEEE Journal of Lightwave Technology*, volume LT-4, pp. 1524-1533, 1986.

Faist, J., Reinhart, F. K., Martin, D., and Tuncel, E., "Orientation dependence of the phase modulation in a p-n junction GaAs/AlGaAs waveguides", *Applied Physics Letters*, volume 50, pp. 68-70, 1987.

Glick, M., Reinhart, F. K., Weimann, G., Schlapp, W., "Quadratic electro-optic light modulation in GaAs/AlGaAs multiquantum well heterostructure near the excitonic gap", *Applied Physics Letters*, volume 48, pp. 989-991, (1986).

C. Jagannath, E. Koteles, J. Lee, J. chen, B. Elman, and Y. Chi, *Physical review B*, volume 34, 1986, P 7027.

Jelley, K. W., Alavi, K., and Engelmann, R. W. H., "Experimental determination of electroabsorption in GaAs/Al_{0.32}Ga_{0.68}As MQW structures as function of well width", *Electronics Letters*, volume 24, pp. 1555-1557, 1988.

Jelley, K. W., and Engelmann, R. W. H., "An etch tunable antireflection coating surface for the controlled elimination of Fabry-Perot oscillations in the optical spectra of transverse modulator structures", *IEEE Photonics Technology Letters* volume 1, 235-237, 1989.

K. Jelly, K. Alavi, and R. Engelman,"Experimental determination of electroabsorption in GaAs/AlGaAs Multiple Quantum Wells as a function of well width", *Electronics Letters*, volume 24, pp 1555-1557, 1988.

Jelley, K. W., Engelmann, R. W. H., Alavi, K., and Lee, H., "Well size related limitations on maximum electro-absorption in GaAs/AlGaAs MQW structures", *Applied Physics Letters*, volume 55, pp. 70-72, July 1989.

Keldysh, L. V., "The effect of a strong electric field on the optical properties of insulating crystals", *Soviet Physical Journal -JETP*, volume 34(7), pp. 788-790, 1958.

Kittel, C., *Introduction to Solid State Physics*, 6th Ed., (John Wiley & Sons, Inc., 1986).

Knuth, Donald E., *The TEXbook*, (Addison Wesley, Reading, Mass., 1986).

Lengyel, G., Jelley, K. W., and Engelmann, R. W. H., "A semi-empirical model for electro-absorption in GaAs/AlGaAs multiple quantum well modulator structures", *IEEE Journal of Quantum Electronics*, volume QE-26, pp. 296-304, 1990.

J. M. Luttinger and W. Kohn, "Motion of electrons and holes in perturbed periodic fields.", *Physical review*, volume 97, 1955, PP 869-883.

J. Manning and R. Olshansky, "The carrier induced index change AlGaAs and 1.3 μm InGaAsP diode lasers", *IEEE Journal of Quantum Electronics*, volume QE-19, pp. 1525-1530, 1983.

Mendoza-Alvarez, J. G., Yan, R. H., Coldren, L. A., "Contribution of the band filling effect to the effective refractive-index change in double heterostructure GaAs/AlGaAs phase modulators", *Journal of Applied Physics*, volume 62, pp. 4548-4553, (1987).

D. Miller, D. Chemla, T. Damen, A. Gossard, W. Wiegman, T. Wood, and C. Burrus, "Band edge electroabsorption in quantum well structures: The quantum confined stark effect.", *Physical Review letters*, volume 53, No. (22), 1984, P. 2173.

D. Miller, D. Chemla, T. Damen, A. Gossard, W. Wiegman, T. Wood, and C. Burrus, "Electric field dependence of optical absorption near the band edge of

quantum well structures." *Physical Review*, volume B32, 1985, P. 1043.

D. Miller, D. Chemla, T. Damen, A. Gossard, W. Wiegman, T. Wood, and C. Burrus, "Electric field dependence of linear optical properties in Quantum well structures: Waveguide electroabsorption and sum rules." *Journal of Quantum Electronics*, volume 22 , no(9), 1986, P.1826.

R. C. Miller, D. A. Kleinman, W. A. Nordland, and A. C. Gossard, *Physical review B*, volume 22, 1980, P863.

Namba, S., "Electro-optical effects of zincblende", *Journal of the Optical Society of America*, volume 51, pp. 76-79, 1961.

K. Nishi and T. Hiroshima,"Enhancement of quantum confined Stark effect in a graded gap quantum well." *Applied Physics Letters*, volume 51, pp.320-322, 1987.

Nye, J. F., *Physical Properties of Crystals*, Oxford University Press, 1957.

Ramo, S., Whinnery, J. R., Van Duzer, T., *Fields and Waves in Communication Electronics*, 2nd Ed., John Wiley & Sons, Inc., (1984).

G. D. Sanders, Yia-Chung Chang, "Optical properties in modulation-doped GaAs-GaAlAs quantum wells.", *Physical review B*, volume 31, 1985, PP 6892-6895.

G. D. Sanders, Yia-Chung Chang, *Physical review B*, Vol 32, 1985, P 4282.

J. N. Schulman, Yia-Chung Chang, "Band mixing in semiconductor superlattices.", *Physical review B*, volume 31, 1985, PP 2056-2068.

Seraphim, B. O., Bottka, N., "Franz-Keldysh effect of the refractive index in semiconductors, *Physical Review*, volume 139, pp. A560–A565, (1965).

M. Shinada, and M. Sugano *Journal of the Physical society of Japan*, volume 21, 1966, P 1396.

Sonek, G. J., Ballantyne, J. M., Chen, Y. J., Carter, G. M., Brown, S. W., Koteles, E. S., and Salerno, J. P., "Dielectric properties of GaAs/AlGaAs multiple quantum well waveguides", *IEEE Journal of Quantum Electronics*, volume QE-22, pp. 1015–1018, 1986.

Sze, S. M., *Physics of Semiconductor Devices*, John Wiley & Sons, Inc., (1969).

Weisbuch, C., in *Semiconductors and Semimetals*, edited by R. Dingle, (Academic Press, San Diego, 1987), volume 24, Chap. 1.

Wood, T. H., Tkach, R. W., and Chraplyvy, A. R., "Observation of large

quadratic electro-optic effect in GaAs/AlGaAs multiple quantum wells", *Applied Physics Letters*, volume 50, pp. 798–800, 1987.

Yariv, A., *Quantum Electronics*, (John Wiley, New York, 1975), 2nd edition, Chap. 14.

Yariv A., and Yeh, P., *Optical Waves in Crystals*, Chap. 7, John Wiley, 1984.

Zucker, J. E., Bar-Joseph, I., Miller, B. I., Koren, U., and Chemla, D. S., "Quaternary quantum wells for electro-optic intensity and phase modulation at 1.3 and 1.55 μm ", *Applied Physics Letters*, volume 54, pp. 10–12, 1989.

Zucker, J. E., Hendrickson, T. L., and Burrus, C. A., "Electro-optic phase modulation in GaAs/AlGaAs quantum well waveguides", *Applied Physics Letters*, volume 52, pp. 945–947, 1988.